

國立臺灣大學土木工程學系

博士論文

Department of Civil Engineering

College of Engineering

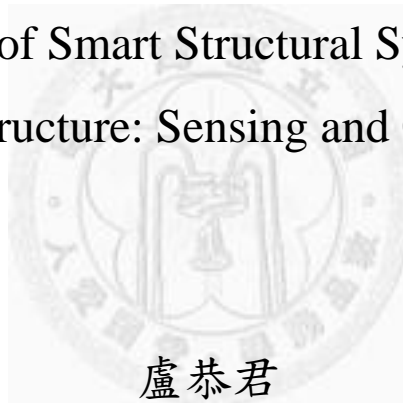
National Taiwan University

Doctoral Dissertation

開發智慧型結構系統於土木基礎建設：感測與控制

Development of Smart Structural System for Civil

Infrastructure: Sensing and Control



盧恭君

Kung-Chun Lu

指導教授：羅俊雄 博士

Advisor: Chin-Hsiung Loh, Ph.D.

中華民國 99 年 12 月

December, 2010

誌謝

首先感謝指導教授 羅俊雄 教授在論文研究期間給予細心的指導及研究方向的指引，使得本論文得以順利完成，在此對恩師致上由衷敬謝之意。感謝史丹佛 Kincho H. Law 教授、喬治亞理工學院 Yang Wang 教授以及密西根大學 Jerome P. Lynch 教授於無線感測技術上的指導與交流。感謝加州大學爾灣分校 J. N. Yang 教授於結構物控制理論上的指導。

於論文口試期間，承蒙 洪宏基 教授、林其璋 教授、張國鎮 教授、呂良正 教授、吳重成 教授以及朱世禹 教授的指導並且提供寶貴的建議，使得本論文更加完備充實，特此予以致謝。

在研究期間感謝學長 林沛暘 博士於研究上的指導及鼓勵，同時也感謝一起努力的研究夥伴 翁建煌 博士、許丁友 博士、趙書賢 博士、譚佳慧 小姐 以及 黃謝恭 先生於研究期間的相互扶持互相激勵。

最後，感謝我親愛的家人，謝謝你們在背後默默的支持我，讓我得以專心求學與研究，並且讓我一次又一次的克服困難，向前邁進。僅以本文獻給你們，願你們跟我共享這份喜悅與榮耀。

摘要

近年來，拜結構感測以及結構控制技術所賜，天然災害所導致的土木基礎結構危害得以減緩。本研究的目的是在於引進嵌入式系統以及無線傳輸技術並且應用於改善傳統結構感測及控制系統的缺點，藉由這樣的研究讓智慧型結構系統的概念得以實踐於真實結構物中。同時，本研究完成了兩套智慧系統的設計，分別為智慧型感測系統以及智慧型結構控制器。

最近研究人員對於嵌入式系統以及無線傳輸技術有著極大的興趣。嵌入式系統的精神在於”軟硬體共同設計”的理念，這樣的理念是依照需求的功能依序完成專用的硬體及軟體設計。無線傳輸技術則是提供一個低成本、有彈性且可重新規劃的傳輸架構，並且藉由此架構取代傳統拉線式的資料傳輸方式。

智慧型感測系統的研發包含了分析方法與設備研發。在設備研發方面開發新的無線感測器以及以即時控制器為基礎的伺服器端，並且運用這些設備完成訊號量測的程序；在分析方法方面，蒐集了數種成熟的分析方法，其中包含了自回歸分析法、頻率域分解法、隨機子空間識別法以及兩階段損害識別法。系統中建置了包含無線感測器網路以及 3G 移動式網路的兩層式無線網路架構。設計完成的智慧型感測系統藉由應用於集鹿橋及牛鬥橋的野外結構微振動反應量測實驗，該系統的可靠度及性能透過實驗的結果獲得驗證；同時藉由本研究所提供的結構物健康診斷方法，結構物的特性也能夠被精確的解析。

智慧型結構控制器的研發中包含了一套新的分散式控制理論（分散式滑模控制）推導，以及針對該方法所設計的專屬控制硬體。透過振動台的實驗，智慧型結構控制器能有效的折減結構物於地震下的反應，該系統也藉由這個實驗獲得驗證。

關鍵詞： 結構物健康診斷、結構控制、分散式控制、損害識別、無線感測、無線傳輸、嵌入式系統

Abstract

In recent years, the techniques of structural sensing and control are used to mitigate the effects of natural hazards on civil infrastructure. The objective of this study is to improve traditional structural sensing and control systems of civil engineering by applying the technologies of embedded system and wireless sensing, and implements the concept of smart structural system on building. Two systems are provided in this study, Smart Sensing System and Smart Control Device.

Recently, the techniques of embedded system and wireless communication have attracted much research interest. The main idea of embedded system is Hardware-Software Co-Design which is a simultaneous design of both hardware and software to implement in a desired function. Wireless communication technology provides a low-cost, flexible and reconfigurable architecture to replace the traditional wired communication.

The development of Smart Sensing System includes a newly developed wireless sensing unit (NTU-WSU) and a Host Node with real-time controller (cRIO) to perform the sensing procedures, and several structural health monitoring techniques (AR, FDD, SSI and two-stage AR-ARX damage detection) are surveyed to extract structural characteristics. Two-layer wireless communication architecture which includes wireless sensor network and 3G Mobile Internet is built in Smart Sensing System. This system is

adopted in the measurement of Gi-Lu Bridge and Niudou Bridge and the result shows the high robustness of wireless sensing system and the structural characteristics are accurately extracted through the provided SHM methods.

The development of Smart Control Device includes a newly developed decentralized control algorithm (decentralize sliding mode control) and a new embedded system which is designed for this specified control algorithm. This system is verified with a shaking table test and the control performance indices show Smart Control Device reduces the structural responses effectively.

Keywords: structural health monitoring, structural control, decentralized control, damage detection, wireless sensing, wireless communication, embedded system

Table of Contents

Abstract (in Chinese)	II
Abstract (in English)	III
Table List	VIII
Figure List	IX
1 Introduction	1
1.1 Background.....	1
1.1.1 Smart Sensing.....	2
1.1.2 Structural Health Monitoring.....	3
1.1.3 Structural Control.....	5
1.2 Research Objectives.....	8
1.3 Thesis Outline.....	9
2 Smart Structural Sensing	11
2.1 Introduction of Smart Sensing System.....	11
2.1.1 The Concept of Smart Sensing System.....	11
2.1.2 The Hardware Overview of Smart Sensing System.....	13
2.1.3 The Communication Overview of Smart Sensing System.....	15
2.2 Hardware Design and Integration of Smart Sensing System.....	18
2.2.1 Hardware Framework.....	18
2.2.2 Sensing Node of Smart Sensing System (NTU-WSU).....	20
2.2.2.1 Computation Core.....	22
2.2.2.2 Wireless Module.....	25
2.2.2.3 Signal Conditioning and Digitalization Module.....	28
2.2.2.4 System Powering Module.....	32

2.2.2.5	Packaging and Specifications of NTU-WSU-V02a.....	35
2.2.3	Host Node of Smart Sensing System.....	38
2.2.3.1	Real-time Controller: cRIO-9022.....	39
2.2.3.2	Wide Area Network: 3G Mobile Router.....	41
2.2.3.3	Wireless Sensor Network: Wireless Receiver.....	42
2.3	Software Design and Arrangement of Smart Sensing System.....	43
2.3.1	Software Framework.....	43
2.3.2	Embedded Software of NTU-WSU.....	45
2.3.2.1	Software Module of MCU Data Bus.....	47
2.3.2.2	Software Module of Peripheral Service Routine.....	49
2.3.3	Embedded Software of Host Node.....	51
2.3.4	User Interface.....	53
2.4	Communication Protocol of Smart Sensing System.....	56
2.4.1	The Main Frame of Sensing Node.....	56
2.4.2	The Main Frame of Host Node.....	59
2.4.3	Synchronization Protocol.....	60
2.4.4	Data Collecting Protocol.....	62
2.5	Summary.....	64
3	Structural Health Monitoring and System Validation	66
3.1	Structural Health Monitoring.....	66
3.1.1	Auto-Regressive Method.....	66
3.1.2	Frequency Domain Decomposition Method.....	71
3.1.3	Stochastic Subspace Identification Method.....	75
3.1.4	Two Stage AR-ARX Damage Detection Method.....	79
3.2	System Validations and Online Embedded Computing.....	83

3.2.1	Field test at Gi-Lu Bridge.....	83
3.2.1.1	First Stage: The Evaluation of Wireless Ambient Measurement.....	84
3.2.1.2	Second Stage: Performance Evaluation of NTU-WSU.....	91
3.2.2	Damage Detection of RC Frame.....	93
3.2.3	Long-term SHM System of NTU CE Research Building.....	112
3.2.4	Field Experiment at Niudou Bridge during FANIPA typhoon period.....	125
3.3	Summary.....	131
4	Smart Structural Control	135
4.1	Decentralized Siding Mode Control.....	138
4.1.1	Experiment Setup.....	139
4.1.2	Decentralized Sliding Mode Control Algorithm.....	146
4.2	Smart Control Device.....	154
4.2.1	Hardware Design of Smart Control Device.....	155
4.2.2	Software of Smart Control Device.....	159
4.3	Discussion on the Experiment Results.....	161
4.4	Summary.....	176
5	Conclusion and Future Work	179
5.1	Conclusion.....	179
5.2	Future Work.....	182
	Reference	185

List of Tables

Table 2.1:	Specification of wireless modules.....	26
Table 2.2:	The specifications of NTU-WSU-V02a.....	36
Table 2.3:	Specification summary of NI cRIO-9022.....	40
Table 2.4:	The function list of embedded program of NTU-WSU.....	48
Table 3.1a:	Estimation of the ratio of residual error through wireless damage detection module (for case of wall frame structure: A1F).....	101
Table 3.1b:	Estimation of the ratio of residual error through wireless damage detection module (for case of wall frame structure: P1F).....	102
Table 3.1c:	Estimation of the ratio of residual error through wireless damage detection module (for case of wall frame structure: P1F).....	102
Table 4.1a:	Mass matrix of 6-DOF test structure.....	141
Table 4.1b:	Stiffness matrix of the 6-DOF test structure.....	141
Table 4.1c:	Damping matrix of the 6-DOF test structure.....	141
Table 4.2:	Voltage dependent parameters of the model of MR damper.....	143
Table 4.3:	Evaluation criteria definition of J indices.....	162
Table 4.4:	Four sets of control parameters considered in SMC1 for Case B structure.....	163
Table 4.5:	Five sets of control parameters considered in SMC4 method for Case B structure.....	165
Table 4.6:	Control parameters and feedback signals for SMC-1, SMC-4 and LQR control methods.....	168
Table 4.7:	Control Parameters for the control methods LQR1 and LQR2 in four test structures.....	169
Table 4.8:	Comparison on the number of control parameters and feedback signals for different control method.....	170

List of Figures

Figure 2.1:	The concept of Smart Sensing System.....	12
Figure 2.2:	Function overview of Smart Sensing System.....	15
Figure 2.3:	The communication overview of Smart Sensing System.....	17
Figure 2.4:	The hardware framework of Smart Sensing System.....	19
Figure 2.5:	The hardware contents of wireless sensing unit (NTU-WSU-V02a).....	21
Figure 2.6:	The hardware of computation core.....	25
Figure 2.7:	The hardware diagram of wireless module and MCU.....	27
Figure 2.8:	The composition diagram of signal conditioning and digitalization module.....	29
Figure 2.9:	The effect of Signal Conditioner of NTU-WSU.....	30
Figure 2.10:	The signal verification of SPC51 and NTU-WSU.....	31
Figure 2.11:	The design of powering module.....	33
Figure 2.12a:	The main board of NTU-WSU-V02a.....	35
Figure 2.12b:	The main board with 9XTend wireless module.....	37
Figure 2.12c:	The pin definitions of NTU-WSU_V02a.....	37
Figure 2.13:	The hardware concept of Host Node.....	38
Figure 2.14:	NI cRIO-9022 (http://www.ni.com).....	41
Figure 2.15:	3.5G Modem D-Link DIR-455, (http://www.dlinktw.com.tw)....	42
Figure 2.16:	The software framework of Smart Sensing System.....	44
Figure 2.17:	The software architecture of Sensing Node (NTU-WSU).....	46
Figure 2.18:	The software architecture of Host Node.....	52
Figure 2.19:	The user interface of Host Node.....	54
Figure 2.20:	The user interface of internet user.....	55
Figure 2.21:	The program structure of Sensing Node.....	57
Figure 2.22:	The main frame of the software of Host Node.....	59
Figure 2.23:	The Synchronization Protocol of Smart Sensing System.....	61
Figure 2.24:	The Data Collecting Protocol of Smart Sensing System.....	63
Figure 3.1:	Signal converter, power source and directional antenna with WiMMS.....	86
Figure 3.2:	Pictures of system calibration and cable installation.....	87
Figure 3.3a:	Front view and top view of the Gi-Lu cable-stayed bridge.....	88
Figure 3.3b:	Installation location of the wireless sensors during Test 3.....	88

Figure 3.4a:	Comparison of the identified bridge deck vertical mode shapes by using Stochastic Subspace Identification and Frequency Domain Decomposition.....	90
Figure 3.4b:	Comparison of the identified bridge deck mode shapes in the transverse direction.....	90
Figure 3.5:	The location of Host node (A) and sensor node (B) on Google Map.....	92
Figure 3.6:	Implementation of the AR-ARX damage detection strategy in a wireless monitoring system to conduct the continuous damage detection of large structural testing in the laboratory.....	96
Figure 3.7a:	Top view of the test specimen (A1F).....	98
Figure 3.7b:	Side view of the test specimen (A1F). Locations of accelerometers (■) and LVDT (▲) are also shown.....	98
Figure 3.8:	Draft of the front view and side view of the two-story RC frame.	99
Figure 3.9:	(a) Photo of the specimen A1F frame, (b) Photo of the specimen P1F frame, (c) Photo of the 2-story RC frame structure	99
Figure 3.10(a):	Restoring diagram of the test structure (A1F) from different input excitation level. (the unit of Y axis is restoring force per unit mass (g)).....	103
Figure 3.10(b):	Restoring diagram of the test structure (P1F) from different input excitation level. (the unit of Y axis is restoring force per unit mass (g)).....	103
Figure 3.10(c):	Restoring diagram of the test structure (P2F) from different input excitation level. (the unit of Y axis is KN).....	104
Figure 3.11(a):	Ratio of AR-ARX two-tier model residual error from test of RC frame (A1F) using off-line data. (Y axis is damage index).....	106
Figure 3.11(b):	Ratio of AR-ARX two-tier model residual error from test of RC frame without walls (P1F). (Y axis is damage index).....	107
Figure 3.11(c):	Ratio of AR-ARX two-tier model residual error from test of 2-story RC frame without walls (P2F).....	107
Figure 3.12:	Three pages to display from the wireless health monitoring system.....	109
Figure 3.13:	Location of dampers and isolators in the isolation floor (between 1st and 2nd floor).....	113
Figure 3.14:	Layout of the velocity sensors for ambient vibration monitoring of the building.....	114
Figure 3.15:	Hardware & Software arrangement of structural health monitoring system.....	116

Figure 3.16:	Flow chart of the software arrangement for building continuous monitoring.....	118
Figure 3.17:	Flowchart of the monitoring system in collecting and analyzing the data.....	118
Figure 3.18:	The automotive analysis flow chart of AR & FDD method.....	120
Figure 3.19:	The modal frequency selector of AR analysis.....	120
Figure 3.20:	The analysis flow chart of data-driven SSI method.....	121
Figure 3.21:	The criteria of mode selector of SSI method.....	121
Figure 3.22:	Display the status of data collection in Wireless Monitoring Module on the screen.....	123
Figure 3.23:	Fourier amplitude spectrum from the recorded ambient vibration data of the CE research building in both longitudinal (a) and transverse (b) direction. The identification natural frequencies and damping ratios from SSI method is also shown.....	124
Figure 3.24:	Identified mode shapes from three different methods: FFT, FDD and SSI.....	124
Figure 3.25:	The concept and instrument of Smart Sensing System on Niudou Bridge.....	127
Figure 3.26:	The photo of Smart Sensing System on Niudou Bridge.....	128
Figure 3.27:	The detail on Sensing Node and Host Node.....	129
Figure 3.28:	The time history of H5 and the analysis results of RSSI.....	130
Figure 4.1:	(a) & (b) schematic diagrams for side view of 6-story steel frame structure; (c) Photo of the 6-story steel frame structure on NCREE shaking table. The V-shape bracing system is for the installation of damper.....	139
Figure 4.2:	The detail view on the bracing of 6-story structure.....	140
Figure 4.3:	Performance test of the 3kN MR damper for four different voltage.....	142
Figure 4.4:	Four different cases of MR damper locations (layouts) in the test frame; (i) damper located on 1st floor, (ii) dampers located on the 1st and 3rd floors, (iii) dampers located on the 1st, 2nd and 3rd floors, (iv) dampers located on the 1st, 3rd, and 5th floors....	144
Figure 4.5:	The detail design of Smart Control Device	155
Figure 4.6:	The detail components of driven box and its connection with MR damper.	156
Figure 4.7:	Components in the driven box.....	159
Figure 4.8:	Photo of the driven box.....	159
Figure 4.9:	The frame work of software design.....	160

Figure 4.10:	Flow chart of calculation in each time step in the microprocessor.	161
Figure 4.11:	Comparison on the performance indices for Case B structure subject to El Centro Earthquake (PGA=100 gal) using the SMC1 method with different sets of control parameters (Passive-off, Passive-on, SMC1-1 ~ 4).....	164
Figure 4.12:	Comparison on the performance indices for Case B structure subject to El Centro Earthquake (PGA=100 gal) using the SMC4 method with different sets of control parameters (Passive-off, Passive-on, SMC3-1, SMC3-2, SMC3-3, SMC3-4, and SMC3-5).....	165
Figure 4.13a:	Comparison for the hysteretic loops of damper on the 1st floor between simulation and experiment results using different pairs of α -value and δ -value in the SMC3 control method.....	167
Figure 4.13b:	Effects of control parameters, α -value and δ -value, on the performance indices of Case B structure using the SMC3 method.....	167
Figure 4.14:	Comparison on the control performance for four different structural systems (from Case A to Case D) using eight different control methods (Passive-off, Passive-on, LQR1, LQR2, SMC1-1, SMC1-2, SMC3-1 and SMC3-1) with El Centro Earthquake (PGA=100 gal) as excitation.....	170
Figure 4.15:	Comparison on the performance indices using three different control methods, Passive-on, LQR1 SMC1-1 and SMC3-1, on four different cases of structural systems.....	171
Figure 4.16:	Comparison on performance indices of Case A structure subjected to four different earthquake excitations (EL Centro-100gal, EL Centro-200gal, Kobe-100gal, Kobe-150gal)...	172
Figure 4.17:	Comparison on the 6th floor acceleration response for case B structure between; (a) Passive-off (0 Volt) and passive-on (0.8Volt) control cases, (b) Passive-off (0 Volt) and LQR1 control cases, (c) Passive-off (0 Volt) and SMC1-1 control cases, (d) Passive-off (0 Volt) and SMC3-1 control cases.....	173
Figure 4.18:	Photos of the Smart Control Device in the first story to control the MR damper.....	174
Figure 4.19:	The performance indices of Case D. (Input is El Centro 100gal)..	175
Figure 4.20:	Comparison on the stroke signal and the command voltage issued by NCREE system and the MSP 430 microprocessor of Smart Control Device.....	176



Chapter 1

Introduction

1.1 Background

Mitigation of the affects of natural hazards on civil and mechanical infrastructure requires that both sensing and control technologies be installed in structures. Specifically, sensors are responsible for recording the response of the structure to time-varying loading conditions while actuators (active and semi-active) are used to physically limit structural response so as to reduce structural damage and avoid catastrophic global collapse. More specifically, “smart” refers to the augmentation of computational intelligence with the sensor or actuator to allow each device to process its own data for determining damage and deciding optimal control actions that limit the dynamic response. Over the past decade, many innovative smart sensing and smart control devices have been explored, with test and field results showing tremendous promise for more widespread implementation in new and existing structural systems. Since the mid 1990’s, researchers have devoted in the fields of sensors, data interrogation algorithms, and smart materials as they apply to mitigation of natural hazards. The pursuit of smart structure research has ushered in a new era of unprecedented multidisciplinary research encompassing a variety of engineering disciplines including, but not limited to, smart materials (materials science and

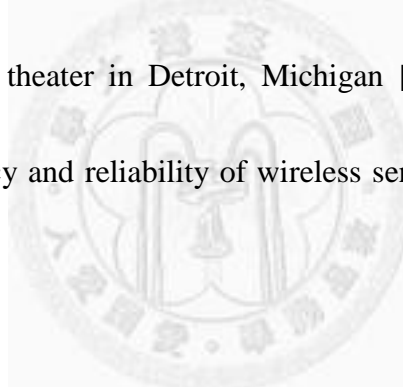
engineering), electronics (electrical engineering), applied mechanics, structural and system dynamics (mechanical engineering), signal processing (computer science), and design and construction (civil engineering). While great advances have already been made, resulting in safer and more durable civil and mechanical infrastructure systems, catastrophes still occur.

1.1.1 Smart Sensing

Through networks of densely deployed smart sensors have the potential to improve structural health monitoring dramatically. To effectively detect arbitrary damage in structures, a dense array of sensors distributed over the entire structure will be required. The essential difference between a standard sensor and smart sensor is the latter's flexible communication and information processing capability. Each sensor has an on-board microprocessor that can be used for digital signal processing and self-diagnostics. Furthermore, all sensor platforms have far employed wireless communication technology. Some of the efforts in developing the smart sensors for application to civil engineering structures were presented by [1]. Several SHM applications with smart sensors have been studied using both scale models and full-scale structure [2 ~ 7].

The use of wireless communications in lieu of wires within a structural monitoring system was initially proposed by Straser and Kiremidjian [1] as a means of reducing

installation costs in large-scale civil structures. In addition, their work illustrated the freedom a wireless system infrastructure provides including rapid and reconfigurable installations. Recently, Lynch et al. has extended their work to include computational microcontrollers in the hardware design of wireless sensors so that various system identification and damage detection algorithms can be embedded for local execution by the sensor [8 ~ 10]. To date, a handful of bridges and buildings have been instrumented with wireless monitoring systems including the Alamosa Canyon Bridge (New Mexico), Geumdang Bridge (Korea), WuYuan Bridge (China), Voigt Bridge (California) and a historic theater in Detroit, Michigan [11]. These extensive field studies attest to the accuracy and reliability of wireless sensors in traditional structural monitoring applications.



1.1.2 Structural Health Monitoring

Structural health monitoring refers to monitoring the health statuses of structures through the techniques of feature extraction and damage detection. The techniques of system identification analyze the structural vibration responses to estimate the dynamic characteristics of structure. Vahid Sotoudeh [12] gives a theoretical formulation of system modeling which is primarily in the discrete-time domain where the z-transform and digital filtering principle can be applied directly. Erdal Safak [13] presents a discrete-time method for system identification by using discrete-time linear filters. The

processing of data, the selection and validation of models in the identification, and the detection of soil-structure interaction are also discussed in the literature. Rune Brincker, et al. [14 ~ 17] presents a new frequency domain technique to extract the structural properties from ambient responses. This technique is called Frequency Domain Decomposition (FDD) which can identify the close modes with high accuracy even in the case of strong noise contamination of the signals. J. H. Weng [18 ~ 22] presents the application of subspace identification techniques on structural system identification and damage detection. Both the theoretical study and the applications on civil infrastructures are shown in this literature.

From the theoretical viewpoint, damage detection using data generated by structural monitoring systems has been extensively studied over the past 30 years and the literature on the subject is rather immense. Doebling, et al. [23] gives a comprehensive survey of vibration based global damage detection techniques. Various approaches on data analysis for system identification and damage detection have been proposed in the literature. In the parametric identification method, Kondo and Hamamoto [24] used an ARMA (Auto-Regressive Moving Average) model to identify the modal frequencies and modal shapes of the structure and detect the location of damage from changes of the curvature of mode shapes. Safak [25,26] used ARMAX (Auto-Regressive Moving Average with eXogenous) models with RPEM (Recursive

Prediction Error Model) to identify the real structure of linear time-varying systems. Andersson [27] used AFMM (Adaptive Forgetting through Multiple Models) methods to trace time-varying parameters of the structure. Loh and Lin [28] also used off-line and on-line identification techniques to accurately determine time-varying system parameters. Recently, an advanced damage detection approach using time series analysis of vibration signals was proposed by Los Alamos National Laboratory (LANL) (2001). The method proposed is based on the “statistical pattern recognition paradigm; the method is attractive for adoption within an automated monitoring system. Following their initial work, a procedure based on the time series analysis of vibration signals for damage detection and localization within a mechanical system was proposed by Sohn, et al. [29,30]. In this method the standard deviation of the residual error, which is the difference between actual measured structural responses and those predicted from a two-stage combination of the AR and ARX models, is used as the damage-sensitive feature to locate damage.

1.1.3 Structural Control

In recent years, many control strategies have been proposed for earthquake and wind hazard mitigation by installing either passive control devices, active control devices, or semi-active control devices. In particular, the semi-active control devices have been shown to be quite effective and robust in reducing the structural responses

when subjected to strong earthquakes. Various control theories have been investigated for implementation of active/semi-active control systems on civil engineering structures, such as H^2 control [31,32,33], H^∞ control [34,35,36], etc.. C. M. Chang and C.H. Loh provided the application of H^2 and H^∞ control on both numerical simulation test and shaking table test [37, 38, 39]. Generally, this type of centralized control system is used to form the control gain and to compute the control force from the global measurements of structural system. Because of the high dimensionality of the finite element model of the structural system, the multiple inputs and outputs, and the complex performance criteria, it is difficult to design a controller so as to achieve the desired control effectiveness for a large-scale structure. Besides, the centralized control system has a risk to shutdown the control server when the external force is so large to cause the malfunction of sensors or computer system. Therefore, the concept of decentralized control has been proposed to replace the global control system by several local control systems. However, the development of effective decentralized control methods is quite challenging.

For the centralized control algorithms, Yang et al. [40, 41] used the concept of continuous sliding mode control and applied the control methods to a variety of linear, non-linear and hysteretic structures. Based on the theory of sliding mode control (SMC), the hybrid control systems, including semi-active control devices and non-linear

isolators, for seismic-excited bridge structures has also been studied by Yang et al. [42]. Using the concept of the Lyapunov direct method for the controller design, Yang et al. [43, 44] had carried out a systematic investigation for the application of sliding mode control to building structures. Besides, skyhook control and a 'clipped' Continuous Sliding Mode (CSM) control were also simulated both numerically and experimentally by Hiemenz et al [45, 46].

In the literature, centralized control strategies have been used to control the MR damper, for instance the popular LQR full-state feedbacks control method [e.g., 47]. Another problem with centralized control is the requirement of wiring to collect all sensor data and to transmit all the data to a central location (computer) for further processing in order to determine the control force for each controller. This could also result in a time delay. Likewise, control robustness may be compromised, since centralized control depends on the identification accuracy of the structural properties. Theoretically, decentralized control is robust and it may need only minimum wiring, because the control action of a controller depends only on the structural responses in the vicinity of the controller's location. Hence, decentralized control strategies have significant advantages, although it is quite challenging to develop effective decentralized control strategies.

1.2 Research Objective

The objective of this research is to implement the concept of smart structural system through the development of Smart Sensing System and Smart Control Device. The development of Smart Sensing System involves the system hardware integration and the techniques of structural health monitoring. The system hardware integration of Smart Sensing System includes (1) developing a newly generated wireless sensing unit, (2) integrating powerful real-time controller and (3) adopting standard industrial communication protocol. Considering the sensing requirements of civil engineering, the sensing node of Smart Sensing System is a newly generated wireless sensing unit National Taiwan University - Wireless Sensing Unit (NTU-WSU) which includes the techniques of wireless sensor network, embedded system and vibration measurement. An industrial real-time controller, NI compact RIO, is also integrated in Smart Sensing System to serve the computation and management functions.

Several structural health monitoring techniques are studied in this research; they are Auto-Regressive (AR), Frequency Domain Decomposition (FDD), Stochastic Subspace Identification (SSI), and Two-stage AR-ARX damage diagnosis. Base on these techniques and considering the requirements of automatic analysis, the software consideration and arrangement are carefully implemented in this system.

The concept of Smart Control Device is to provide a new and easy approach to

implement structural control on civil infrastructures. In order to reduce the complex computation and sensing requirements of traditional control method, the decentralized sliding mode control algorithm which is a decentralized computing method and only requires local measurement is studied in this research. A new control system which is designed to embed with the decentralized sliding mode control algorithm is also developed in this research.

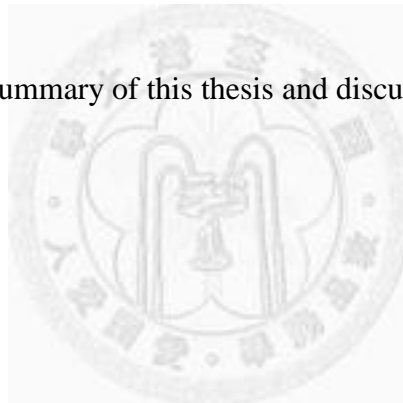
1.3 Thesis Outline

The thesis is organized as follows:

- **Chapter 2** introduces the smart structural sensing and the development of Smart Sensing System. The hardware overview and communication overview of Smart Sensing System are described first. The development of hardware and software are introduced in **Section 2.2** and **2.3**. Finally is the communication protocol which includes the main frames of software and operating protocols.
- **Chapter 3** introduces the techniques of structural health monitoring and the system validations of Smart Sensing System. Three system identification methods and one damage detection method are introduced in **Section 3.1**; they are Auto-Regressive, Frequency Domain Decomposition, Stochastic Subspace Identification and Two-stage AR-ARX damage detection. **Section 3.2** shows a

series experimental studies which are used to validate the results of SHM techniques and the performance of Smart Sensing System.

- **Chapter 4** introduces the smart structural control which includes the introduction of decentralized sliding mode control and Smart Control Device. Both the theoretical formulation and experimental study of decentralized sliding mode control are presented in **Section 4.1**. The hardware and software design of Smart Control Device and the device validation are introduced in **Section 4.2**.
- **Chapter 5** is the summary of this thesis and discusses possible future work.



Chapter 2

Smart Structure Sensing

The objective of this chapter is to develop Smart Sensing System which is a continuous monitoring system for building structure. Based on the wireless sensing and monitoring system Smart Sensing System was developed. The smart sensors are employed in the same manner as traditional wired sensors with all data being synchronously collected for processing at a centralized location. With the management of data processing and identification in the server, the dynamic characteristics of the building structure can be reported continuously.

2.1 Introduction of Smart Sensing System

2.1.1 The Concept of Smart Sensing System

The development of wireless sensing system for structural health monitoring is studied by Lu et al., 2010 [48, 49], the preliminary concept of Smart Sensing System is provided in this study. *Figure 2.1* shows the concept of Smart Sensing System, there are three nodes in this system and they are Sensor Node, Server Node and User Node. Sensor Node is a smart sensor which is constructed with a transducer and an embedded system. The transducer transforms structural vibration response into voltage signal. This voltage signal is sampled and processed in the embedded system. Sensor Node also

supports the flexible communication. Here, wireless communication is adopted in Sensor Node. So Sensor Node includes three major functions and they are signal sampling, distributed computing and wireless communication.

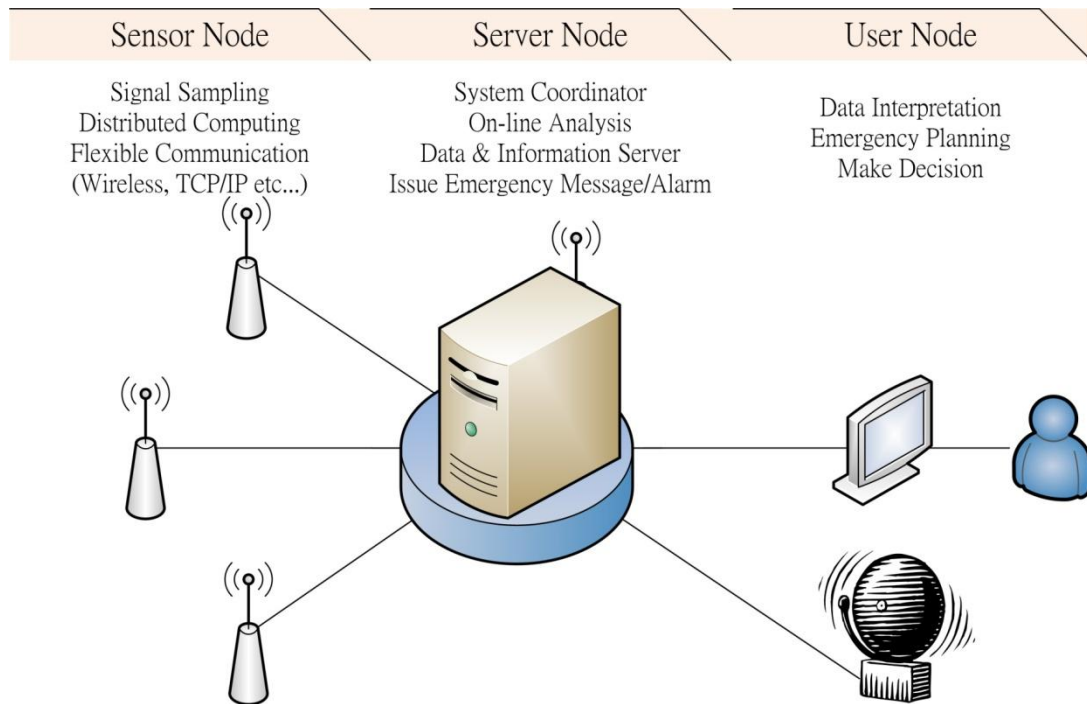


Figure 2.1: The concept of Smart Sensing System.

Also, Server Node is an embedded system which includes more powerful computation core and larger memory size than Sensor Node. Server Node performs the system coordinator of this wireless sensor network, manages the entire status of wireless sensor nodes and dominate wireless sensor network to complete the issued event. After the issued event is completed and the data is feedback to Server Node, Server Node executes the on-line analysis to generate the useful information and base on this information to alarm emergency message. Server Node saves information in memory

space and to be a data & information server for user to access it. Finally is User Node, User Node is designed to be any general purposed electoral information machine (ex. PC, Laptop, PDA, Smart Phone, etc...). User can get information from Smart Sensing System easily through these equipments. And the interface between Smart Sensing System to Wide Area Network follows the standard internet protocol (ex. TCP/IP, FTP, Webpage, etc...).

2.1.2 The Hardware Overview of Smart Sensing System

Smart Sensing System is designed for the application of civil engineering, the function of Smart Sensing System must be defined first and the hardware is also decided.

According to the concept of Smart Sensing System, Sensor Node includes transducer and embedded system. Considering the application of civil engineering and the requirements of continuous structural health monitoring, there are two requirements of transducer. Mostly of structural health monitoring methods require the structural vibration responses to be the input data, i.e. the transducer must be a vibration type sensor. Smart Sensing System continuously collects the structural responses under ambient excitation level. The transducer needs to be sensitive to detect the weak vibration motion of structure. Base on the above considerations, the transducer needs to be a sensitive vibration sensor. According to the past experiments, the ambient sensor

VSE-15D is selected. The VSE-15D sensor is a servo velocity meter produced by Tokyo Sokushin Co., Ltd. The detail description of VSE-15D is on the official website [www.to-soku.co.jp]. A newly generated wireless sensing unit (NTU-WSU) is the embedded system of Sensor Node which provides the function of signal sampling, data buffering, data pre-processing and wireless communication. This new generated wireless sensing unit is based on the original hardware of WiMMS [50], with the consideration of the requirements of structural health monitoring and named it as “NTU-WSU” wireless sensing unit. The detail design of NTU-WSU will be described in *Section 2.2.2*.

Server Node of Smart Sensing System is NI-cRIO 9022 which is a configurable real-time input/output controller. Server Node plays a very important role in Smart Sensing System. It coordinates the full wireless sensors, triggers event, executes on-line analysis and plays the data server of user interface. So Server Node must be a highly robust machine with real-time OS, the general purposed personal computer is difficult to match these requirements and cRIO is selected to be the Server Node of Smart Sensing System. By the way, cRIO supports civil engineers an easy way to embed program, this can reduce the development time and improve the efficiency of system implementation and validation. The detail operation of Server Node will be introduced in *Section 2.2.3*.

User Node of Smart Sensing System is not limited to special machine, i.e. general digital computer with the function of internet explorer and FTP is accepted. In the system validation and test, both laptop and smart phone are used to be User Node.

The overall function and hardware are shown in **Figure 2.2**, where the sensor is ambient velocity sensor (VSE-15D), wireless sensing unit is NTU-WSU and Server Node is configurable real-time I/O controller (cRIO). The hardware and software of Smart Sensing System will be presented in **Section 2.2** and **2.3**.



Figure 2.2: Function overview of Smart Sensing System.

2.1.3 The Communication Overview of Smart Sensing System

An important feature of Smart Sensing System is flexible communication. The communication overview of Smart Sensing System is presented here. There are two different communication levels in Smart Sensing System.

First is the wireless sensor network between Sensor Node and Server Node. The

system commands and data strings are propagated through this wireless sensor network which is a specified local area network. In this study, the wireless sensor network is performed by Digi wireless solution. Two types of wireless module are compactable with Smart Sensing System, they are 9XTend and 24XStream. By adjusting the wireless module, Smart Sensing System can suit to different application scenarios. The hardware of wireless module is described in *Section 2.2.2.2*; the communication protocol is in *Section 2.4*.

Another communication is Wide Area Network (WAN) of Smart Sensing System. In order to share the information of Smart Sensing System, Server Node requires the link of Internet. User and Smart Sensing System can exchange data on Internet. The linkage of Internet makes Smart Sensing System to contact with user. There are several different application scenarios of civil engineering which are indoor, outdoor and field tests. Monternet (Mobile-Internet) is included in Server Node to perform the linkage of WAN. The operation of Wide Area Network is described in *Section 2.2.3.2*.

Figure 2.3 shows the communication overview of Smart Sensing System which includes

1. The wireless sensor network between Sensor Node and Server Node;
2. Digital data bus (RS232) of wireless receiver and cRIO;
3. Local area network between cRIO and 3G modem;

4. 3G communication between 3G modem and telecom tower.

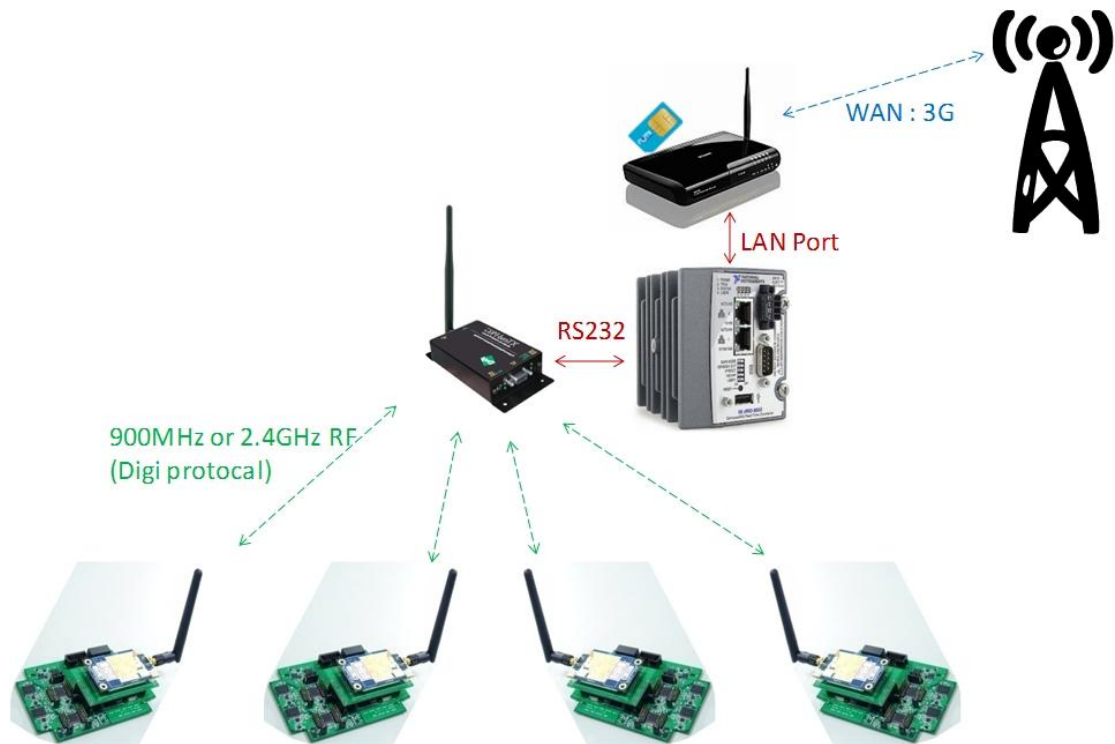


Figure 2.3: The communication overview of Smart Sensing System.

2.2 Hardware Design and Integration of Smart Sensing System

The details of hardware design and system integration of Smart Sensing System are described in the following sections. The hardware framework will be introduced first which includes the hardware organization and the working procedure. The hardware design of Sensor Node and Server Node will also be introduced in sequent.

2.2.1 Hardware Framework

The detail description of hardware framework is presented in *Figure 2.4*. Smart Sensing System includes three major components; they are: sensors, wireless sensing units (NTU-WSU) and Server Node (cRIO). Ambient velocity meters (VSE-15D) sense the structural vibration responses and convert the vibration signals into analog voltage signals. These voltage signals are fed into the wireless sensing unit (NTU-WSU) and sampled as digitalized and discrete-time data series. Server Node can acquire these sampled data through the wireless communication from all distributed wireless sensing units. After getting the required data, the host node will execute the SHM process and generate a report. User can access the host node through File Transfer Protocol (FTP) or Internet Explorer (IE) to get the structural responses and on-line analysis results.

The wireless sensing unit (NTU-WSU) is responsible to (1) supply the sensor power, (2) sample and buffer the sensor signals and (3) communicate with Server Node through wireless radio. There are four major subsystems included in the wireless

sensing unit (NTU-WSU), they are (1) computation core, (2) wireless module, (3) signal conditioning and digitalization module and (4) system powering module. The detail of these subsystems is described in *Section 2.2.2*.

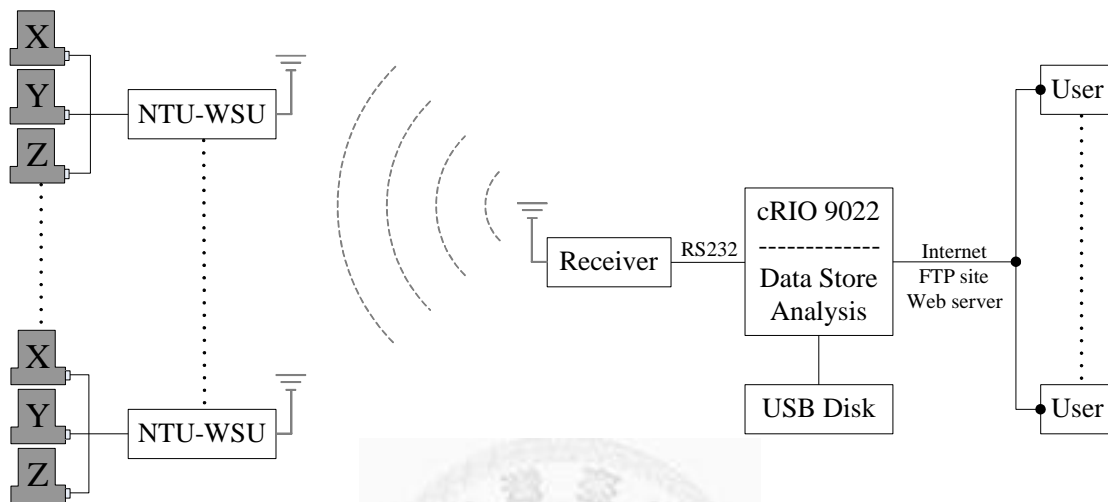


Figure 2.4: The hardware framework of Smart Sensing System

Server Node communicates with Sensor Node through wireless radio, after the data of Sensor Node is feedback to Server Node; Server Node saves these data and processes these data. Server Node also allows user to access these analysis results and recorded data. Base on the above description, the Server Node includes four major components, and they are: (1) real-time controller (cRIO-9022), (2) wireless receiver, (3) USB disk and (4) Wide Area Network machine (D-Link DIR-455). These components are introduced in *Section 2.2.3*.

2.2.2 Sensing Node of Smart Sensing System (NTU-WSU)

Sensing Node of Smart Sensing System is NTU-WSU which is newly generated wireless sensing unit from WiMMS[50]. This newly generated wireless sensing unit NTU-WSU considers the requirements of structural health monitoring and the environment of civil infrastructure. For structural health monitoring, the correction of analysis result is depending on the accuracy of recorded signal, especially on signal noise effect. Signal conditioning and digitalization module is designed to meet this requirement. Considering the environment of civil infrastructure, like office building, large scale bridge, etc..., there are several requirements on wireless communication. Buildings are usually constructed with concrete; the wireless radio should be strength enough to propagate in the building. In general, an office building is covered by several wireless network stations, and these wireless networks are usually in the frequency band 2.4GHz which is a noisy radio band. The design of wireless module needs to prevent this noisy radio band.

By the definition of Sensor Node of Smart Sensing System, Sensor Node includes the ability of data processing. Computation core with microcontroller (MCU), random accessible memory (RAM) and latch are used to handle the data processing and measurement procedure. Finally, the wireless sensing unit requires power to operate, the powering module is designed for system powering which is used to reduce the power

consumption and prevent the system noise to influence the performance of signal sampling.

Figure 2.5 shows the hardware contents of NTU-WSU and also includes the data bus between each component. The voltage signal of sensor is fed into NTU-WSU, this voltage signal is first amplified by selected gain (there are 4 different gain here, they are (1, 10, 100, 1000 V/V)). This amplified voltage signal is converted into the range of ADC sampling (0~5V). Each sensing unit supports four analog input channels and each channel with the same amplifying setting and conversion. After these signals are converted into the sampling range, the ADC digitalizes and samples this analog voltage signal. This digital signal is fed into microcontroller through Serial Peripheral Interface (SPI).

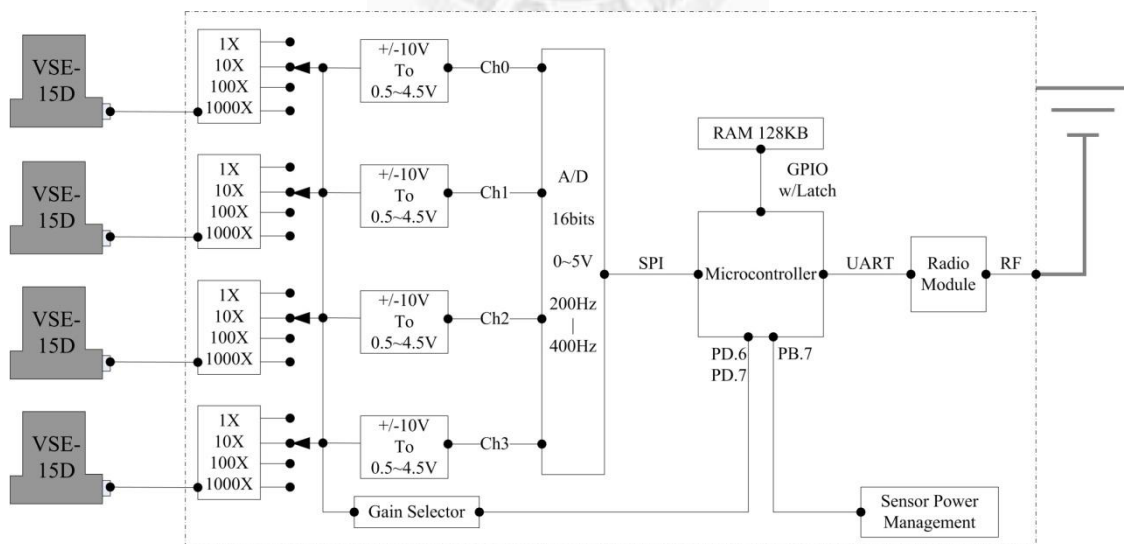


Figure 2.5: The hardware contents of wireless sensing unit (NTU-WSU-V02a).

The microcontroller is the main core of wireless sensing unit which is used to control all peripherals to complete the assigned event. After the digitalized structural response is received by microcontroller, the microcontroller accords the requirements of issued event to buffer this data in RAM or send this data to server through wireless radio. The data bus between RAM and MCU is General Purpose Input and Output (GPIO) with Latch; between wireless module and MCU is Universal Asynchronous Receiver/Transmitter (UART). The microcontroller also controls the Gain Selector and Sensor Power Management. Gain Selector is used to adjust the amplifying ratio (1, 10, 100, 1000 V/V) which is the pre-amplifying gain of sensor signal. Sensor Power Management is a digital switch used to turn on/off the sensor. This design is used to improve the power efficiency and extend the supplying time of system power. The detail design of each component is described in the following sections.

2.2.2.1 Computation Core

The computation core is used to execute the embedded program of wireless sensing unit. The embedded program includes the main loop of wireless sensing unit and the communication protocols (driver) of other peripherals. The design of computation core is base on the requirements of wireless sensing unit. As the function definition of wireless sensing unit, the computation core is used to control other peripherals, buffer data and execute required computation. The computation core

includes three components; they are microcontroller, SRAM and latch. The microcontroller is used to control other on-board peripherals and execute main program (idle loop) and required computation. Large memory space is required to buffering sampled signal and store variable of computation. SRAM and Latch are used to extend the memory size of computation core.

The microcontroller is Atmel ATmega128 which is a low-power 8-bit Reduced Instruction Set Computing (RISC) microcontroller. The 128K Bytes In-System Programmable Flash of ATmega128 is used to store the embedded program and this memory size (128KB) is large enough to cover most applications of wireless sensing. ATmega128 also includes 4KB EEPROM and 4KB SRAM. The measurement of structural response and the signal processing require large space of memory to store and operate raw data (time histories); therefore, the internal SRAM is not enough for this application. And an external SRAM is considered in this system to extend the space of system SRAM.

The integrated hardware interface of ATmega128 includes one Serial Peripheral Interface (SPI), two Universal Asynchronous Receiver/Transmitter (UART) and External Memory Interface. SPI is the interface of ADC (ADS8341EB); UART is the interface of wireless module (9XTend/24XStream); External Memory Interface is the interface of external SRAM (CY62128). The complete introduction of ATmega128 is

shown in Atmel Datasheet [51].

The composition diagram is shown in **Figure 2.6**. The capacity of External Memory Interface of ATmega128 is 64KB ($2^{16} \times 8$ bits) which includes 16 address control bits and 8 data bits. The interface includes (1) AD7:0: Multiplexed low-order address bus and data bus. (2) A15:8: High-order address bus. (3) ALE: Address latch enable. (4) \overline{RD} : Read strobe. (5) \overline{WR} : Write strobe. A latch (74AHC573) is required to keep the lower-order address bus from AD7:0. The external SRAM control procedure of ATmega128 is to issue the required memory address through (AD7:0 & A15:8) then output a 8-bits data contents through (AD7:0) and the operation (read or write) is selected by \overline{RD} and \overline{WR} . The size of external SRAM (CY62128) is 128KB ($2^{17} \times 8$ bits) which requires 17 address bits (A[16:0]). The ATmega128 only supports 16 address bits and is not enough to control CY62128, therefore a GPIO pin (PF3) of ATmega128 is arranged to control the last address bit (A[16]) of CY62128. Finally, the computation core of NTU-WSU is implemented through these hardware designs.

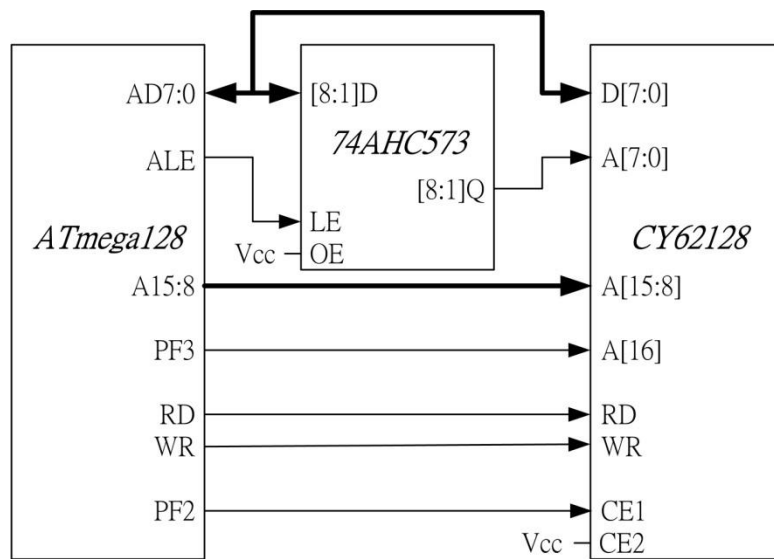


Figure 2.6: The hardware of computation core.

2.2.2.2 Wireless Module

The wireless module is the interface between Sensor Node and Server Node. The considered features of wireless module include (1) Data rate, (2) Frequency band of radio, (3) Communication protocol, (4) Radio signal strength (propagation distance) and (5) Power consumption. High data rate is good to reduce the data communication time but is usually with shorter propagation distance and higher power consumption. The frequency band of radio is a very important issue. The most commonly used band is 2.4GHz which is international ISM (Industrial, Science and Medical) band; and the wireless machine operated in 2.4GHz band is permitted using in most of countries. In general environment, the frequency band 2.4GHz is very busy which includes wireless access point, Bluetooth peripherals and Wi-Fi equipments, etc., this status is also considered in the design of wireless sensing unit. The communication protocol includes

the function of radio operation which is a very complicated rule. The selection of communication protocol is depended on the requirement of wireless sensor network. The propagation distance is controlled by the signal strength of radio and operating environment. For the application of civil engineering, the sensor is usually installed in the building, and wireless signal is required to propagate in the building. Another application is field test, the wireless sensor is installed on a large bridge and the wireless signal is required to propagate several hundred meters away.

Table 2.1: Specifications of wireless modules

Specification	9XTend		24XStream	
Frequency Range	902-928 MHz		2.4000-2.4835 GHz	
Channel Capacity	10 hop sequences shear 50 frequencies		7 hop sequences shear 25 frequencies	
Supply Voltage	2.8 ~ 5.25V		4.75 ~ 5.25 V	
Data Interface	COMS UART		COMS UART	
Network Topology	Peer-to-Peer, Point-to-Multipoint, Point to Point		Peer-to-Peer, Point-to-Multipoint, Point to Point	
Receive Current	80mA		80mA	
Transmit Power Output	1mW ~ 1Watt		50mW	
Throughout Data Rate	9600 bps	115200 bps	9600 bps	19200 bps
RF Data Rate	10000 bps	125000 bps	10000 bps	20000 bps
Indoor Range	900m	450m	180m	
Outdoor Range (w/ high-gain antenna)	22km (64km)	11km (32km)	5km (16km)	

The wireless sensing unit is a portable device with limited power source. So the power consumption is an important index of power supplying time. The design of NTU-WSU includes the ambient sensor (VSE-15D) which consumes about

0.9W/per-sensor (+/-15V @ 30mA) power and is larger than the power consumption of wireless radio. As the ambient sensor consumes the most power, the power consumption of wireless radio is not considered in the design of NTU-WSU.

The design of wireless sensing unit is compatible with two different wireless modules; they are Digi 9XTend and 24XStream. The comparison of 9XTend and 24XStream is shown in **Table 2.1**. 9XTend is operated in 900 MHz; 24XStream is operated in 2.4 GHz. By the selection of wireless module, wireless sensing unit (NTU-WSU) can prevent the busy frequency band of test environment. The data rate and signal range of 9XTend module is better than 24XStream; the power consumption of 9XTend is also larger than 24XStream. Wireless sensing unit can depend on the requirement of application to adopt different wireless module.

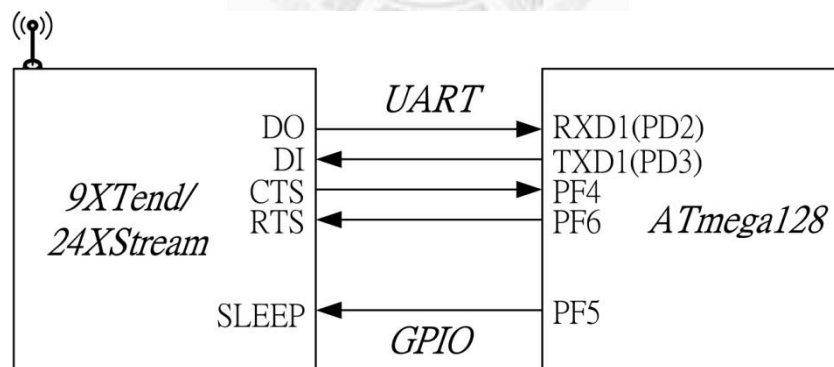


Figure 2.7: The hardware diagram of wireless module and MCU.

The hardware diagram of wireless module is shown in **Figure 2.7**. The interface between wireless module and MCU is CMOS UART interface, the wireless module

(9XTend/24XStream) is connected with the UART1 of ATmega128 and the communication data rate is adjustable. Two GPIO (PF4, PF6) of ATmega128 are used to change status flags (Clear to Send (CTS), Request to Send (RTS)) of wireless module; the GPIO (PF5) of ATmega128 is used to control the sleep mode of wireless module. Actually, 9XTend and 24XStream are not pin to pin compatible devices, there is an adapter board (9XTend-to-24XStream) used to connect with 9XTend.

2.2.2.3 Signal Conditioning and Digitalization Module

The design of signal conditioning and digitalization module is to satisfy the measurement of Smart Sensing System. For the purpose of routinely structural health monitoring, the structural response under ambient excitation is acquired and used for the analysis of structural health monitoring. The structural ambient response is a very slight signal and a high performance sampling hardware is required.

There are four components in the signal conditioning and digitalization module, they are Programmable Gain Instrumentation Amplifier (PGA204), Differential Amplifier (INA159) and Analog-to-Digital Converter (ADS8341EB). The PGA204 is used to amplify the sensor signal with selected gain. The gains of PGA204 are digitally selected through two GPIO pins (PD6, PD7) of ATmega128. There are four different gains of PGA204, they are 1, 10, 100, 1000 V/V and they are controlled through the software setting of embedded program. Microcontroller can base on the level of input

signal to select a suitable gain value to get the best sampling performance. The Differential Amplifier (INA159) is used to convert the amplified signal ($\pm 10\text{V}$) into the sampling range of ADC ($0 \sim 5\text{V}$). The analog-to-digital converter (ADS8341EB) is a four channel 16-bits Delta-Sigma ADC with maximum sampling rate 100 kHz. The sensor signal is pre-process with PGA204 and INA159 then finally sampled by ADS8341EB. The interface between ADS8341EB and ATmega128 is Serial Peripheral Interface (SPI) with 2 MHz data rate. An accurate reference voltage is generated by REF5050 and is used for the voltage reference of INA159 and ADS8341EB. A clean and accurate reference voltage is used to improve the sampling noise effect and sampling accuracy. REF5050 is a 5 V precision voltage reference with low-noise and low-drift features. The detail composition diagram is shown in **Figure 2.8**.

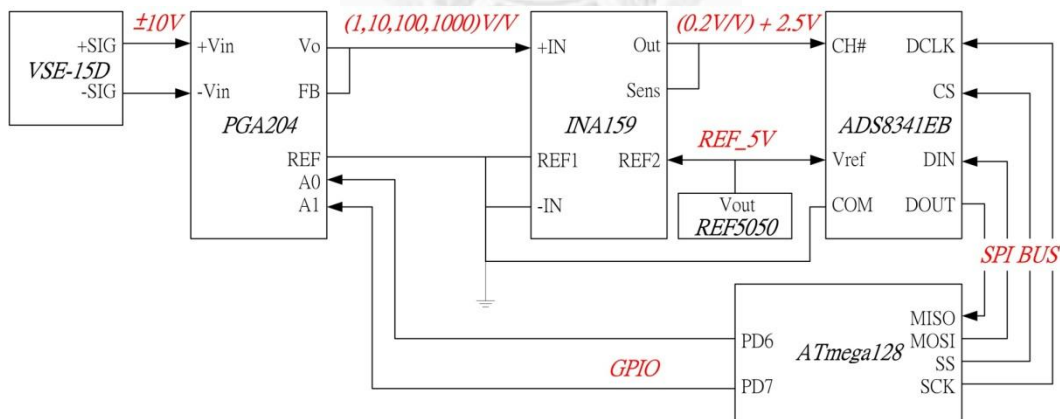


Figure 2.8: The composition diagram of signal conditioning and digitalization module.

In order to verify the sampling performance of NTU-WSU, two verifications and one experiment studies are presented here. These verifications and experiment studies

are focus on the performance of wireless sensing unit (NTU-WSU-V02a). First, laboratory test is used to verify the effect of signal conditioner of NTU-WSU. Two VSE-15D sensors are collocated and one is measured without signal conditioner, another is measured through signal conditioner with amplifier gain setting ($G = 100V/V$). The differences are shown in *Figure 2.9*.

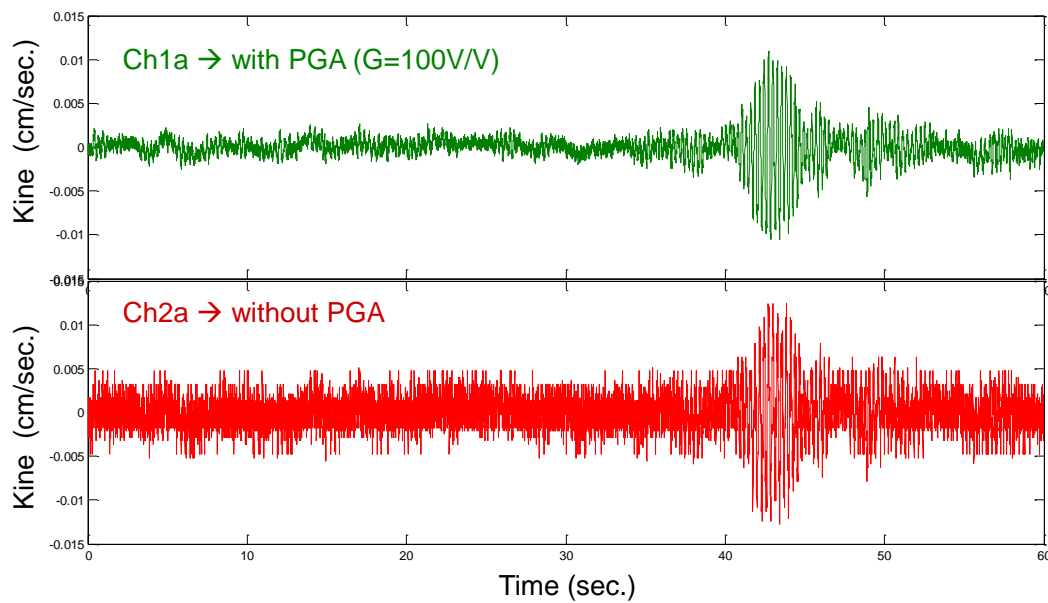


Figure 2.9. The effect of Signal Conditioner of NTU-WSU

There are two obvious differences in *Figure 2.9*, one is the system noise effect another is the insufficient resolution of ADC for ambient measurement. The system noise level is usually in a fixed level, the operation of amplifying signal is to increase the SNR (Signal to Noise Ratio) to prevent the noise effect. Generally, the ambient vibration signal is about several mille Kine (cm/sec.).

$$\frac{\pm 10 \text{Kine}}{2^{16} \text{ section}} = \frac{\pm 1.5 \times 10^{-4} \text{ Kine}}{1 \text{ section}} \quad (2.1)$$

Comparing the level of ambient signal with the resolution of 16-bits ADC, Equation (2.1) shows that the corresponding resolution is 1.5×10^{-4} Kine. The matched effective resolution is only about 30 sections.

The above evaluation is an ideal case. Actually, according to the datasheet of ADS8341[52], the SINAD is 86.3db (i.e. noise free bit is 14bit). By considering these device performances, the corresponding resolution is 6×10^{-4} Kine which is 4 times larger than ideal case. The resolution of VSE-15D [53] sensor is 10μ Kine. Comparing the resolution of ADC and VSE-15D sensor, the ADC performance is not good enough to match VSE-15D. The signal conditioner is used to improve this problem.

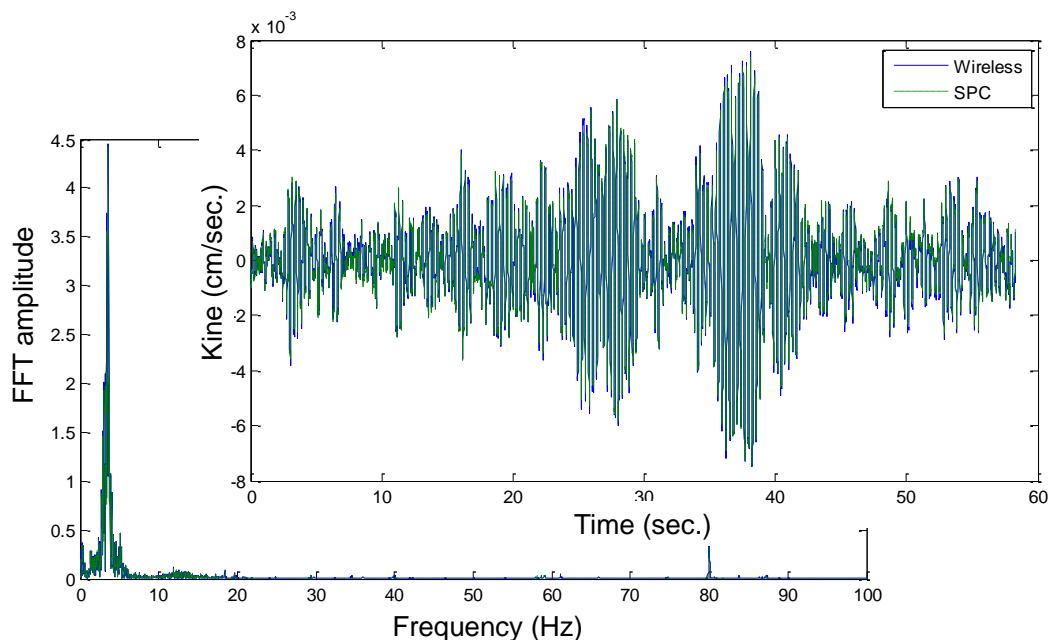


Figure 2.10. The signal verification of SPC51 and NTU-WSU

The other test is to use the data acquisition system (SPC51, Tokyo Sokushin Co., Ltd) as benchmark model to verify the NTU-WSU unit. Two VSE-15D sensors are

collocated. One is sampled by SPC51 and the other is sampled by NTU-WSU unit. The signal comparison is shown in *Figure 2.10*. Only slight difference between these two sampled signal, that they are almost the same in time domain and frequency domain. This means that the system performance is good as official system (SPC51) which includes the effects of system noise, the performance of system powering and the accuracy of ADC sampling.

2.2.2.4 System Powering Module

The purpose of powering module is to serve as a pure and accurate DC power for wireless sensing unit. Also the powering efficiency is considered in this design. The system reliability, ADC sampling noise, wireless radio performance and power supplying time are decided by the performance of powering module. The design of powering module is to enhance the system reliability, prevent system noise, improve radio performance and manage the powering efficiency.

The detail of powering module is presented in *Figure 2.11*. A rechargeable Li-Battery (7.4V / 3200mAh) is selected to be the standard power source of wireless sensing unit (NTU-WSU). There are two regulators (LP2986 Regulator_A & B) and one DC-DC converter (EC3SA-05D15) under the Li-Battery. These three chips are used to convert the power source (7.4V Li-Battery) to the system required power (5V/1W, 5V/1W and +/-15V / 3W). LP2986 Regulator_A is used to supply the power for

wireless radio; LP2986 Regulator_B is used for the main board of wireless sensing system (main component of embedded system); EC3SA-05D15 is used to supply the power of sensors and PGA204 (programmable gain amplifier).

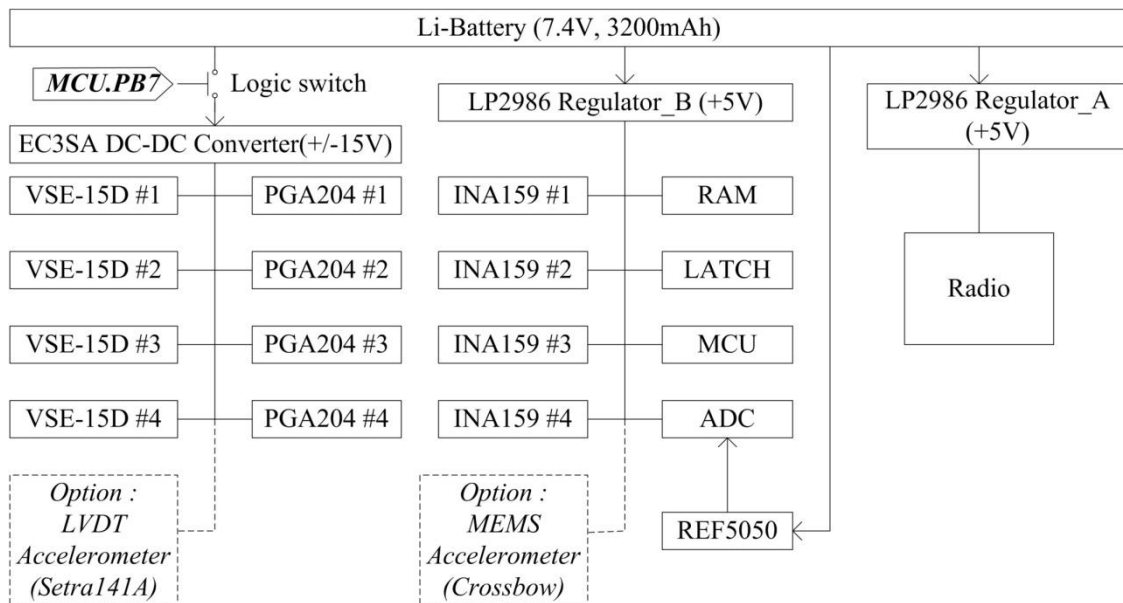


Figure 2.11: The design of powering module.

Both the wireless module and the main board of wireless sensing unit require the same powering voltage (+5V), but they are supplied by individual powering regulators. This design is considering the noise effect of radio operating, the wireless module sinks a large current at the moment of transmitting data and this large current sinking will influence the stability of power, if the sampling module shears the same source of power and this unstable power will generate a digital noise in the sampled signal. The separated powering design of wireless radio and sampling module can reduce this kind of digital noise effect. The loading capacity of LP2986 Regulator_A is 5V with 200mA

which is enough for wireless module (9XTend & 24XStream). The powering component of main board of wireless sensing unit is LP2986 Regulator_B, This regulator is used to cover the power requirements of embedded system and MEMS sensors. Actually, the embedded system consumes lightly current which is less than 40 mA and the loading capacity of LP2986 is 200mA, there is still a large residual loading capacity. The residual capacity is reserved for the sensors which are achieved by 5V power. So the wireless sensing unit reserves an extra 5V power for other expansions (ex. Crossbow accelerometers and strain gauge, etc...).

EC3SA-05D15 is a DC-to-DC converter which requires input voltage 5 ~ 9V and converts to +/-15V. A lot of high definition sensors require this power which is dual pole, low drift and low noise. But the power efficiency of EC3SA-05D15 is only about 80%, this is not good for portable device (battery powered device). A power manager is designed to improve this problem. This power manager is a digital logic switch controlled by the GPIO pin (the 7th pin of port B of ATmega128 → PB7), when MCU pulls up the voltage status of GPIO (PB7) of ATmega128, the EC3SA-05D15 is turned off to save power. Finally, an extra component under Li-Battery is REF5050, it is a precision reference voltage chip, in order to prevent the digital disturbance of embedded system, REF5050 is directly powered by Li-Battery and feedback into ADC (ADS8341EB) to be a pure and accurate 5V voltage reference.

2.2.2.5 Packaging and Specification of NTU-WSU-V02a

The main board of wireless sensing unit is a four-layer printed circuit board. This PCB is designed by optimizing the sampling noise of ADC, there are two considerations (1) a powering panel and grounding panel are used to stable powering route and grounding trace; (2) The placement is schemed with the consideration of dividing digital components and analog components to prevent the disturbances of digital and analog signal.

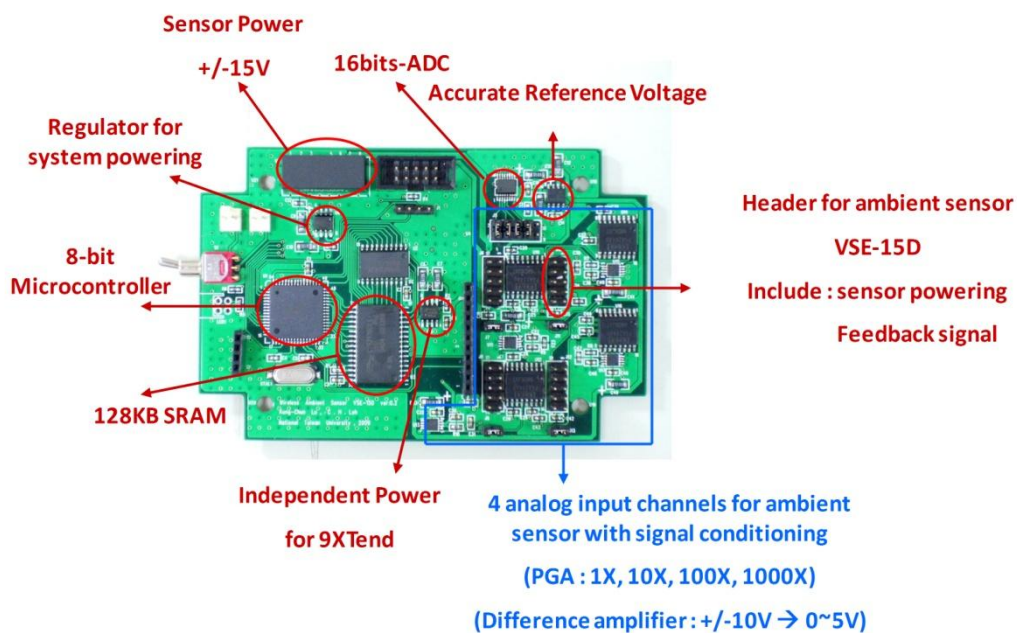


Figure 2.12a: The main board of NTU-WSU-V02a

In *Figure 2.12a*, the analog signal zone which is framed by blue line is used to place the analog and sampling circuits. Outside the analog signal zone is digital zone which is used to place embedded system and wireless module. The dimension of main board is a 117x77 mm and the wireless module is plug-in through the reserved digital

pin connection header, the main board mounted with 9XTend module is shown in **Figure 2.12b**. The housing of NTU-WSU-V02a is a plastic water weatherproof case, the picture is shown in **Figure 2.12b**. **Figure 2.12c** shows the pin definitions of NTU-WSU_V02a, the definitions of J6 (Ch0), J8 (Ch1), J10 (Ch2) and J12 (Ch3) are the same. And the overall specifications of NTU-WSU-V02a are shown in **Table 2.2**.

Table 2.2: The specifications of NTU-WSU-V02a

Specification			
Cost	About NT 7000 (\$ 215)		
Form Factor	117 X 77 X 45 mm		
Power Source	7.4V/ 3200mA Rechargeable Li battery		NT 2100
RF module	Two compatible wireless modules (see Table 2.1)		
	9XTend	24XStream	
Radio Range @ 9600bps	In door : 900 m, Out-door:22 km (64 km)	In door : 180 m, Out-door : 5 km (16 km)	(w/ high gain antenna)
Data rate	57.6 kbps	19.2 kbps	
Sampling Rate	Software Adjustable: 100/200/400 Hz		
Input signal	Software Adjustable: +/- (10V, 1V, 0.1V, 0.01V)		
Sensor power	+/-15V/ 3W (for VSE-15D, etc...), 5V/ 500mW (for accelerometer, etc...)		

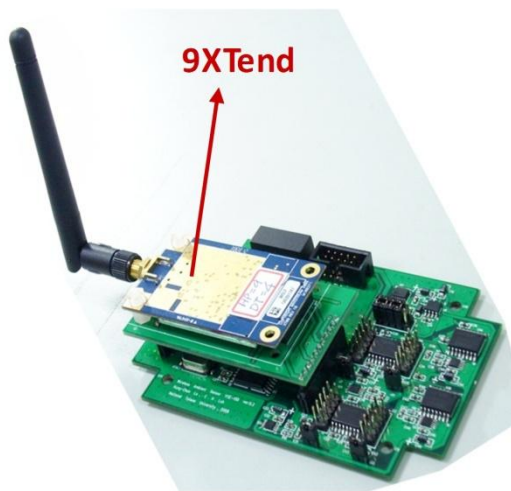


Figure 2.12b: The main board with 9XTend wireless module

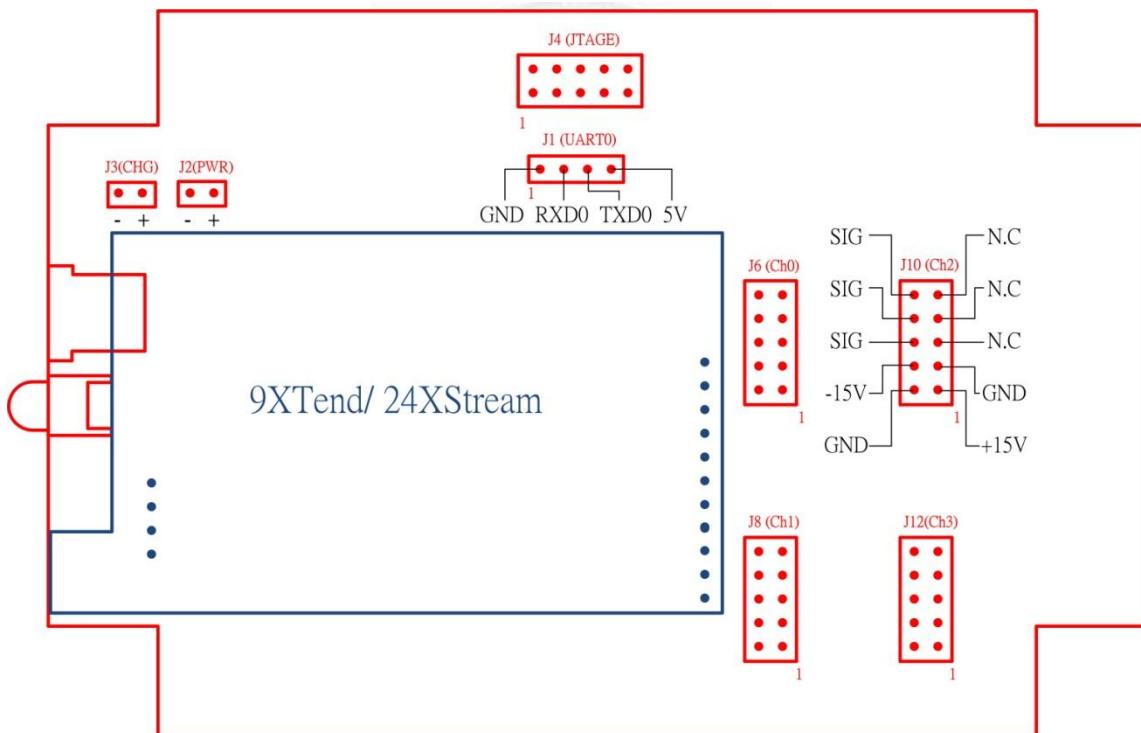


Figure 2.12c: The pin definitions of NTU-WSU_V02a

2.2.3 Host Node of Smart Sensing System (NI-cRIO w/ 3G)

There are three rules included in Host Node of Smart Sensing System; they are (1) Coordinator of wireless sensor network, (2) Analysis machine of Structural Health Monitoring, (3) Data Server of User Interface. The hardware integration of Host Node is to satisfy these three major functions and there are four components inside the Host Node; they are (1) Real-time Controller (NI cRIO-9022), (2) Wide Area Network (WAN) access modem (D-Link 3.75G Modem), (3) Wireless Sensor Network (WSN) Receiver, (4) USB Disk. **Figure 2.13** shows the hardware concept of Host Node.

Real-time Controller is the computation core of Host Node; this computation core is used to execute the embedded program of host service routine. And there are three peripherals controlled by Real-time Controller, WSN Receiver is used to communicate with wireless sensor nodes; 3.75G Modem is used to link Internet (WAN); USB Disk is used to store measurement data and analysis results.

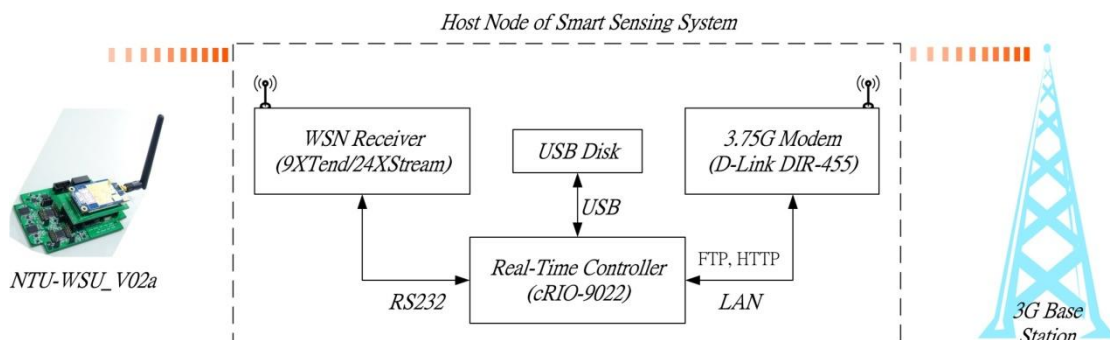


Figure 2.13: The hardware concept of Host Node

Real-time Controller (NI cRIO-9022) communicates with WSN Receiver through RS232 bus, the command and measured data are exchanged through this interface. When Real-time Controller issues a command for wireless sensor nodes, the WSN Receiver will get this command through RS232 interface and send this command through wireless radio. In the other hand, when a wireless data is received by WSN Receiver, WSN Receiver sends this data to Real-time Controller through RS232 interface.

Host Node is the data server of user interface; this means Host Node needs to exchange information with users on Internet. 3.75G Modem performs this Internet link for Host Node. Real-time Controller communicates with 3.75G Modem through 10/100BASE-T Ethernet port (RJ45 header) with embedded Web (HTTP) and file (FTP) server. Finally is USB Disk which is used to extend the storing space of Real-time Controller and they communicate through USB interface.

2.2.3.1 Real-time Controller: cRIO-9022

The purposed application scenario is to install a Host Node in the measurement environment with wireless sensor nodes and the Host Node will individually execute the pre-designed task by timing trigger or event trigger. To complete this pre-designed task, the Host Node must embedded the detail procedure of required task and execute the embedded procedure automatically. During the operating period, Real-time

Controller is required to coordinate wireless sensor nodes, store data and link Internet.

NI cRIO-9022 is the computation core (Real-time Controller) of Host Node and is used to coordinate wireless sensor network through WSN Receiver, store data on USB Disk and link Internet through 3.5G Modem. Reliable and deterministic for stand-alone control, monitoring and logging are the reasons to select cRIO-9022 as the solution of Host Node.

cRIO-9022 is an embedded real-time controller which is one of the high-performance programmable automation controller (PAC) platform. It includes an industrial real-time processor (Freescale MPC8347, 533MHz), 256MB of DDR2 RAM, 2GB of flash memory and three communication interfaces (RS232, USB and Ethernet ports). A reconfigurable chassis is used to extend optional interfaces into cRIO-9022. The specifications of NI cRIO-9022 are listed in **Table 2.3**. The picture of NI cRIO-9022 is shown in **Figure 2.14**.

Table 2.3: Specifications summary of NI cRIO-9022

Specifications	
Processor Type	533MHz Freescale MPC8347
System Memory	256MB DDR2 RAM
Nonvolatile Memory	2GB Flash
Network	Two Ethernet ports (10/100 & 10/100/1000 Mbps)
Serial Interface	RS-232 DTE Serial Port (up to 230.4 kbps)
USB Interface	Hi-speed USB host port for USB flash devices
Power Requirement	DC 9 ~ 35 V (35W) (Typical application is 7 ~ 10W)
Operating temperature	-20 ~ 55°C
Factor	77.3 x 90.2 x 88.1 mm

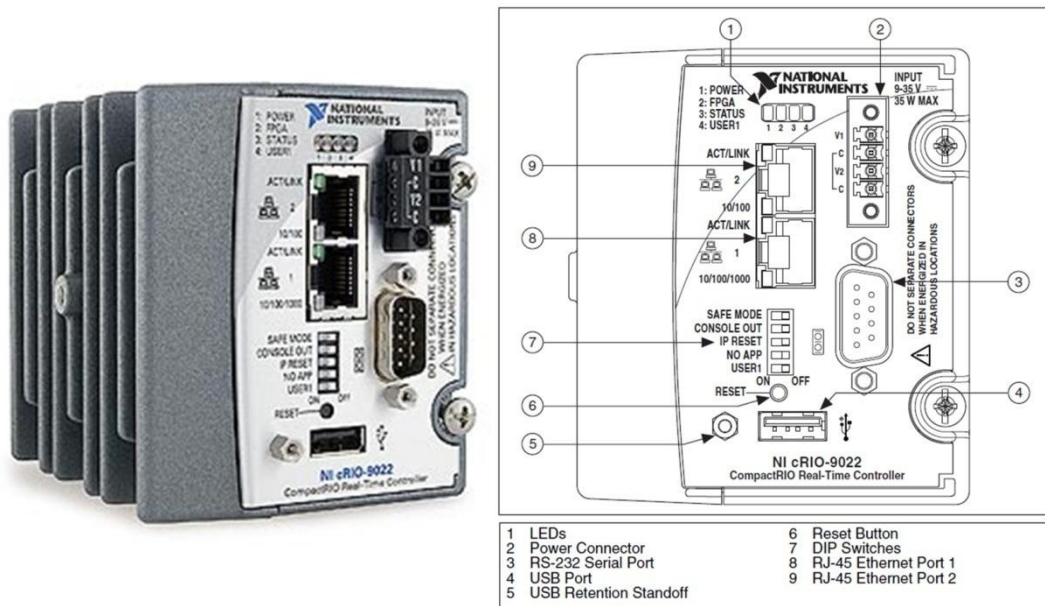


Figure 2.14: NI cRIO-9022 (<http://www.ni.com>)

2.2.3.2 Wide Area Network: 3G Mobile Router

Host Node requires Internet link to let user to access the information from Smart Sensing System. D-Link DIR-455 is selected to connect Internet and it is a 3.5G HSDPA Mobile Communication Router. A SIM card with 3G telecom service is required to plug in DIR-455 to link Internet. DIR-455 supports Dynamic Domain Name Service (DDNS) which is very important for Smart Sensing System. When a device is connecting to the Internet through 3G telecom service, a floating internet protocol (IP) address is assigned for this device. The floating IP address means that this device without a fixed address and this induces difficulty that users don't know how to get this floating address. DDNS solves this difficulty and makes user to link Smart Sensing

System easily. The picture of D-Link Dir-455 and its specification are shown in *Figure*

2.15.

Technical Specifications


GSM Band (GSM/GPRS/EDGE) <ul style="list-style-type: none">▪ 850 / 900 / 1800 / 1900 MHz▪ Power Class 4 (850 / 900 MHz)▪ Power Class 1 (1800 / 1900 MHz)	VPN <ul style="list-style-type: none">▪ L2TP/PPTP/IPSEC VPN Pass-through▪ 5 Dedicated IPsec tunnels
UMTS/HSDPA Band * <ul style="list-style-type: none">▪ 850 / 1900 / 2100 MHz▪ Power Class 3	Antenna <ul style="list-style-type: none">▪ 3 Internal antennas
Data Rates ** <ul style="list-style-type: none">▪ 6/9/11/12/18/24/36/48/54Mbps in 802.11g mode▪ 1/2/5.5/11Mbps in 802.11b mode	Ports <ul style="list-style-type: none">▪ 4 x LAN (RJ-45)▪ 1 x WAN (RJ-45)▪ 1 x Phone (RJ-11)
Standards <ul style="list-style-type: none">▪ 802.11g▪ 802.11b▪ 802.3▪ 802.3u	USIM Slot <ul style="list-style-type: none">▪ Standard 6-pin SIM card interface
Wireless Security <ul style="list-style-type: none">▪ 64/128-bit WEP (Wired Equivalent Privacy)▪ WPA & WPA2 (Wi-Fi Protected Access)	LED Status Indicators <ul style="list-style-type: none">▪ WPS▪ WAN▪ LAN▪ WLAN▪ 2G/2.5G▪ 3G/3.5G▪ SMS▪ Signal
Firewall <ul style="list-style-type: none">▪ Network Address Translation (NAT)▪ Stateful Packet Inspection (SPI)	

Figure 2.15: 3.5G Modem D-Link DIR-455, (<http://www.dlinktw.com.tw>)

The concept of DDNS is introduced on the web site (<http://www.dyndns.com>). In a word, there is a DNS server on Internet; Host Node enrolls a hostname (<http://polarbearlu.homelinux.org>) from DNS server and updates its IP address to DNS server when the address is changed. When someone want to link to Host Node with website name (<http://polarbearlu.homelinux.org>), the DNS server will converter this website name to the current IP address of Host Node.

2.2.3.3 Wireless Sensor Network: Wireless Receiver

The wireless receiver is used communicate with wireless sensor node; it includes a

wireless module (9XTend or 24XStream) and a receiver main board. The wireless module was introduced in *Section 2.2.2*. The receiver main board is used to link wireless module and computer (or cRIO-9022). In Smart Sensing System, the official receiver is selected which includes the wireless module, main board and housing. The official receiver is 9XTend-PKG RF Modem for 9XTend wireless module and 24XStream-PKG RF Modem for 24XStream wireless module.

2.3 Software Design and Arrangement of Smart Sensing System

After the system concept and hardware integration of Smart Sensing System, the software of Smart Sensing System is introduced in this section. First, the Software Framework is presented in *Section 2.3.1*, the Smart Sensing System includes Sensing Node, Server Node and User Node, the software of these nodes works together to serve the function of Smart Sensing System which is described in *Section 2.1*. Then the detail software design of these three nodes is presented in sequence.

2.3.1 Software Framework

The Smart Sensing System includes three nodes; Sensing Node, Server Node and User Node, each of these nodes are implemented on different hardware platform with individual function definitions. Sensing Node is a microcontroller (ATmega128) based embedded system, the software of Sensing Node is an embedded program which is

designed to control all peripherals of Sensing Node and is in charge of the communication between Server Node. Server Node is an embedded system with real-time controller (NI cRIO-9022); the software of Server Node includes the hosting function of wireless sensor network, the analysis of Structural Health Monitoring and the communication of Sensing Node and User Node. User Node is a computer or general digital machine which supports the software of internet tool (Internet Explorer (IE) and FTP Client). User can access the information of Smart Sensing System through these internet tools.

The detail of software framework of Smart Sensing System is shown in *Figure 2.16*. And the detail of each software design is described in the following sections.

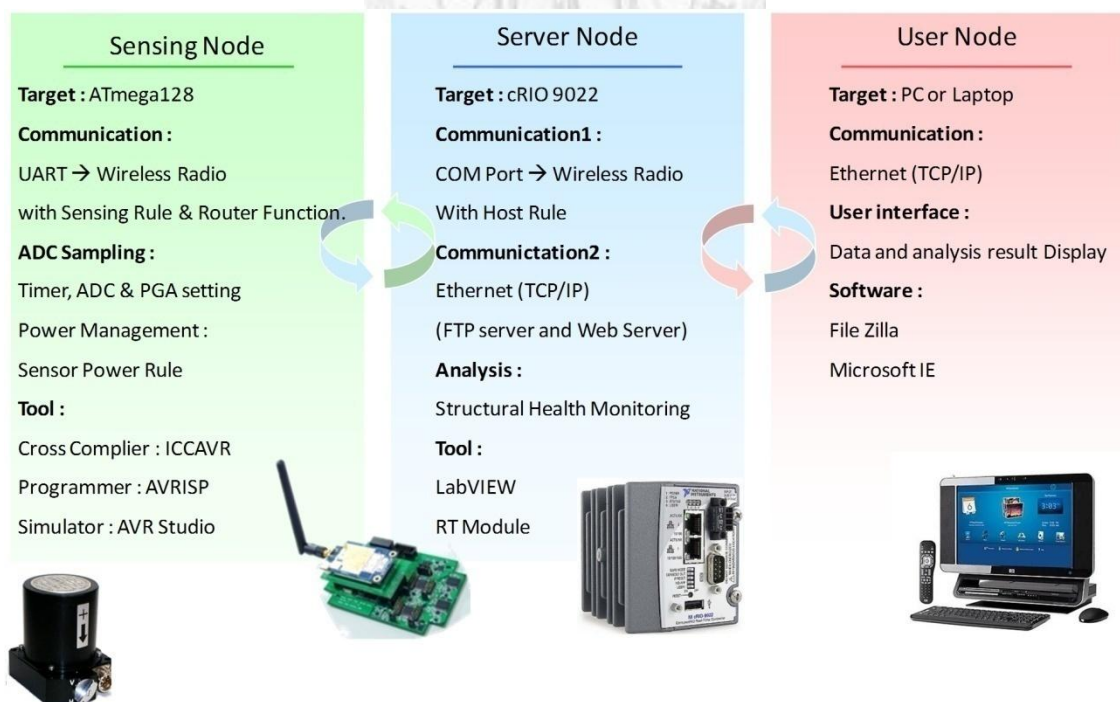


Figure 2.16: The software framework of Smart Sensing System.

2.3.2 Embedded Software of NTU-WSU

NTU-WSU is the Sensing Node of Smart Sensing System and its computation core is ATmega128 microcontroller. As shown in *Figure 2.16*, for Sensing Node, the embedded target is ATmega128 microcontroller and there are two functions included; they are communication function and ADC sampling function. In order to implement these two functions, a software architecture shown in *Figure 2.17* is applied.

There are three levels in the software architecture; they are MCU Data Bus, Math Function & Peripheral Service Routine and Application Software. The level, MCU Data Bus, is the basement of software architecture which includes the digital communication bus and timer interrupt. The middle level includes Math Function and Peripheral Service Routine, the Peripheral Service Routine is the working procedure of hardware and the Math Function includes the basic functions which are used for data pre-processing of microcontroller. The top level is Application Software which is depending on the application scenarios. Working Procedure of Smart Sensing System and Working Procedure of Damage Detection are two implemented application software of Sensing Node.

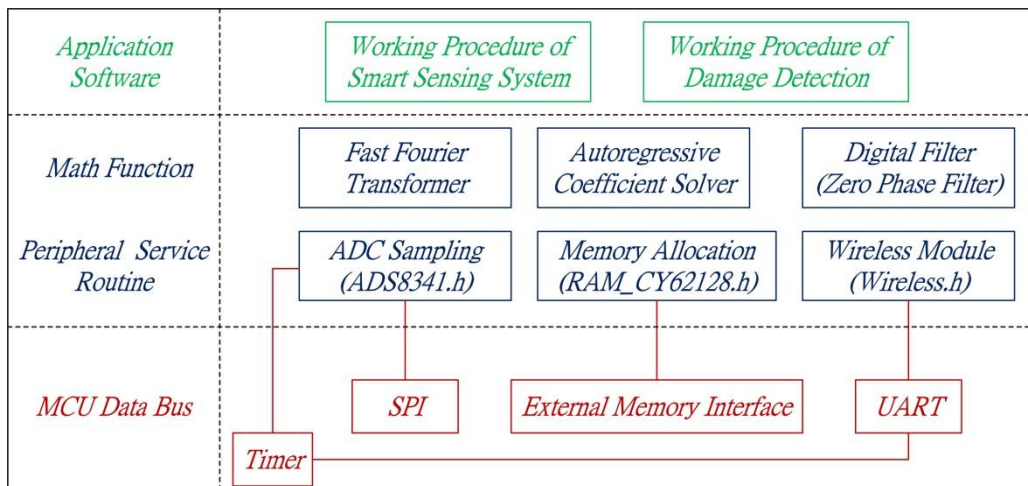


Figure 2.17: The software architecture of Sensing Node (NTU-WSU)

The hardware framework of NTU-WSU is already introduced in **Section 2.2.2**; it decides the arrangement of software architecture of NTU-WSU and is briefly described as below: The analog-to-digital converter (ADS8431EB) communicates with MCU (ATmega128) through SPI Bus; MCU controls the external SRAM (CY62128) through External Memory Interface; the wireless module (9XTend/24XStream) communicates with MCU through UART1 Bus.

Base on these hardware relationships and the software architecture which is shown in **Figure 2.17**, the hardware drivers (SPI, External Memory Interface and UART) are used to support the peripheral service routines (ADC Sampling, Memory Allocation and Wireless Module). And the timer interrupts which controls the time-out status of digital data communication and the timing of ADC Sampling is also included in MCU Data Bus. Peripheral Service Routine and Math Function are located in the middle level and

used to support the top level, Application Software. The software modules (MCU Data Bus, Peripheral Service Routine) are introduced in the following sections. Math Function of NTU-WSU is depending on the analysis requirement and its detail is not introduced here. The Application Software is introduced in the communication protocol of Smart Sensing System (*Section 2.4*).

2.3.2.1 Software Module of MCU Data Bus

The function list of embedded program of NTU-WSU is shown in *Table 2.4*. The software module of MCU Data Bus includes SPI, UART, External Memory Interface and Timer interrupt. External Memory Interface is implemented with Memory Allocation of Peripheral Service Routine and is introduced in next section; Timer Interrupt supports the functions which require timing constrain and is introduced when used. SPI and UART are introduced in this section.

As shown in *Table 2.4*, there are two subroutines in the header file of SPI (SPI.h). The [SPI_MasterInit] subroutine declares the Master SPI communication of MCU with bus frequency at 2MHz. The [SPI_MasterTransceive] subroutine sends one byte data to slave machine and get one byte data from slave machine.

Table 2.4: The function list of embedded program of NTU-WSU

Header File	Function Name
ADS8341.h	void StartA2DIntrpt(unsigned short Sampling_Freq); void StopA2DIntrpt(void); void Set_ADC_Buffer(unsigned short EVENT_TYPE, unsigned short Num_pts); void InitPGA204(unsigned short PGA_Gain);
RAM_CY62128.h	void InitExSRAM(void); void EnLowHalfExSRAM(void); void EnHighHalfExSRAM(void); void DisableExSRAM(void); void EnableExSRAM(void);
Wireless.h	void InitWireless(void); unsigned short ReceiveCMD(void); unsigned short ReceiveCMDTimeOut(unsigned short timeOutTicks); void SendCMD(unsigned short CMD_U16); unsigned char RadioNumber(void); void Timer3ADelay(unsigned short delayTicks); unsigned char HexCharToNibble(unsigned char ch); void SendData(unsigned short ptr, unsigned short size, unsigned char lowOrHighHalf); void SendWirelessByte(unsigned char byte); unsigned char ReceiveBytesVectorTimeOut(unsigned short Num_Bytes, unsigned short timeOutTicks);
UART.h	void InitUART1(unsigned char BD); void TransmitByteUART1(unsigned char data); unsigned char ReceiveByteUART1(void); unsigned char ReceiveByteUART1TimeOut(unsigned short timeOutTicks, unsigned char* timeOutFlag); void TransmitStringUART1(char* str);
SPI.h	void SPI_MasterInit(void); unsigned char SPI_MasterTransceive(unsigned char cData);

There are five subroutines in the header file of UART (UART.h). The [InitUART1] declares the UART1 of MCU with required baud rate (57.6kbps for 9XTend and

19.2kbps for 24XStream). The [TransmitByteUART1] outputs one byte data through UART1 of MCU; the [TransmitStringUART1] sends a string data which includes several bytes of data from MCU at one time. The [ReceiveByteUART1] receives one byte data into MCU through UART1; the [ReceiveByteUART1TimeOut] is like [ReceiveByteUART1] but with time limitation of receiving time and this time limitation is controlled by Timer3A (output compare channel A of timer 3). This function is used for wireless communication to prevent the communication error to hold the full working procedure of NTU-WSU.

2.3.2.2 Software Module of Peripheral Service Routine

The software module of peripheral service routine includes ADC Sampling (ADS8314.h), Memory Allocation (RAM_CY62128) and Wireless Module (Wireless.h); they are listed in *Table 2.4*.

The ADC Sampling works with SPI of MCU Data Bus, ADC receives command from MCU and feedbacks data to MCU by calling the SPI subroutines. The ADC Sampling includes four subroutines and they are introduced as below. The [StartA2DIntrpt] enables the interrupt service routine of A2D sampling with specified sampling time. This interrupt service routine is controlled by Timer1A (Compare Match A of Timer 1) and the [StopA2DIntrpt] stops this interrupt service routine. The [InitPGA204] sets the digital control pins of programmable gain amplifier (PGA204) to

adjust the amplifying gain. The [Set_ADC_Buffer] arranges the memory space to buffer the sampled data.

Memory Allocation (RAM_CY62128) includes five subroutines. Base on the hardware description of computation core that the External Memory Interface of ATmega128 is not enough to address the CY62128 (128kB) and a GPIO pin of ATmega128 is used to control the highest address pin of CY62128. The detail is shown in *Section 2.2.2.1*. This design makes the CY62128 is divided into two spaces, high half and low half and only one space can be accessed at one time. The [EnLowHalfSRAM] and [EnHighHalfSRAM] subroutines are used to select memory space to access with MCU. The [InitExSRAM] initials External Memory Interface of ATmega128. The [EnableExSRAM] and [DisableEXSRAM] control the CS (Chip Select) pin of CY62128 to enable or disable this SRAM chip.

Wireless Module includes the wireless communication protocol and the mechanism of wireless transmission. The communication protocol is shown in following section (*Section 2.4*). The basic radio operation and protocol are introduced in the datasheets of 9XTend and 24XStream Module. There are two types of wireless data bus, one is wireless command bus which is a two bytes data and presents in the format of unsigned short; another is wireless data bus which contents series bytes data arranged in a vector. Wireless Module includes twelve subroutines, as shown in *Table 2.4*. The

[ReceiveCMD] and [ReceiveCMDTimeOut] receive the issued command from Server Node, and the [SendCMD] sends a command to Server Node. The [ReceiveCMDTimeOut] receives command with time limitation by calling the subroutine [ReceiveByteUART1TimeOut] which is introduced in MCU Data Bus. The [ReceiveBytesVectorTimeOut] is the same as [ReceiveCMDTimeOut] and extends to receive a wireless data bus which is a vector constructed with specified data length (bytes). The [SendData] subroutine gets the data from external SRAM of Sensing Node and sends to Host Node.

2.3.3 Embedded Software of Host Node

NI cRIO-9022 is the Host Node of Smart Sensing System; its development environment is completely integrated in LabVIEW which is a popular graphically programming language.

The software architecture of Host Node is shown in *Figure 2.18*; there are three levels in this software. The level, LabVIEW Basement, is the foundation of software to work with hardware (cRIO-9022). VxWorks is a real-time operating system (RTOS) of cRIO-9022; NI RIO is the hardware driver of cRIO-9022; NI Real-time Module is the general real-time software package of RTOS; NI Serial RT is the hardware service routine of serial communication (RS232); NI MathScript RT is the tool to embedded MatScript code into cRIO system. The LabVIEW Basement includes system OS, system

driver and software communication protocol, engineers can develop application software under these basement in an easy and effective way.

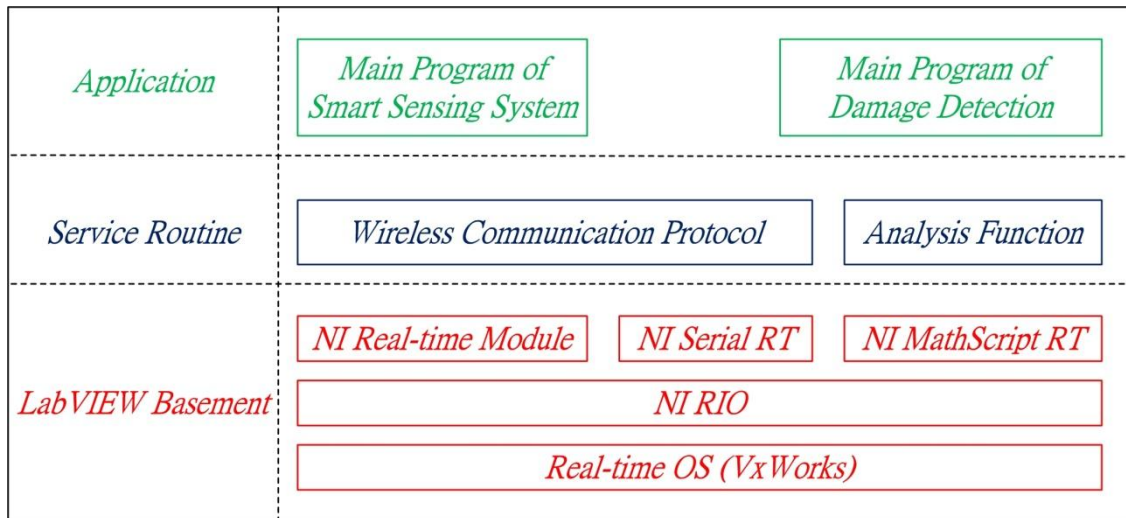


Figure 2.18: the software architecture of Host Node

The middle level is the service routine which includes Wireless Communication Protocol and Analysis Function. Wireless Communication Protocol includes the functions of wireless sensor network; Analysis Function includes the program of Autoregressive method, Fast Fourier Transform, Stochastic Subspace Identification and Damage detection method, etc.... NI MathScript RT is compatible with Matlab script, so the system developer can easily to deploy the analysis program which is in Matlab format into Host Node.

The top level is Application which is the main program of Host Node. This main program includes the servo procedures of Smart Sensing System and is introduced in **Section 2.4**. Another is Main Program of Damage Detection which is the main loop of

two stage AR-ARX damage detection and is presented in *Section 3.2.3*.

2.3.4 User Interface

There are two user interfaces of Smart Sensing System. One is the user interface of Host Node and engineer manipulates Smart Sensing System through this interface. Another is the user interface for internet user who can get information from Smart Sensing System.

The user interface of Host Node is the main page of System Control. This main page includes three functions; they are System Editor, Collecting Data and Analysis. The System Editor function includes the operation of system settings which controls the working procedure of Smart Sensing System. The Collecting Data function achieves wireless sensing network and displays the status of wireless communication. The Analysis function executes the deployed analysis and generates report. All of these operations are only available when user connects to Host Node directly. When there is no local user to control Smart Sensing System, the Smart Sensing System will work automatically according to the system settings and internet user is accepted to access this system. *Figure 2.19(a)* shows the main page; functions can be executed through the bottom pressing; *(b)* System Editor; user sets the system parameters in this page; *(c)* Collecting Data is the state machine of wireless sensing system.

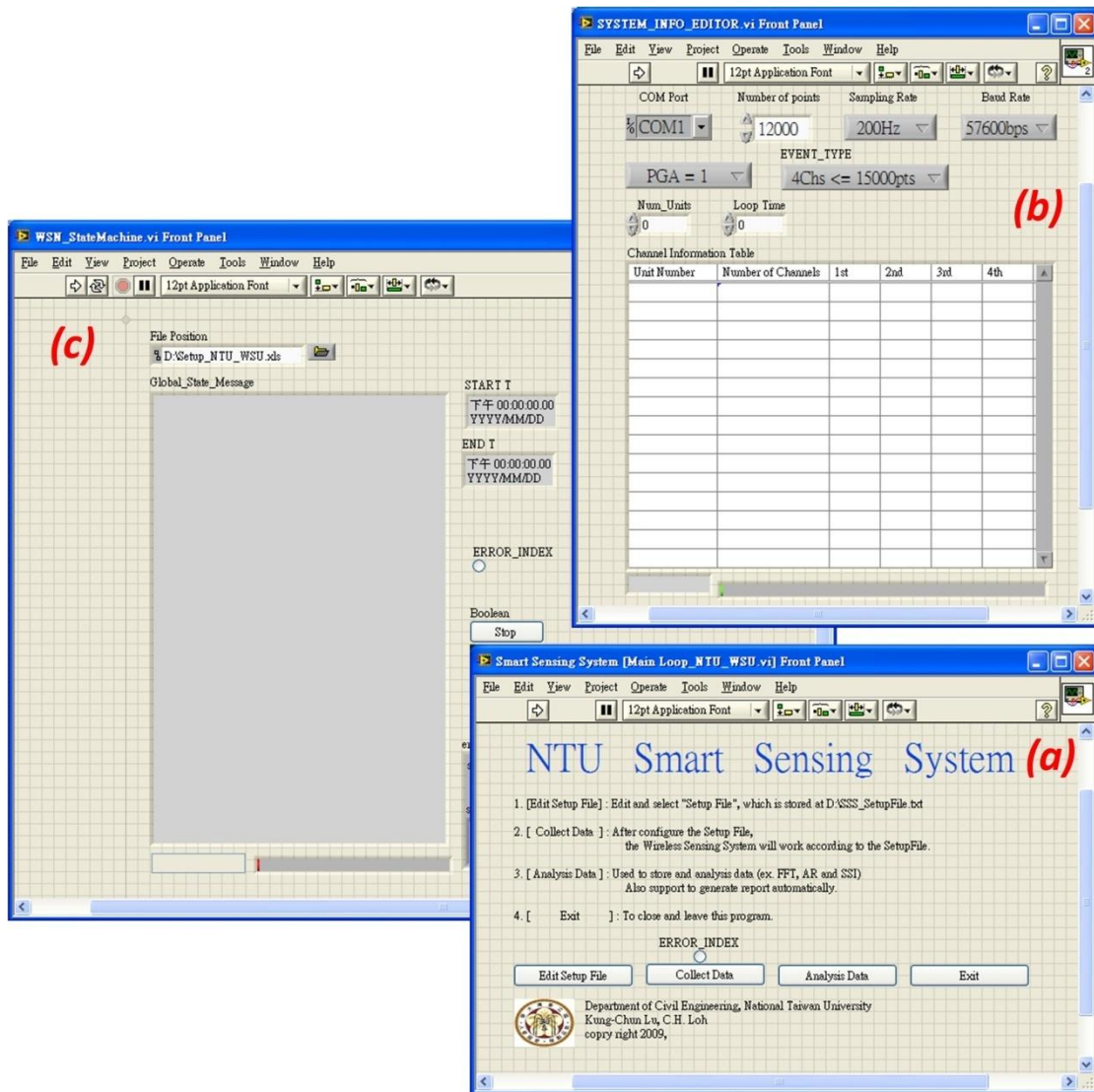


Figure 2.19: the user interface of Host Node.

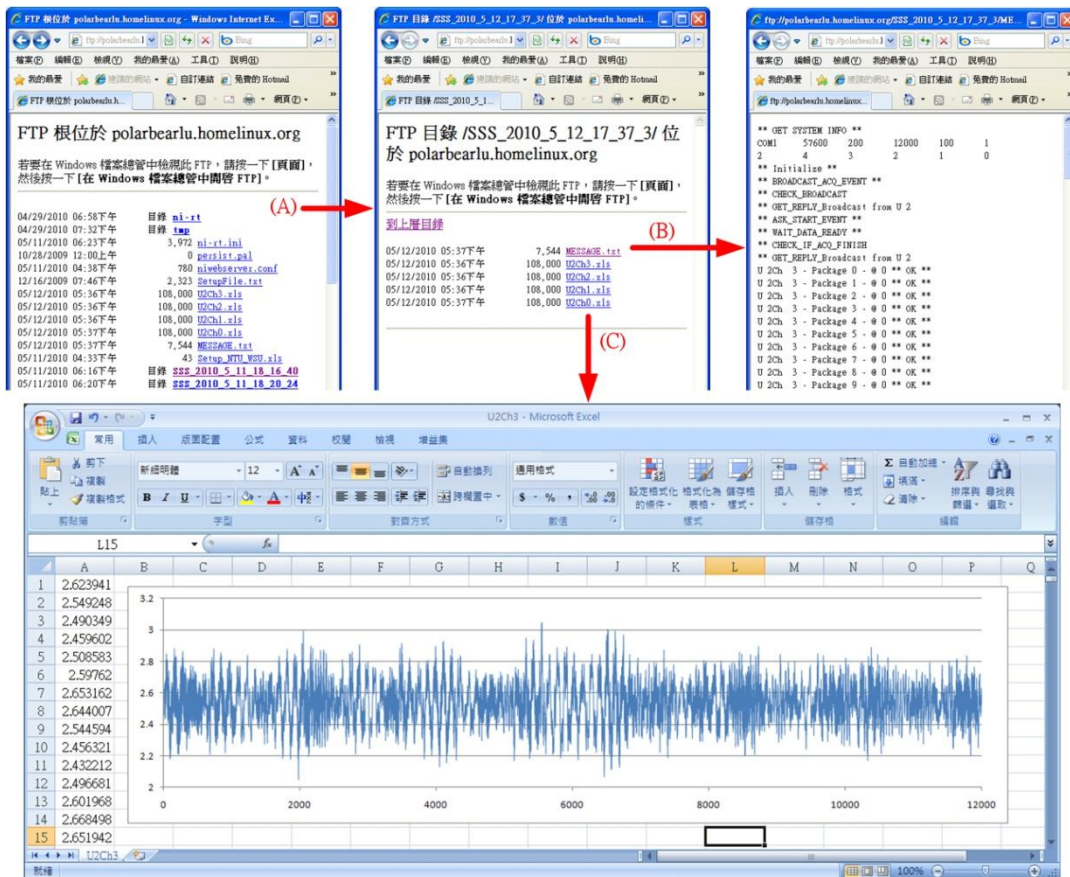


Figure 2.20: The user interface of internet user

The user interface of internet user displays and downloads the information from Smart Sensing System through Internet Explorer (IE) and File Transform Protocol (FTP). The user interface of internet user is shown in **Figure 2.20**, using the Microsoft IE with the address of Smart Sensing System (<ftp://polarbearlu.homelinux.org>), the data of Smart Sensing System is listed in IE and user can download these data or open it directly. The step (B) is to open the message of wireless sensing network and step (C) is to download the time histories and plot on MS Excel.

2.4 Communication Protocol of Smart Sensing System

The communication protocol of Smart Sensing System is the main frame of software design. The main frame of Sensing Node and Host Node is introduced here and the details of system Synchronization Protocol and Data Collecting Protocol are also introduced in the following sections.

2.4.1 The Main Frame of Sensing Node

The main frame of Sensing Node is first appeared in the section, Embedded Software of NTU-WSU (*Section 2.3.2*); “Working Procedure of Smart Sensing System” is the main frame. According to the application scenario of Smart Sensing System, Sensing Node is possible to install at the position which is far away or difficult to maintain, in this scenario the robustness of Sensing Node is very important to prevent user to maintain system at the position of Sensing Node. Another scenario is to use Smart Sensing System to measure the structural response under inclement weather, like typhoon, flood and etc..., Smart Sensing System must be installed on the structure before the inclement weather and working in inclement condition. In order to enhance the software robustness of Sensing Node, the program is an idle mode structure with implicit state machine as shown in *Figure 2.21*.

The idle mode means the main program will release hardware resources when there is no process executing. The operation of hardware release makes the system more

robust and low power. As shown in **Figure 2.21**, the center of idle modes structure is a *Receive_CMD* state, this state detects the command from Host Node. When Host Node sends a command to Sensing Node, the *Receive_CMD* state is achieved. The *Receive_CMD* state receives this command and according to the contents of command to triggers the required action states. There are seven action states around the center state (*Receive_CMD*); they are *BOOT_UP*, *REBOOT*, *GET EVENT_INFO*, *REPLY_STATE_INFO*, *START EVENT*, *REPLY PACKAGE_DATA* and *CLEAR COM*.

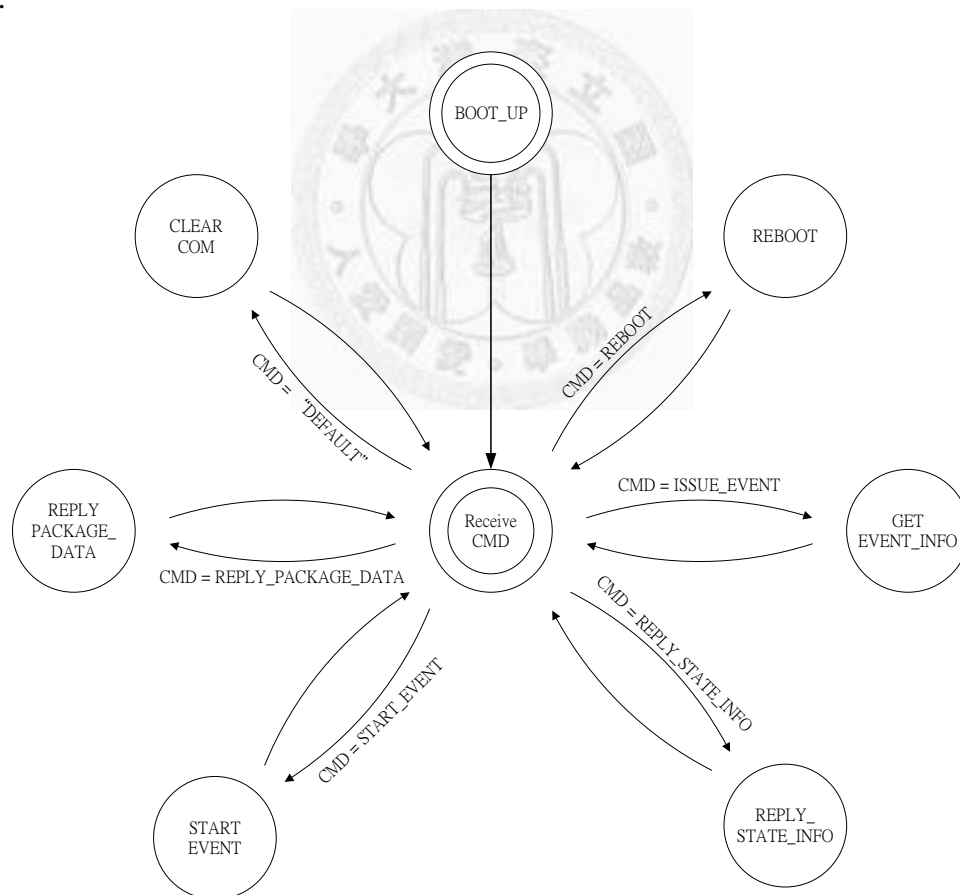


Figure 2.21: the program structure of Sensing Node

BOOT_UP is the initial state of Sensing Node; when Sensing Node is rebooting, the state is setting to *BOOT_UP*. *BOOT_UP* state enters the center state (*Receive_CMD*) of idle mode without any condition. *REBOOT* state is achieved when the state *Receive_CMD* gets a “REBOOT” command from Host Node, and this state resets all hardware peripherals and system variables. The state *GET_EVENT_INFO* receives the event information from Host Node and saves this information for the following procedures. *REPLY_STATE_INFO* replies the state information of Sensing Node to Host Node; Host Node can judge the system status by this information. *START_EVENT* triggers the event which is pre-assigned by Host Node. *REPLY_PACKAGE_DATA* replies the requested package data to Host Node; this requested package data is issued by Host Node and is a container packaged with a series of data. *CLEAR_COM* clears the buffer zone of COM port which includes the received data of RS232 communication.

The implicit state machine controls the action type of the state of idle mode. For example, if a command from Host Node to achieve the state *START_EVENT*, but the implicit state machine shows the system state is not ready to execute then *START_EVENT* does not achieve this event and replies the message that system is not ready. Both Sensing Node and Server Node are with state machine and they interplay on these two nodes. Synchronization Protocol and Data Collecting Protocol of Sensing

Node include a lot operation of implicit state machine and they are individually introduced in *Section 2.4.3* and *2.4.4*.

2.4.2 The Main Frame of Host Node

The main frame of Host Node is shown in *Figure 2.22* which is a standard state machine. The solid line shows the normal process sequence of Host Node and the dotted line shows the error procedures.

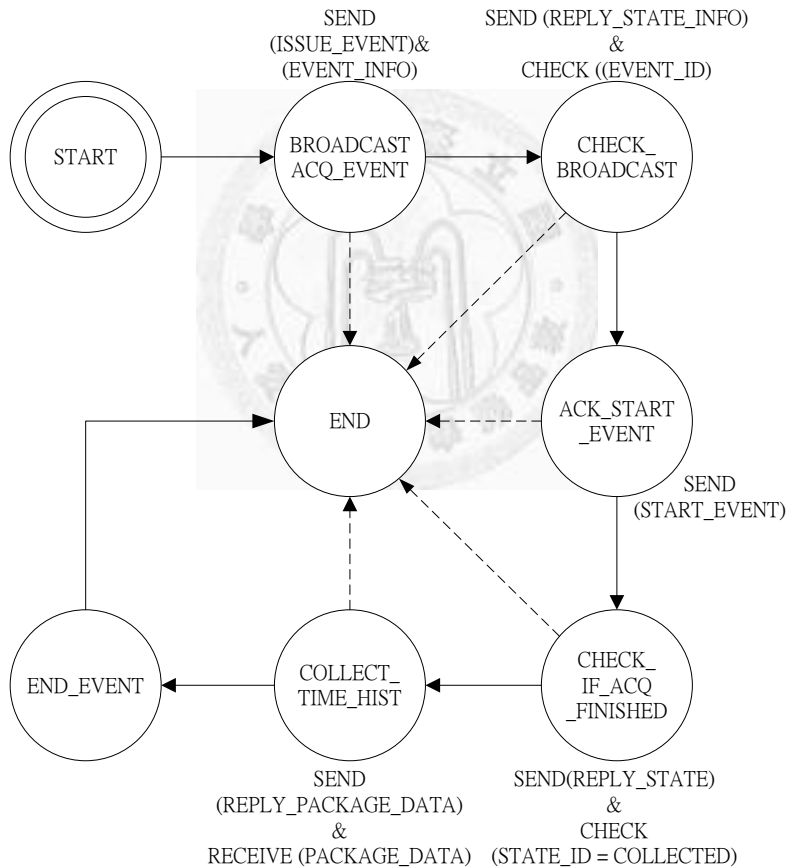


Figure 2.22: The main frame of the software of Host Node

The initial state is *START*, this is a default state of system when system is booting.

The state *START* goes to the state *BROADCAST_ACQ_EVENT* without any condition;

the state *BROADCAST_ACQ_EVENT* broadcasts the data acquisition event which includes “ISSUE_EVENT” and “EVENT_INFO” to the whole wireless sensor network. *CHECK_BROADCAST* requires Sensing Nodes to reply their current implicit state and system parameters; according this feedback information, Host Node can confirm if Sensing Node receives its broadcasted event. After the broadcasted event is confirmed, *ACK_START_EVENT* triggers Sensing Node to execute the required event. *CHECK_IF_ACQ_FINISHED* checks the status of Sensing Node; when the required event is done, Sensing Node will send a message to Host Node and the state of Host Node will go to *COLLECT_TIME_HIST* which includes the procedure to collect data from Sensing Node. Finally, when all data is collected by Host Node, the state is going to *END_EVENT* and this event is end here. During the event, the dotted line shows the error procedures and changes the state to the state *END* to stop this event. This design considers the application of Smart Sensing System to prevent the error status to hold the whole process.

2.4.3 Synchronization Protocol

The synchronization of recorded time histories is very important for mostly system identification methods. The synchronization protocol synchronizes the trigger time of Smart Sensing System to make the collected data are synchronized. The synchronization protocol is shown in *Figure 2.23*, the right side is Host Node and left side is Sensing

Node. The dotted line between Host Node and Sensing Node is wireless communication message and inside in the Sensing Node is the implicit state message.

Host Node broadcasts the event information through *BROADCAST_ACQ_EVENT*, and Sensing Node receives this message through *GET_EVENT_INFO* and changes the implicit state to “GET_ACQ_EVENT”. After the broadcasting of Host Node, Host Node confirms its broadcast through *CHECK_BROADCAST*, the Sensing Node receives this command and replies the system information through *REPLY_STATE_INFO*. Host Node checks the received system information, if the broadcasting is success then goes to *ACK_START_EVENT*, else if the broadcasting is fault then goes to the error process.

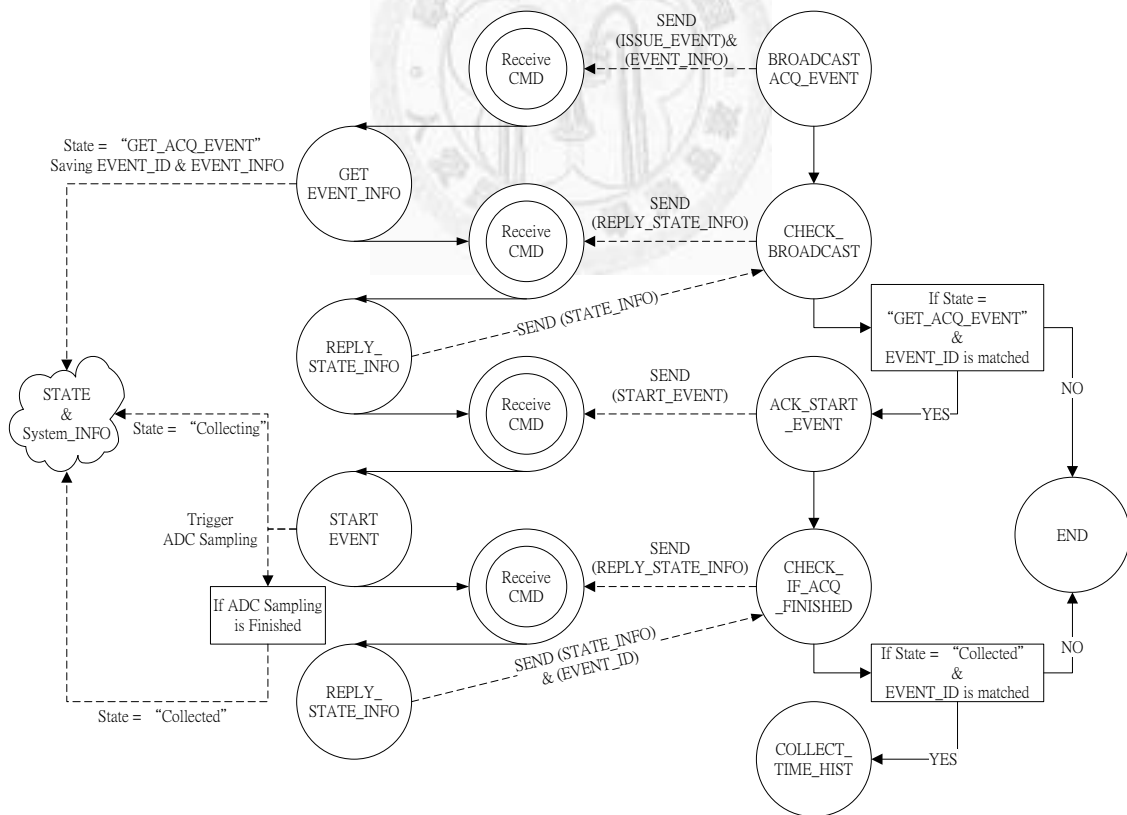


Figure 2.23: The Synchronization Protocol of Smart Sensing System

Host Node sends a synchronization message through *ACK_START_EVENT* to achieve Sensing Nodes to start the sampling at the same time. After Sensing Node receives this synchronization message, the action state goes to *START_EVENT* with time constrain and changes the implicit state to “Collecting”. After the ADC sampling is completed, the implicit state changes to “Collected”. Host Node and Sensing Node stop the radio operation to get the best quality of sampled time histories. After the sampling is finished, Host Node checks the system current state through *CHECK_IF_ACQ_FINISHED* and collects data through *COLLECT_TIME_HIST* when the system is ready to feedback data.

2.4.4 Data Collecting Protocol

The data collecting protocol collects the data from Sensing Node to Host Node after the event is finished. The data losing and error of wireless communication are considered in this protocol. The data collecting protocol is shown in *Figure 2.24*, the right side is Host Node and left side is Sensing Node. The dotted line between Host Node and Sensing Node is wireless communication message.

In this protocol, Host Node goes into *COLLECT_TIME_HIST* state and sends “PKG_NUM” and “REPLY_PACKAGE_DATA” to request data from Sensing Node. “PKG_NUM” means the number of package; “REPLY_PACKAGE_DATA” is a command for Sensing Node. Sensing Node receives these messages from Host Node

and feedbacks the required data package to Host Node. After Host Node receives the feedback package, Host Node interprets this package with three processes. First is *Check_PKG_DATA*, this process checks the status of wireless package, if the package is health then Host Node goes to the process *If_PKG_NUM=End_of_PKG*; else goes to the process *If_PKG_RETRY=MAX_RETRY*. *If_PKG_NUM=End_of_PKG* checks if all of the required packages are collected, if all packages are received then Host Node goes to *END_EVENT*; else goes back to *COLLECT_TIME_HIST* to continue collecting other packages. When package error occurs, *If_PKG_RETRY=MAX_RETRY* counts the error time of communication, if the error time arrives the limit “MAX_RETRY” then Host Node gives up this package and goes to *If_PKG_NUM=End_of_PKG*; else Host Node goes to *COLLECT_TIME_HIST* to request the same package again.

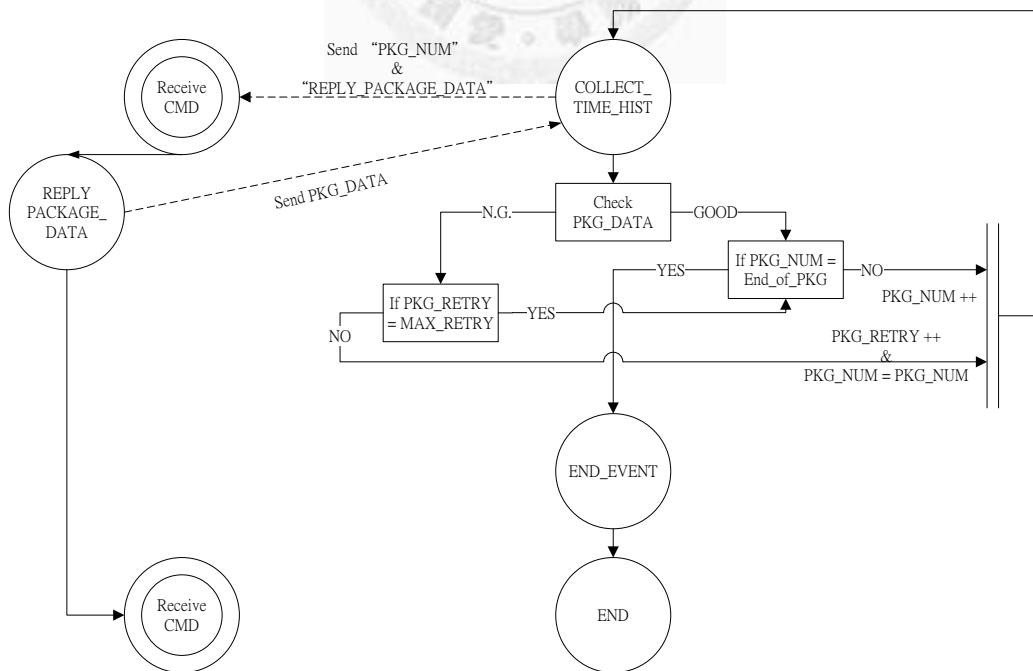


Figure 2.24: The Data Collecting Protocol of Smart Sensing System

2.5 Summary

In this chapter, both the system concept and design of Smart Sensing System are described. The system concept shows the specific description of the word “Smart” of Smart Sensing System. This chapter also provides the detail design on developing Smart Sensing System. These contents are summarized as below.

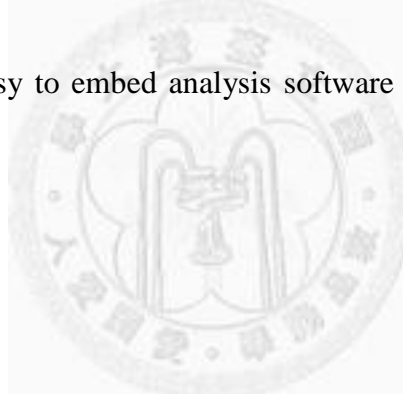
In order to reduce the cost on system installation and improve the system reliability for the application of civil engineering, Smart Sensing System provides a flexible communication through the integration of wireless sensor network and 3G mobile internet. The wireless sensor network is constructed with Digi wireless solution, two different wireless modules 9XTend and 24XStream are compatible with NTU-WSU. According to the application scenario, Smart Sensing System adopts a suitable wireless module to get the best performance on wireless communication. The techniques of 3G mobile internet and Dynamic Domain Name Service provide a communication solution between Host Node and User Node.

Through the development of new wireless sensing unit (NTU-WSU_V02a), the purposed idea to acquire structural ambient responses by wireless sensors is achieved. The noise effect, powering requirement and the difficulties of wireless communication are all considered and implemented in the design of NTU-WSU_V02a.

Two software architectures, “Idle Mode” and “Implicit State Machine”, are

implemented in the embedded software of NTU-WSU and reinforce the software robustness. The emphases of Data Collecting Protocol are on the data correctness and completeness; the mechanisms of data checking and package resending are implemented and running in this protocol. Synchronization Protocol provides a synchronization broadcasting to trigger the sampling process and makes the recorded data to be synchronized.

Smart Sensing System integrates with a real-time controller (NI cRIO-9022). cRIO provides Smart Sensing System to interface with industry standard. This integration makes the system to be easy to embed analysis software and extend the hardware on Host Node.



Chapter 3

Structural Health Monitoring and System Validation

Smart structural sensing includes both hardware and software. In *Chapter 2*, Smart Sensing System which is a hardware prototype of smart structural sensing is introduced. The software of smart structural sensing is the techniques of structural health monitoring. Several structural health monitoring methods will be introduced in *Section 3.1*. In *Section 3.2*, both the proposed hardware and software of smart structural sensing will be verified through experimental studies.

3.1 Structural Health Monitoring

In this section, four structural health monitoring methods are introduced (AR, FDD, SSI and AR-ARX damage detection). Auto-Regressive (AR) and Stochastic Subspace Identification (SSI) are time domain system identification techniques. Frequency Domain Decomposition (FDD) is frequency domain system identification technique. Finally, a time domain damage detection method, two stage AR-ARX damage detection, is introduced. The theoretical formulation of these methods will be presented in this section and their application will be in *Section 3.2*.

3.1.1 Auto-Regressive Method

For long-term structural health monitoring, the emphasis of system identification is

on the extraction of system dynamic features through the signal analyzing of structural ambient responses. Auto-Regressive method is one of the system identification methods and is suitable for this application. The basic theory formulation is as following [12]:

For SDOF system, the differential equation of SDOF system is shown as below:

$$m\ddot{y}(t) + c\dot{y}(t) + ky(t) = x(t) \quad (3.1)$$

Or (if system with proportional damping)

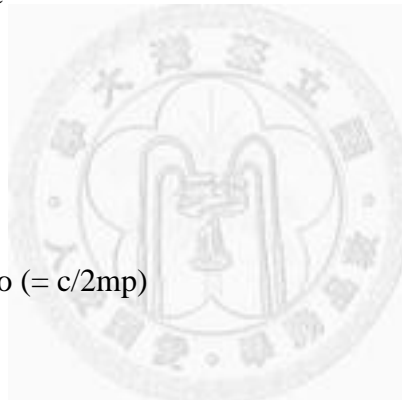
$$\ddot{y}(t) + 2\xi p\dot{y}(t) + p^2y(t) = \frac{1}{m}x(t) \quad (3.2)$$

$y(t)$ displacement

$x(t)$ input force

m mass

ξ damping ratio ($= c/2mp$)



The solution of Equation (3.2) is

$$y(t) = h(t) * x(t) \quad (3.3)$$

The symbol “*” is convolution and p_D is the damped frequency ($p_D = p\sqrt{1 - \xi^2}$). $h(t)$

is the impulse response function:

$$h(t) = \frac{1}{mp_D} e^{-p\xi t} \sin(p_D t) \quad (3.4)$$

In Z domain, Equation (3.3) can be written as below:

$$Y(z) = H(z) \cdot X(z) \quad (3.5)$$

The z domain transfer function is shown as below:

$$H(z) = Z\{T h(nT)\} = \frac{T}{m p_D} \frac{z^{-1} e^{-p \xi T} \sin(p_D T)}{1 - 2z^{-1} e^{-p \xi T} \cos(p_D T) + e^{-2p \xi T} z^{-2}} \quad (3.6)$$

The poles of $H(z)$ is a conjugate pair (z_1, z_2) , and are related to the system properties shown as below:

$$|z_1| = |z_2| = e^{-p \xi T} \quad (3.7)$$

$$\text{Arg}(z_1) = -\text{Arg}(z_2) = p_D T \quad (3.8)$$

Where T is the sampling time

To present Equation (3.6) in simplified notation:

$$H(z) = Z\{T h(nT)\} = \frac{\theta z^{-1}}{1 - \varphi_1 z^{-1} - \varphi_2 z^{-2}} \quad (3.9)$$

According to equation (3.9) taking the inverse z transform of Equation (3.5) and $T=1$,

$$y(n) - \varphi_1 y(n-1) - \varphi_2 y(n-2) = \theta x(n-1) \quad (3.10)$$

Assume the input is a white noise process (that is zero mean, independent identically distributed), multiplying both sides of Equation (3.10) by $y(n-k)$ and taking the expectations we get

$$R_y(k) - \varphi_1 R_y(k-1) - \varphi_2 R_y(k-2) = \begin{cases} \theta^2 \sigma_x^2 & k = 0 \\ 0 & k \geq 1 \end{cases} \quad (3.11)$$

Where $\sigma_x^2 = E[x^2(n)]$ is the variance of $x(n)$.

Equations (3.1) to (3.11) are the basic formulation of SDOF system with displacement measurement.

In actual application, displacement is difficult to be get; acceleration and velocity

are much easily. So the formulation of acceleration and velocity measurement is discussed as below:

The transfer functions of velocity and acceleration response are shown in Equation (3.12) and (3.13):

$$H_v(z) = \frac{T}{m} \frac{1 - [\cos(p_D T) + (\xi/\sqrt{1 - \xi^2}) \sin(p_D T)] z^{-1} e^{-p \xi T}}{1 - 2z^{-1} e^{-p \xi T} \cos(p_D T) + e^{-2p \xi T} z^{-2}} \quad (3.12)$$

$$H_a(z) = \frac{pT}{m} \frac{-2\xi + \{2\xi \cos(p_D T) + [(2\xi^2 - 1)/\sqrt{1 - \xi^2}] \sin(p_D T)\} z^{-1} e^{-p \xi T}}{1 - 2z^{-1} e^{-p \xi T} \cos(p_D T) + e^{-2p \xi T} z^{-2}} \quad (3.13)$$

By comparing Equations (3.6, 3.12, and 3.13), their denominators are the same.

This is reasonable that the system poles are consistent and not changed by different measurement. So the basic formulations are also worked with acceleration and velocity responses.

For MDOF system, any response $y(t)$ is linear related to the normal coordinates and shown as follows.

$$y(t) = \sum_{m=1}^M B_m y_m(t) \quad (3.14)$$

Where B_m is modal coefficient of m^{th} mode and $m=1,2,\dots,M$. $y_m(t)$ is modal response of m^{th} mode.

For the case when $y(t)$ is displacement response, the z-domain transfer function is shown as below.

$$H(z) = \sum_{m=1}^M \frac{B_m \theta z^{-1}}{1 - \varphi_{1m} z^{-1} - \varphi_{2m} z^{-2}} = \frac{A(z^{-1})}{\prod_{m=1}^M (1 - \varphi_{1m} z^{-1} - \varphi_{2m} z^{-2})} \quad (3.15)$$

$$= \frac{Y(z)}{X(z)}$$

In the above equation $A(z^{-1})$ is a polynomial of order $2M-1$, the denominator is an order of $2M$. The input-output difference equation can be obtained by taking the inverse z -transform of both side of Equation (3.15) to get

$$y(n) - \varphi_1 y(n-1) - \dots - \varphi_{2M} y(n-2M)$$

$$= \alpha_1 x(n-1) + \dots + \alpha_{2M-1} x(n-2M+1) \quad (3.16)$$

Multiplying both sides of this equation by $y(n-k)$ and taking expectations for $k \geq 2M$ we have

$$R_y(k) - \varphi_1 R_y(k-1) - \dots - \varphi_{2M} R_y(k-2M) = 0 \quad (3.17)$$

which is the difference equation of the response autocorrelation function given that the forcing function is a white noise process. For ambient vibration survey, this is a correct assumption. The estimated autocorrelation function is defined as:

$$\hat{R}_y(k) = \frac{1}{N} \sum_{n=k}^N y(n)y(n-k) \quad (3.18)$$

A least squares estimate of the coefficient vector $\hat{\Phi}$ becomes

$$\hat{\Phi} = (\mathbf{X}^T \mathbf{X})^{-1} \mathbf{X}^T \mathbf{Y} \quad (3.19)$$

Where

$$\hat{\Phi}^T = [\varphi_1 \quad \dots \quad \varphi_{2M}] \text{ and } \mathbf{Y}^T = [\hat{R}_y(2M) \quad \dots \quad \hat{R}_y(k_{\max})] \quad (3.20a)$$

And

$$\mathbf{X} = \begin{bmatrix} \widehat{R}_y(2M-1) & \widehat{R}_y(2M-2) & \cdots & \widehat{R}_y(0) \\ \widehat{R}_y(2M) & \widehat{R}_y(2M-1) & \cdots & \widehat{R}_y(1) \\ \vdots & \vdots & \ddots & \vdots \\ \widehat{R}_y(k_{\max}-1) & \widehat{R}_y(k_{\max}-2) & \cdots & \widehat{R}_y(k_{\max}-2M) \end{bmatrix} \quad (3.20b)$$

By taking z-transform of the correlation equation, the complex roots of the characteristics equation will provide necessary information for the estimation of the modal frequencies and damping. Since all the coefficients of the characteristics equation are real, the roots will appear as complex conjugate pairs corresponding to one of the M observed modes. The modal frequencies and damping ratios can be calculated by Equation (3.7) and (3.8).

$$p_D = \frac{\text{Arg}(z_1)}{T} = \frac{\tan^{-1}\left(\frac{\text{Im}(Z_1)}{\text{Re}(Z_1)}\right)}{T} \quad (3.21a)$$

$$\xi = \frac{\ln\left(\frac{1}{|z_1|}\right)}{\sqrt{\left(\tan^{-1}\left(\frac{\text{Im}(Z_1)}{\text{Re}(Z_1)}\right)\right)^2 + \left(\ln\left(\frac{1}{|z_1|}\right)\right)^2}} \quad (3.21b)$$

The above formulation is for system with proportional damping; the non-proportional damping is discussed by Safak, E. etc. [13].

3.1.2 Frequency Domain Decomposition (FDD) Method

Frequency Domain Decomposition Method [16] is introduced as below. The relationship between the unknown inputs $x(t)$ and the measured responses $y(t)$ can be expressed as [54]

$$\mathbf{G}_{yy}(j\omega) = \bar{\mathbf{H}}(j\omega)\mathbf{G}_{xx}(j\omega)\mathbf{H}(j\omega)^T \quad (3.22)$$

where $\mathbf{G}_{xx}(j\omega)$ is the $(r \times r)$ power spectral density (PSD) matrix of the input, r is the number of inputs, $\mathbf{G}_{yy}(j\omega)$ is the $(m \times m)$ PSD matrix of the responses, m is the number of responses, $\mathbf{H}(j\omega)$ is the $(m \times r)$ frequency response function (FRF) matrix and the overbar and superscript T denote the complex conjugate and transpose, respectively. The FRF can be written in partial fraction, i.e. pole/residue, form

$$\mathbf{H}(j\omega) = \sum_{k=1}^n \frac{\mathbf{R}_k}{j\omega - \lambda_k} + \frac{\bar{\mathbf{R}}_k}{j\omega - \bar{\lambda}_k} \quad (3.23)$$

where n is the number of modes, λ_k is the pole and \mathbf{R}_k is the residue.

$$\mathbf{R}_k = \boldsymbol{\phi}_k \boldsymbol{\gamma}_k^T \quad (3.24)$$

$$\lambda_k = -\alpha_k + j\omega_k \quad (3.25)$$

where $\boldsymbol{\phi}_k$ and $\boldsymbol{\gamma}_k$ are the mode shape vector and the modal participation vector.

In order to simplify Equation (3.22), an assumption of white noise input is required,

i.e. $\mathbf{G}_{xx}(j\omega) = \mathbf{C}$, then Equation (3.22) becomes

$$\begin{aligned} \mathbf{G}_{yy}(j\omega) &= \bar{\mathbf{H}}(j\omega)\mathbf{C}\mathbf{H}(j\omega)^T \\ &= \sum_{k=1}^n \sum_{s=1}^n \left[\frac{\mathbf{R}_k}{j\omega - \lambda_k} + \frac{\bar{\mathbf{R}}_k}{j\omega - \bar{\lambda}_k} \right] \mathbf{C} \left[\frac{\mathbf{R}_s}{j\omega - \lambda_s} + \frac{\bar{\mathbf{R}}_s}{j\omega - \bar{\lambda}_s} \right]^H \end{aligned} \quad (3.26)$$

where superscript H denotes a complex conjugate and transpose. Applying Heaviside partial fraction theorem and mathematical manipulation, the output PSD can be reduced to a pole/residue form as follows

$$\mathbf{G}_{yy}(j\omega) = \sum_{k=1}^n \left[\frac{\mathbf{A}_k}{j\omega - \lambda_k} + \frac{\bar{\mathbf{A}}_k}{j\omega - \bar{\lambda}_k} + \frac{\mathbf{B}_k}{-j\omega - \lambda_k} + \frac{\bar{\mathbf{B}}_k}{-j\omega - \bar{\lambda}_k} \right] \quad (3.27)$$

In the case of a lightly damped structure, at a certain frequency ω only a limited number of modes will contribute significantly; let this set of modes be denoted by $\text{Sub}(\omega)$. The response spectral density can always be written

$$\mathbf{G}_{yy}(j\omega) = \sum_{k \in \text{Sub}(\omega)} \frac{\mathbf{d}_k \boldsymbol{\phi}_k \boldsymbol{\phi}_k^T}{j\omega - \lambda_k} + \frac{\bar{\mathbf{d}}_k \bar{\boldsymbol{\phi}}_k \bar{\boldsymbol{\phi}}_k^T}{j\omega - \bar{\lambda}_k} \quad (3.28)$$

In the FDD identification, the first step is to estimate the PSD matrix. The estimate of the output PSD $\hat{\mathbf{G}}_{yy}(j\omega)$ known at discrete frequencies $\omega = \omega_i$ is then decomposed by taking the SVD of the matrix

$$\hat{\mathbf{G}}_{yy}(j\omega_i) = \mathbf{U}_i \mathbf{S}_i \mathbf{U}_i^H \quad (3.29)$$

where the matrix $\mathbf{U}_i = [\mathbf{u}_{i1} \quad \mathbf{u}_{i2} \quad \cdots \quad \mathbf{u}_{im}]$ is a unitary matrix holding the singular vectors \mathbf{u}_{ij} , and \mathbf{S}_i is a diagonal matrix holding the scalar singular values s_{ij} . Near a peak corresponding to the k^{th} mode in the spectrum this mode, or maybe a possible close mode, will be dominating. If only the k^{th} mode is dominating there will only be one term in Equation (3.29). Thus, in this case, the first singular vector \mathbf{u}_{i1} is an estimate of the mode shape

$$\hat{\boldsymbol{\phi}} = \mathbf{u}_{i1} \quad (3.30)$$

and the corresponding singular value is the auto-PSD function of the corresponding SDOF system. This PSD function is identified around the peak by comparing the mode shape estimate $\hat{\boldsymbol{\phi}}$ with the singular vectors for the frequency lines around the peak. As long as a singular vector is found that has a high modal assurance criterion (MAC)

value with φ , the corresponding singular value belongs to the SDOF density function.

Modal damping can also be estimated by FDD [55]. From the identified auto-PSD function (\mathbf{S}), the natural frequency and damping are obtained by taking the spectral density function back to time domain by inverse FFT. The damping can be estimated by the logarithmic decrement which is from free decay time domain function of auto-correlation function of the SDOF system, the natural frequency is found by estimating crossing times.

Logarithmic decrement is shown as below

$$\delta = \frac{2}{k} \ln \left(\frac{r_0}{|r_k|} \right) \quad (3.31)$$

where r_0 is the initial value of correlation function and r_k is the k^{th} extreme.

The damping ratio is given by

$$\zeta = \frac{\delta}{\sqrt{\delta^2 + 4\pi^2}} \quad (3.32)$$

To implement the FDD method, some prior knowledge of the modal frequencies is required. Peak picking and crossing time methods are difficult to be automated process. In our procedure, it is important to note that the least square AR method must be applied first to identify the model parameters of the structure. Based on the identified model frequencies from statistical analysis, the FDD can be applied to extract the model shape at that particular model frequency.

3.1.3 Stochastic Subspace Identification (SSI) Method

Recently, Weng et al. [18] applied the subspace identification method to structural health monitoring and damage detection. The Stochastic Subspace Identification method is an output-only method with the assumption of white noise input. The basic formulation is described as below:

Consider a discrete-time stochastic state-space model:

$$\begin{aligned}\mathbf{x}_{k+1}^s &= \mathbf{A}\mathbf{x}_k^s + \mathbf{w}_k \\ \mathbf{y}_k^s &= \mathbf{C}\mathbf{x}_k^s + \mathbf{v}_k\end{aligned}\quad (3.33)$$

where the superscript “s” denoting “stochastic” since the system is assumed to be excited by a stochastic component (i.e. broad-band noise). The SSI method is used to identify the system matrices, \mathbf{A} and \mathbf{C} , from the system output measurements, \mathbf{y}_k^s (i.e. ambient vibration measurements). The procedure of SSI method is shown as below:

1. Using output measurement data, the Hankel matrix, \mathbf{Y}^s , can be constructed:

$$\mathbf{Y}^s \equiv \begin{bmatrix} y_0^s & y_1^s & \cdots & y_{j-1}^s \\ y_1^s & y_2^s & \cdots & y_j^s \\ \vdots & \vdots & \ddots & \vdots \\ y_{i-1}^s & y_i^s & \cdots & y_{i+j-2}^s \\ y_i^s & y_{i+1}^s & \cdots & y_{i+j-1}^s \\ y_{i+1}^s & y_{i+2}^s & \cdots & y_{i+j}^s \\ \vdots & \vdots & \ddots & \vdots \\ y_{2i-1}^s & y_{2i}^s & \cdots & y_{2i+j-2}^s \end{bmatrix} \equiv \begin{bmatrix} \mathbf{Y}_p^s \\ \mathbf{Y}_f^s \end{bmatrix} \in \mathbb{R}^{2li \times j} \quad (3.34)$$

where i is a user-defined index and must be larger than the order, n , of the system.

Since there are only 1 degrees-of-freedom measured, the output vector \mathbf{y}_k^s must

contain l rows and the matrix \mathbf{Y}^s must contain $2li$ rows. Here, j corresponds to the number of columns of the Hankel matrix. To ensure all of the r time samples of the output vector \mathbf{y}_k^s populate the Hankel matrix, the number j can be equal to $(r - 2i + 1)$. According to the expression of Equation (3.34), the Hankel matrix is divided into the past, $\mathbf{Y}_p^s \in \mathbb{R}^{li \times j}$, and the future, $\mathbf{Y}_f^s \in \mathbb{R}^{li \times j}$, parts. For the reference-based stochastic subspace identification method, the Hankel matrix plays a critically important role in the SSI algorithm.

2. Row Space Projections:

The orthogonal projection of the row space of the matrix $\mathbf{Y}_f^s \in \mathbb{R}^{li \times j}$ on the row space of the matrix $\mathbf{Y}_p^s \in \mathbb{R}^{li \times j}$ is defined as $\mathbf{Y}_f^s / \mathbf{Y}_p^s$ which can be calculated by the following formula:

$$\mathbf{Y}_f^s / \mathbf{Y}_p^s \equiv \mathbf{Y}_f^s \mathbf{Y}_p^{sT} (\mathbf{Y}_p^s \mathbf{Y}_p^{sT})^\dagger \mathbf{Y}_p^s = \mathbf{O}_i^s \in \mathbb{R}^{li \times j} \quad (3.35)$$

where “ / ” denotes the projection operator, T denotes the transpose operator and

† denotes the pseudo-inverse operator. The projection operator can also be computed quickly by using QR-decomposition. QR-decomposition of the block Hankel matrix ($\mathbf{H} = \mathbf{R}\mathbf{Q}^T$) results in a reduction of the computational complexity and memory requirements of the SSI implementation by projecting the row space of future outputs into the row space of the past reference outputs. Orthogonal projection relates the Hankel matrix to the observability matrix; hence, the observability matrix can be

estimated by factoring the orthogonal projection of the Hankel matrix.

3. Singular value decomposition (SVD) of the orthogonal projection:

In linear algebra, SVD is an important factorization tool used for rectangular real or complex matrices. SVD is used to decompose the orthogonal projection of the Hankel matrix:

$$\mathbf{O}_i^s = \mathbf{USV}^T = (\mathbf{U}_1 \quad \mathbf{U}_2) \begin{pmatrix} \mathbf{S}_1 & 0 \\ 0 & \mathbf{S}_2 \end{pmatrix} \begin{pmatrix} \mathbf{V}_1^T \\ \mathbf{V}_2^T \end{pmatrix} \approx \mathbf{U}_1 \mathbf{S}_1 \mathbf{V}_1^T \quad (3.36)$$

The matrix $\mathbf{U} \in \mathbb{R}^{li \times li}$ contains a set of orthonormal “output” basis vector directions for

\mathbf{O}_i^s while $\mathbf{V} \in \mathbb{R}^{j \times j}$ contains a set of orthonormal “input” basis vector directions for \mathbf{O}_i^s .

The matrix $\mathbf{S} \in \mathbb{R}^{li \times j}$ contains singular values of the decomposition along its diagonal;

here, \mathbf{S} is block separated into two parts \mathbf{S}_1 and \mathbf{S}_2 . The smallest singular values in

the matrix \mathbf{S} are grouped as $\mathbf{S}_2 \in \mathbb{R}^{(li-n) \times (j-n)}$ and are neglected. In contrast, the

largest set of singular values, \mathbf{S}_1 , dominate the system and provide a means of

assessing the system order. The order, n , is the number of dominant singular values

where $\mathbf{S}_1 \in \mathbb{R}^{n \times n}$. Thus a reduced version of the SVD is described by the matrices

$\mathbf{U}_1 \in \mathbb{R}^{li \times n}$, $\mathbf{S}_1 \in \mathbb{R}^{n \times n}$ and $\mathbf{V}_1 \in \mathbb{R}^{j \times n}$. A reduced SVD helps to catch the principle

components of the system and reduce noise effects.

4. Calculate the extended observability matrix, Γ_i :

$$\Gamma_i = \mathbf{U}_1 \mathbf{S}_1^{1/2} \quad (3.37)$$

Since the dimension of Γ_i in Equation (3.37) is $(li \times n)$, it can be extracted from the reduced order SVD of the orthogonal projection as described above. The extended observability matrix Γ_i is defined as:

$$\Gamma_i = \begin{bmatrix} \mathbf{C} \\ \mathbf{CA} \\ \mathbf{CA}^2 \\ \vdots \\ \mathbf{CA}^{i-1} \end{bmatrix} \in \mathbb{R}^{li \times n} \quad (3.38)$$

which contains information on the system matrix, \mathbf{A} .

5. Calculate the system parameter matrices \mathbf{A} and \mathbf{C} from Γ_i :

$$\mathbf{A} = \underline{\Gamma}_i^\dagger \overline{\Gamma}_i \quad (3.39)$$

where $\underline{\Gamma}_i \in \mathbb{R}^{l(i-1) \times n}$ denotes Γ_i without the last l rows and $\overline{\Gamma}_i \in \mathbb{R}^{l(i-1) \times n}$ denotes Γ_i without the first l rows. The matrix \mathbf{C} can be determined from the first l rows of Γ_i as shown in equation (3.38).

6. Calculate the eigenvalues, λ_N , and eigenvectors, $\phi_{\lambda_N} \in \mathbb{R}^{n \times 1}$, of \mathbf{A} :

$$\det(\mathbf{A} - \lambda_N \mathbf{I}) = 0, (\mathbf{A} - \lambda_N \mathbf{I})\phi_{\lambda_N} = 0 \quad (3.40)$$

It should be noted that the eigenvalues of \mathbf{A} occur in complex conjugated pairs and the subscript “N” denotes the number of these pairs.

7. Determine the frequency ω_N and damping coefficient ξ_N from λ_N :

$$\omega_N = \frac{a_N}{\Delta t}, \xi_N = \frac{|b_N|}{\sqrt{a_N^2 + b_N^2}} \quad (3.41)$$

Where

$$a_N = \left| \tan^{-1} \left(\frac{\text{Im}(\lambda_N)}{\text{Re}(\lambda_N)} \right) \right|, b_N = \ln(\lambda_N) \quad (3.42)$$

8. Determine mode shapes Φ_N (with corresponding frequency ω_N) from C and

ϕ_{λ_N} :

$$\Phi_N = C\phi_{\lambda_N} \quad (3.43)$$

The elements in the vector, Φ_N , are always complex numbers in practice. It can be imagined that the absolute value of the complex number is interpreted as the amplitude and the argument as the phase of a sine wave at a given frequency, ω_N .

In the SSI method, first, the output data collected from the ambient vibration survey is arranged to form the Hankel matrix. Second, the projection theorem is introduced to establish the relation between the extended observability matrix and the matrix corresponding to the orthogonal projection. Finally, the SVD algorithm is used to determine the system matrix, A , from which the dynamic characteristics (Φ_N, ω_N, ξ_N) of the system can be identified.

3.1.4 Two Stages AR-ARX Damage Detection Method

A procedure based on the time series analysis of vibration signals for damage detection and localization within a mechanical system had been developed by Sohn et al.

[30]. In this method the standard deviation of the residual error, which is the difference between the actual measurement and the prediction derived from a combination of the AR and ARX models, is used as the damage-sensitive feature to locate damage. This approach is easy to be implemented in microcontroller of embedded system to detect the structural damage at different stage. This method is described as below.

As proposed by Sohn, et al.[29], the AR-ARX model is implemented for damage diagnosis problems. First, AR models are constructed for a reference signal $x(t)$ and a new signal $y(t)$:

$$x(t) = \sum_{j=1}^p \phi_{xj}x(t-j) + e_x(t) \quad (3.35a)$$

$$y(t) = \sum_{j=1}^p \phi_{yj}y(t-j) + e_y(t) \quad (3.35b)$$

Then, an ARX model is formed with $x(t)$ as output and $e_x(t)$ as input:

$$x(t) = \sum_{i=1}^a \alpha_i x(t-i) + \sum_{j=1}^b \beta_j e_x(t-j) + \varepsilon_x(t) \quad (3.36)$$

Then α_i and β_j are used to reproduce the output and input relationship between $y(t)$ and $e_y(t)$:

$$\varepsilon_y(t) = y(t) - \sum_{i=1}^a \alpha_i y(t-i) + \sum_{j=1}^b \beta_j e_y(t-j) \quad (3.37)$$

The coefficients α_i and β_j are associated with the reference signal $x(t)$ and are obtained from equation (3.36). Therefore, if the ARX model, obtained from $x(t)$ and

$e_x(t)$, were not a good representative of the $y(t)$ and $e_y(t)$ pair, there would be a significant change in the probability distribution of the residual error $\varepsilon_y(t)$ associated with the new signal $y(t)$. Finally, the residual error $\varepsilon_y(t)$ is a damage sensitive feature, and the damage can be identified by comparing the residual error of damaged case and referenced case.

Equations (3.35) ~ (3.37) are the basic formulation of AR-ARX method, for real-world implementation and application, the analysis procedure is introduced as below.

First, before the damage diagnosis, a reference data base is required. Preparing several reference time histories and using Equation (3.35a) to establish reference data base which includes the AR coefficients ϕ_{xj} and residual error $e_x(t)$.

After the reference base is established and a new response $y(t)$ is collected, using Equation (3.35b) to generate the AR coefficients ϕ_{yj} and residual error $e_y(t)$. In order to search a suitable reference data set that is closest to this new response $y(t)$, a criterion to minimize the difference of AR coefficients is shown as below:

$$\text{Difference} = \sum_{j=1}^p (\phi_{xj} - \phi_{yj})^2 \quad (3.38)$$

The reference data set is decided by Equation (3.38), and using these selected ARX coefficients α_i , β_j and the residual error $e_y(t)$ into Equation (3.37) to reproduce the response and get the residual error ($\varepsilon_y(t)$) of the reproduced ARX model.

Finally, the ratio of $\sigma(\varepsilon_y)/\sigma(\varepsilon_x)$ is defined as the damage-sensitive feature of this new response $y(t)$.

$$\frac{\sigma(\varepsilon_y)}{\sigma(\varepsilon_x)} \geq h, \text{ where } (h > 1) \quad (3.39)$$

Where $\sigma(\varepsilon_y)$ and $\sigma(\varepsilon_x)$ are the standard deviations of $\varepsilon_y(t)$ and $\varepsilon_x(t)$. Once, if the ratio is larger than some threshold value h , the system is considered to have some system changes.



3.2 System Validation

Several experiments are studied in this section; they are field test at Gi-Lu Bridge [57], Damage detection of RC frame [58, 59] and long-term SHM system of NTU CE research building [60]. Both Smart Sensing System (*Chapter 2*) and Structural Health Monitoring methods (*Section 3.1*) are applied in these experiments. Smart Sensing System is verified through the results of these experiments and evaluated by these real applications.

3.2.1 Field Test at Gi-Lu Bridge

Gi-Lu Bridge is a cable-stayed bridge, located in Nantou County, Taiwan. This bridge is a modern pre-stressed concrete cable-stayed bridge which crosses the Juosheui River. The bridge has a single pylon (with a 58 meter height above the deck) and two rows of harped cables (68 cables in total) on each side. The bridge deck consists of a box girder section 2.75 m deep and 24 m wide and is rigidly connected to the pylon; the deck spans 120 m on each side of the pylon. On September 21, 1999, during the final construction stages of the Gi-Lu Bridge, a significant earthquake (Chi-Chi Earthquake) with $ML = 7.3$ struck the central part of Taiwan. Only three kilometers away from the epicenter, Gi-Lu Bridge was subjected to very strong ground motions resulting in the damage of several of the bridge's critical structural elements. Reconstruction work undertaken to repair the bridge damage was completed at the end of 2004. At that time,

the bridge owner elected to develop an experimentally-calibrated finite element model of the bridge so that bridge safety could be verified over the bridge operational lifespan. To accurately calibrate the model, ambient vibration survey was conducted to extract the modal characteristics of the bridge.

In order to collect the dynamic responses of Gi-Lu Bridge under ambient excitation conditions, wireless monitoring system is suitable for this field measurement.

There are two stages of Gi-Lu Bridge test. The first stage is from 2005~2008 which is to integrate ambient sensor with wireless sensing unit and apply this system to collect the ambient responses of Gi-Lu Bridge. The second stage is start from 2009 after the newly developed wireless sensing unit (NTU-WSU-v02) is completed. In this stage, the performances of newly system (NTU-WSU-v02) are evaluated through the field test of Gi-Lu Bridge.

3.2.1.1 First stage: the evaluation of wireless ambient measurement

From 2005~2008, this field test is to employ the prototype of wireless sensing system (WiMMS) which is developed by Wang, et al. for monitoring long-span bridges during ambient excitation conditions. There are two objectives in this stage, one is to evaluate the feasibility of wireless sensing system on ambient response measurement; another is to determine the dynamic properties of the newly retrofitted Gi-Lu cable-stayed bridge (Nantou County, Taiwan) using ambient vibration responses

recorded by a wireless structural monitoring system. The wireless monitoring system consists of a distributed network of wireless sensors in direct communication with a high-performance data repository where data is stored and analyzed. To extract the bridge modal characteristics, three methods were used to identify the dynamic properties of Gi-Lu Bridge, they are Auto-Regressive (AR), Frequency Domain Decomposition (FDD) and Stochastic Subspace Identification (SSI) methods.

Instrumentation and data acquisition: The instrumentation installed in the bridge consisted of the following components: (1) Wireless sensors: twelve wireless sensors each containing a four-channel sensor interface with high-resolution analog-to-digital conversion are used; (2) Transducers: interfaced to each wireless sensor node is a highly sensitive Tokyo Sokushin VSE-15D velocity meter whose sensitivity constant is 0.25Volt/Kine (this sensitivity is calculated after signal conditioner); (3) Data repository computer: one high-performance laptop computer with a wireless receiver serves as the core of the system responsible for triggering the system, archiving recorded response data, and autonomously extracting the bridge modal characteristics.

In order to interface VSE-15D sensor to the wireless sensing node (WiMMS), an signal converter is required to convert the sensor voltage signal from $\pm 10V$ (the output of VSE-15D) into 0~5V (the ADC range of WiMMS). Here, an operational amplifier

OP400 [56] (Analog Device, Inc.) is selected to implement this function of signal converter.



Figure 3.1: Signal converter, power source and directional antenna with WiMMS.

The powering requirement of ambient sensor (VSE-15D) is $\pm 15V@15mA$. The WiMMS system does not support this powering requirement, so an extra power source of ambient sensor is required. Two sets of 14.4V Li rechargeable battery are serial connected to offer the $\pm 14.4V$ power. About the range of wireless sensor network, the length of Gi-Lu Bridge is about 240 meter and it's difficult to be handled by the original antenna of WiMMS. In order to extend the wireless signal range, a directional high gain antenna (D-Link 6dbi directional antenna) is used to replace the original antenna of WiMMS (2.1dbi Omin-directional antenna). The signal converter, power source and directional antenna are integrated with WiMMS system and shown in **Figure 3.1**.

Figure 3.2 shows the picture of system calibration and the installation of cable.



Figure 3.2: pictures of system calibration and cable installation.

Due to the limited number of sensing nodes available (only 12 wireless sensor-velocity meter pairs), the wireless monitoring system is reconfigured during testing to achieve three different test configurations: (1) Test 1: Ten wireless sensor-velocity meter pairs are installed along the bridge deck to record its vertical vibration at locations denoted as V01 through V10 as shown in *Figure 3.3a*; (2) Test 2: The ten wireless sensor-velocity meter pairs used during Test 1 are reoriented to record the deck's transverse vibration (denoted as H01 through H10 in *Figure 3.3a*); (3) Test 3: All twelve wireless sensors are installed on one side of the bridge to simultaneously record the cables and deck vibrations at sensor location T01 through T12 (*Figure 3.3b*).

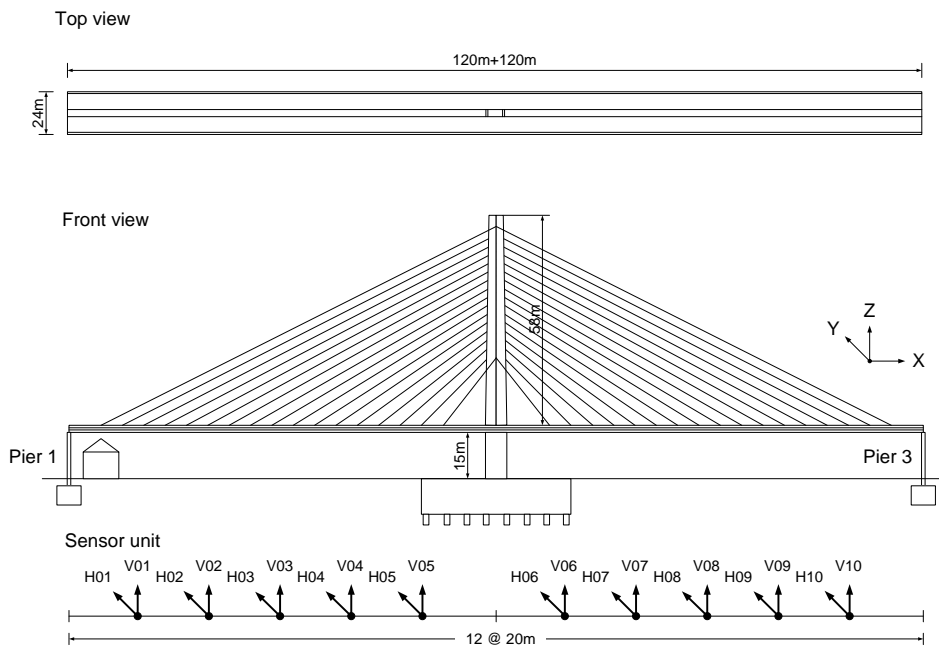


Figure 3.3a: Front view and top view of the Gi-Lu cable-stayed bridge.

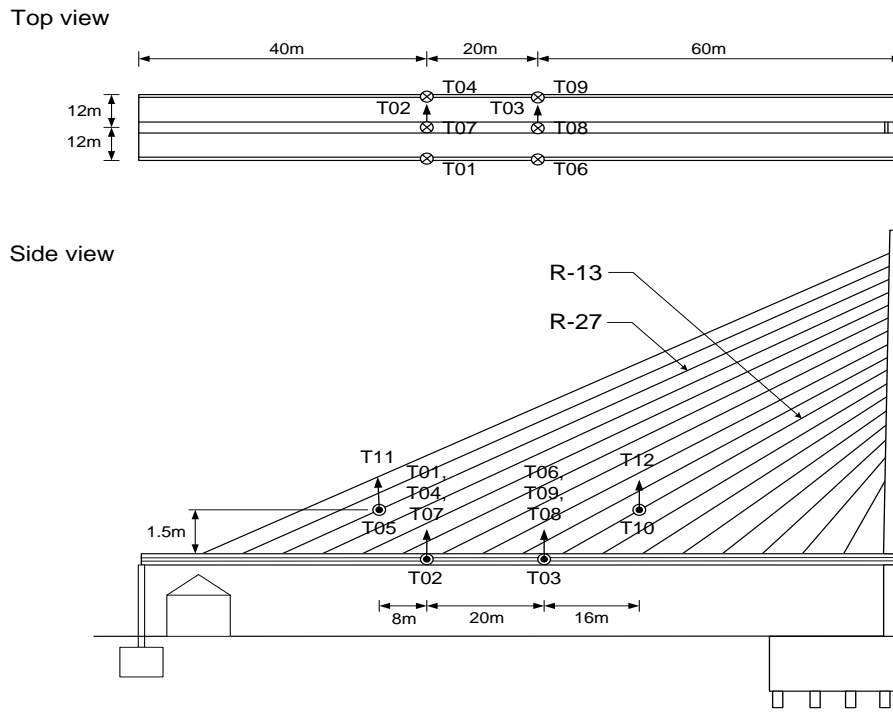


Figure 3.3b: Installation location of the wireless sensors during Test 3.

Data was sampled at 100 points per second on each channel to provide good waveform definition. The analog voltage output of the velocity meter was converted to a

digital signal with 16-bit resolution by each wireless sensor. The synchronized time-histories collected by the wireless monitoring system were wirelessly broadcasted to the high-performance laptop computer serving as the monitoring system's sole data repository.

Analysis of bridge ambient vibration data: Using the output only system identification methods (AR, FDD and SSI) described in *Section 3.1*, the dynamic characteristics of the Gi-Lu cable-stayed bridge are accurately identified from the wireless sensor data collected during field study.

In addition, the first ten bridge deck mode shapes determined by the SSI and FDD methods during Test 1 are shown in *Figure 3.4a*. The modal frequencies decided by SSI and AR methods and these results are matched. The estimated mode shapes of the bridge deck using both methods are consistent. Using the time history data collected during Test 2, the identified mode shapes of the bridge deck in the transverse direction are also shown in *Figure 3.4b*. Again, excellent agreement between SSI- and FDD-derived mode shapes is evident.

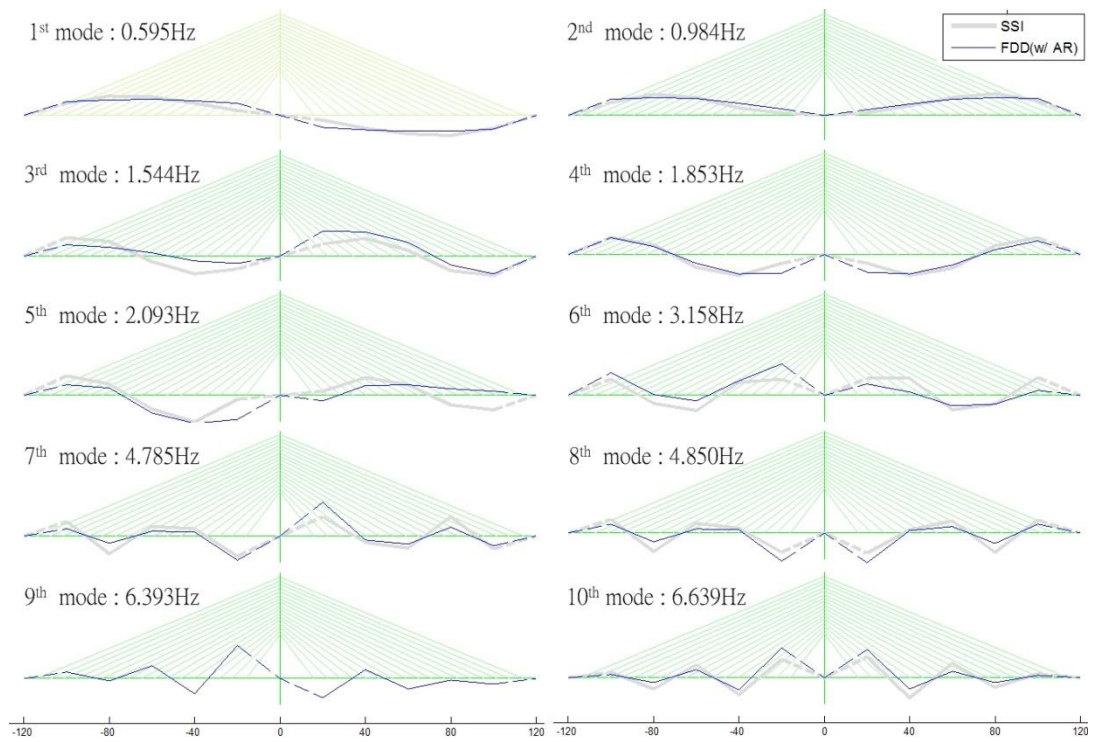


Figure 3.4a: Comparison of the identified bridge deck vertical mode shapes by using Stochastic Subspace Identification and Frequency Domain Decomposition.

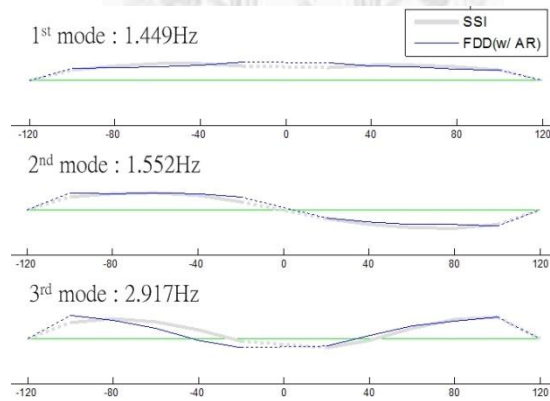


Figure 3.4b: Comparison of the identified bridge deck mode shapes in the transverse direction.

3.2.1.2 Second stage: Performance evaluation of NTU-WSU

The second stage focuses on the performance test of newly wireless system and the measurement of bridge responses under severe flood loading.

After the newly wireless sensing unit (NTU-WSU-v02a) is developed which is described in *Chapter 2*, the field experiment of Gi-Lu Bridge is also conducted. The vibration of Gi-Lu Bridge under severe flood loading was measured. In this field experiment the NTU-WSU-V02a unit with 9XTend wireless module is installed on the deck of Gi-Lu Bridge to record the vibration responses under flooding condition. The server node is installed at a location which is about 2 km away from Gi-Lu Bridge which is shown in *Figure 3.5*. In this case, the NTU-WSU unit can successful record and transmit the response data of bridge. For field test, 9XTend is a good solution for this kind application. In this test, although the performance of wireless communication is influenced by environment condition, ex. heavy raining and wind etc..., the data is feedback to host node successfully. In some applications the environment effect may need to be considered.

From stage1 to stage2, there are several obviously improvements, they are shown as below:

1. NTU-WSU-v02a successful supports the power requirement of ambient sensor. A multi-function powering module is included in NTU-WSU-v02a

which is able to supply various different kind of sensors (ex. Crossbow accelerometer, MTS LVDT, VSE-15D, etc...).

2. The programmable gain amplifier of NTU-WSU-v02a is good to adjust the signal range to prevent the noise effect and increase the signal resolution.
3. 9XTend wireless module of NTU-WSU-v02a presents the high performance on propagation distance and transmission data rate.



Figure 3.5: The location of Host node (A) and sensor node (B) on Google Map.

In Gi-Lu Bridge field test, NTU-WSU unit with 9XTend successfully performs the long distance wireless communication under poor weather conditions. There are three computation platforms (including sensor node, host node and user end) allow user to embed analysis algorithms. How to arrange the SHM computation algorithms into these spaces and consider the features of each space is an important issue in the future. Base

on the framework of smart sensing system, users and engineers can implement their structural health monitoring program on this system.

3.2.2 Damage Detection of RC Frame

In this test, a wireless monitoring system assembled from wireless sensor prototypes proposed by Wang *et al.* was used and installed on a full-scale RC frame structure with and without brick wall during the shaking table test in the laboratory. A damage detection method described in *Section 3.1.4* was adopted and embedded in the wireless sensing unit to continuously identify the structural damage situation in almost real time during the shaking table test. With a flexible and capable hardware design on wireless sensing unit, this proposed core idea can be implemented with the computational task required by a SHM and damage detection system. Based on the embedded damage detection algorithm on the calculation of the AR-ARX model coefficients by the wireless sensing and monitoring system, the damage feature of the structural system is calculated. A graphical user interface, in connection with wireless sensing and monitoring system, is also implemented in this damage detection system for on-line and almost real time monitoring.

The procedure of damage detection: The damage detection monitoring system contains one wireless sensing unit with one accelerometer to collect the structural response and one receiver unit (server) outside the structure. Integration of the wireless

sensing system and the damage detection algorithm the monitoring system can be used for on-line damage detection of structure. The on-line damage detection algorithm and data broadcasting between sensing unit and receiver (server) is described as follows:

1. The wireless sensing unit continuously collects a series of ambient vibration of structural responses and broadcasts the collected structural responses to the receiver (to the server side). This ambient signal, $x(t)$, will serve as the reference data of the structure.
2. Under the assumption of stationary response time history of the structure at a single measurement location (for case of white noise excitation), the response data, $x(t)$, an autoregressive (AR) time series model is fitted to the data. By **Equation (3.35a)**, the order of AR model ($p=22$) is assumed for this structure. Then the AR coefficients ϕ_{xj} and residual error $e_x(t)$ of AR model are solved here. After the AR model is established, The residual error, $e_x(t)$, and response data, $x(t)$, will be used as the input and output of ARX model (**Equation (3.36)**). The input order ($a = 12$) and output order ($b = 10$) of ARX model are assumed for this structure. Therefore, the output coefficients (α_i), input coefficients (β_j) and residual error ($\varepsilon_x(t)$) of ARX model are solved. And the standard deviation ($\sigma(\varepsilon_x)$) of residual error is also calculated. Each reference response $x(t)$ with a set of AR-ARX parameters ($\phi_{xj}, \alpha_i, \beta_j$ and $\sigma(\varepsilon_x)$) and this set of parameters is arranged

in the reference data base. There are several sets of parameters held in the reference data base.

3. When an unknown (damaged) structural response time history $y(t)$ is measured by wireless sensing unit, and its AR coefficients ϕ_{yj} are solved on wireless sensing unit and feedback to the server node.
4. The server node will select a suitable reference model by minimizing the difference of received ϕ_{yj} and ϕ_{xj} of data base (**Equation (3.38)**). Then the ARX coefficients (α_i, β_j) and the standard deviation $(\sigma(\varepsilon_x))$ of suitable model are uploaded to the wireless sensing unit.
5. The wireless sensing unit uses this received ARX coefficients to fit the measured time history $y(t)$ and solve the fitted residual error $\varepsilon_y(t)$ by **Equation (3.37)**. Finally calculate the damage index (F) and feedback to server node.

$$F = \frac{\sigma(\varepsilon_y)}{\sigma(\varepsilon_x)} \quad (3.40)$$

After these five steps of on-line damage detection system, the damage index is displayed on the screen through graphical user interface (which is implemented by LabVIEW) and user can get this information in almost real-time.

Figure 3.6 shows the major program flow for damage detection strategy in a wireless monitoring system. The AR-ARX time series damage detection method is well suited for automated execution by a wireless monitoring system.

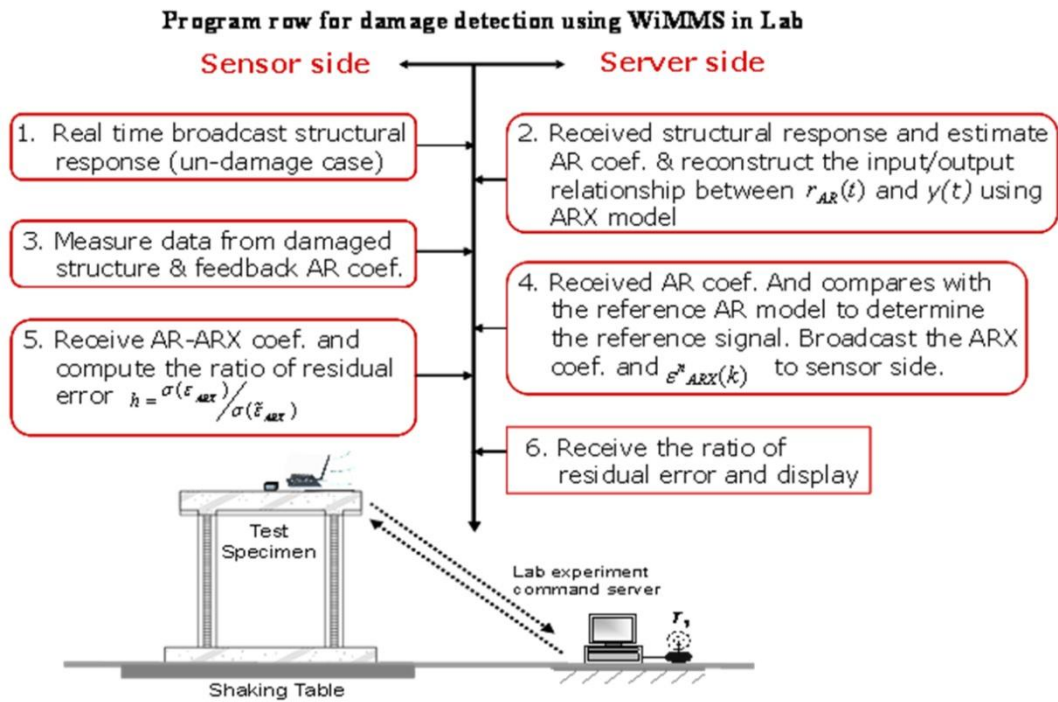


Figure 3.6: Implementation of the AR-ARX damage detection strategy in a wireless monitoring system to conduct the continuous damage detection of large structural testing in the laboratory.

Test Structures: To verify the proposed on-line damage detection technique using wireless sensing and monitoring module, shaking table test on three different types of reinforced concrete frame structure with different excitation level are conducted. Three sets of full-scale RC frames were designed, constructed and tested at the National Center for Research on Earthquake Engineering (NCREE) in Taipei, Taiwan, to study the dynamic behaviors of RC frame without and with infill wall (along out-of-plane direction). The three different RC frames are specified with: (1) Frame A1F, (2) Frame P1F, and (3) Frame P2F. Frame A1F, which is an RC frame with two 12cm thick post-laid brick walls. As shown in *Figure 3.7a* (top views), the A1F structure consists

of four RC columns, a strong top floor, a strong foundation and two side walls. The distances between the center lines of columns along X and Y directions are 2.1m and 3.05m, respectively. The height of the columns is 2.8m. The column section is 0.35 by 0.3m with eight #5 longitudinal steel bars and #3 transverse ties with spacing of 0.25m. The nominal strengths of concrete and steel are 180kg/cm² and 2800kg/cm², respectively. The 10-ton top floor and the 13-ton foundation are both designed to be strong compared with the columns and are considered as rigid diaphragms. Accelerometers (Setra 141A in range of $\pm 4g$) are installed at the top and basement of the floor and four Linear Variable Differential Transformer (LVDT) displacement measurement devices are positioned on each brick wall so as to measure the deformation of the wall, as shown in *Figure 3.7b*.

Preliminary modal analysis using displacement-based beam-column elements with fiber sections using OpenSees (ver. 1.7.1) shows that the dominant natural periods of the specimen is 0.24sec. Frame P1F is designed with the same details as frame A1F but without infill wall. Another 2-story RC frame structure is also designed for this stud. The detail design drawing of this structure is shown in *Figure 3.8*. The dominant frequency of this 2-story RC frame is 12.0 Hz. *Figure 3.9* shows the photos of these three frame structures.

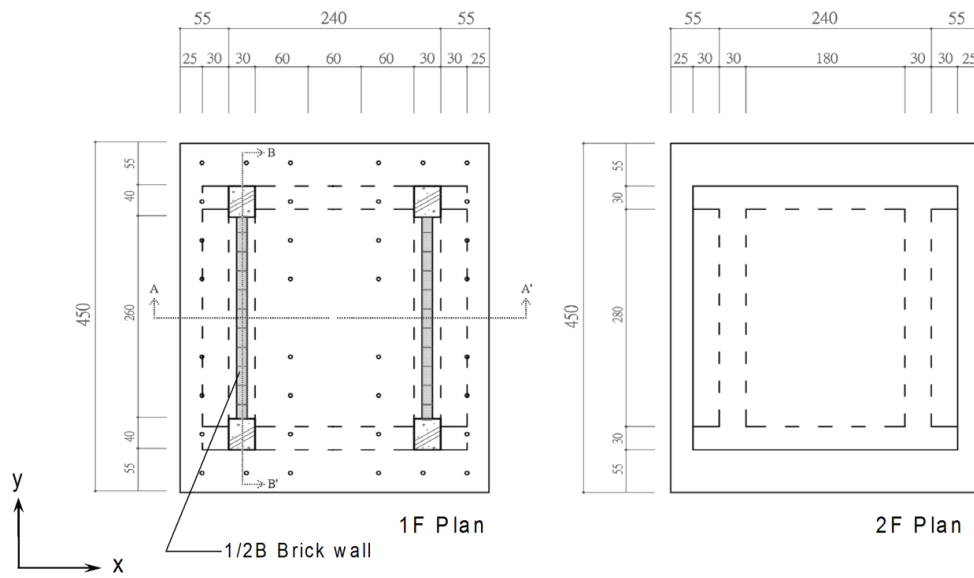


Figure 3.7a: Top view of the test specimen (A1F).

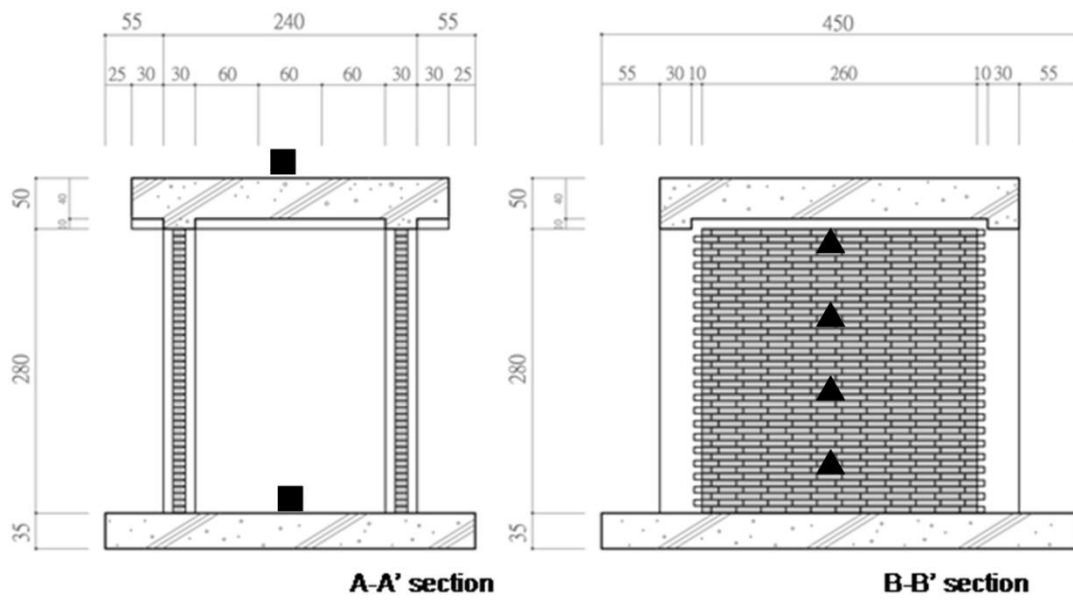


Figure 3.7b: Side view of the test specimen (A1F). Locations of accelerometers (■) and LVDT (▲) are also shown.

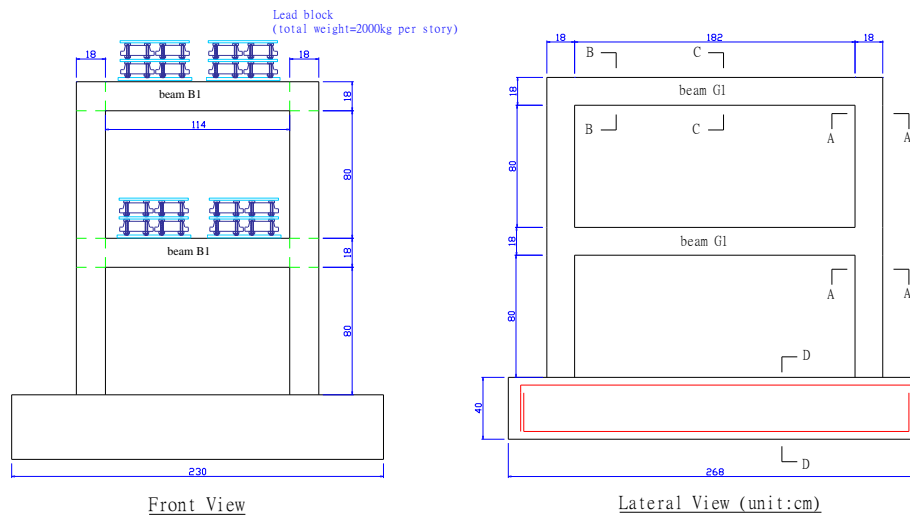


Figure 3.8: Draft of the front view and side view of the two-story RC frame.

(3.9a)



(3.9b)



(3.9c)



Figure 3.9: (a) Photo of the specimen A1F frame, (b) Photo of the specimen P1F frame, (c) Photo of the 2-story RC frame structure.

There are three objectives in this study: 1) to assess the accuracy of the wireless monitoring systems, 2) to utilize the computational capabilities of the sensing unit design for continuous damage detection, 3) to evaluate the reliability of damage detection and the capability of visualization on almost real-time structural damage monitoring. Both conventional wired sensors and the wireless sensing unit are installed on each specimen to monitor their response excited by the shaking table. To quantify the accuracy of the wireless monitoring system, the laboratory data acquisition system (Pacific Instrument Series 5500 data acquisition classis) is also used to offer high-resolution data acquisition with sampling rate of 200 Hz. In the wireless communication a sampling rate of 100Hz is used. To excite these three structures, respectively, various intensities of base excitations are applied by the shaking table. It should be noted that the white noise and seismic ground motion records are applied back to back sequentially in uni-axial direction. *Table 3.1* summarizes the excitations during the laboratory study for each of the structure. The ground motion of Chi-Chi 1999 earthquake collected at station TCU078 seismic are used for this study. Comparison on the recorded roof acceleration response between wired and wireless system with nearly identical results on the data acquisition are observed. Comparison on the floor acceleration collected from wired and wireless systems was also verified. Good agreement between the wired and wireless system is observed. From the recorded

acceleration response of the frame structure during earthquake excitation, the restoring force diagrams of different test stages are also examined. *Figure 3.10* shows the restoring force diagram of the three structures from the response of different level of excitation. From the observation of restoring force diagram among different test cases the inelastic hysteretic behavior were observed for case of large excitation.

Table 3.1a: Estimation of the ratio of residual error through wireless damage detection module (for case of wall frame structure: A1F)

Wall Frame (A1F)		Ratio of residual error
Excitation	Intensity	
White Noise 1	50 gal	Reference
TCU078EW	150 gal	
White Noise 2	50 gal	0.902
TCU078EW	500 gal	
White Noise 3	50 gal	1.027
TCU078EW	1000 gal	
White Noise 4	50 gal	1.377
TCU078EW	1500 gal	
White Noise 5	50 gal	1.545

Table 3.1b: Estimation of the ratio of residual error through wireless damage detection module (for case of pure frame structure: P1F).

Pure Frame (P1F)		Ratio of residual error
Excitation		
White Noise 1	50 gal	Reference
TCU078EW	150 gal	
White Noise 2	50 gal	0.955
TCU078EW	500 gal	
White Noise 3	50 gal	0.930
TCU078EW	1000 gal	
White Noise 4	50 gal	2.354
White Noise 5	50 gal	1.706
White Noise 6	50 gal	1.407
TCU078EW	1500 gal	
White Noise 7	50 gal	1.616
TCU078EW	1800 gal	

Table 3.1c: Estimation of the ratio of residual error through wireless damage detection module (for case of 2 story RC frame: P2F).

Excitation		Ratio of residue error
White Noise 1	50 gal	Reference
TCU078EW	200 gal	
White Noise 2	50 gal	1.018
TCU078EW	400 gal	
White Noise 4	50 gal	1.102
TCU078EW	600 gal	
White Noise 5	50 gal	1.064
TCU078EW	800 gal	
White Noise 6	50 gal	1.206
TCU078EW	1000 gal	
White Noise 7, 8,	50 gal	1.659
TCU078EW	1200 gal	
White Noise 9	50 gal	1.638
TCU078EW	1500 gal	
White Noise 10, 11	50 gal	2.176
TCU078EW	2000 gal	
White Noise 12	50 gal	2.410
TCU078EW	1200 gal	
White Noise 13	50 gal	2.609

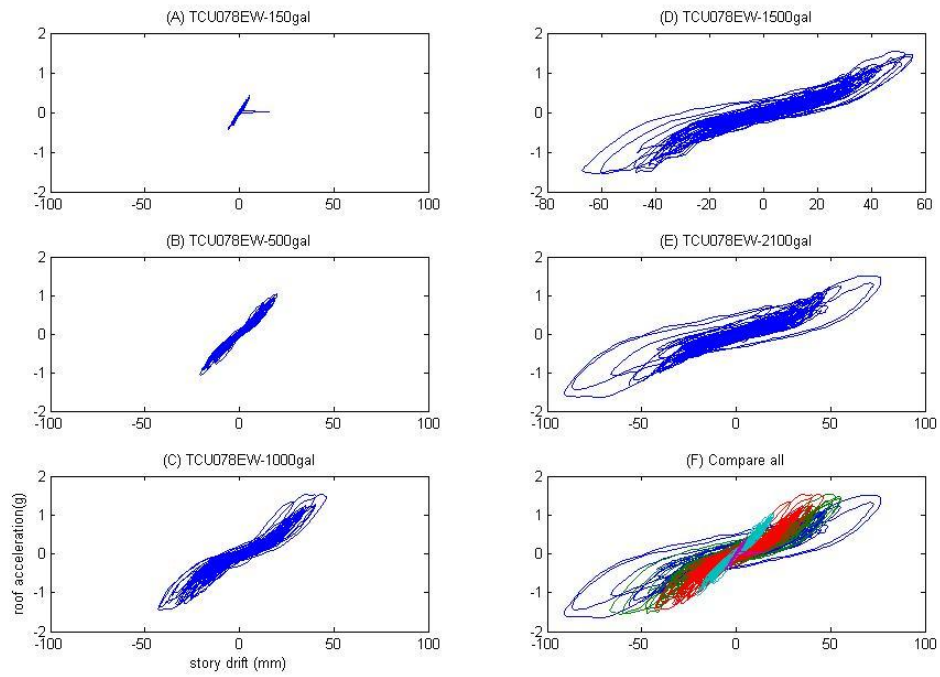


Figure 3.10(a): Restoring diagram of the test structure (A1F) from different input excitation level. (the unit of Y axis is restoring force per unit mass (g))

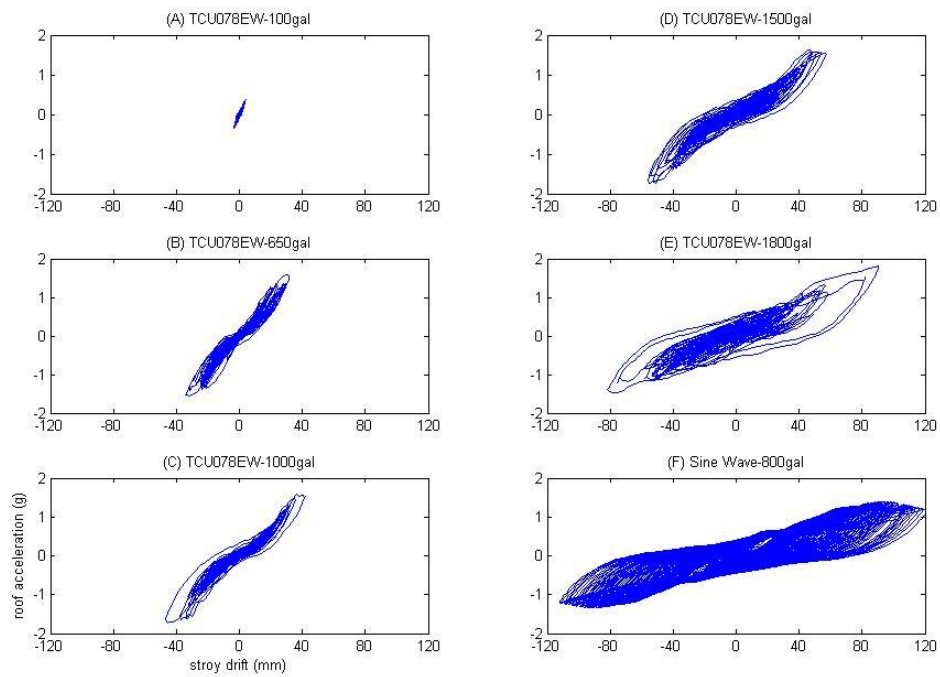
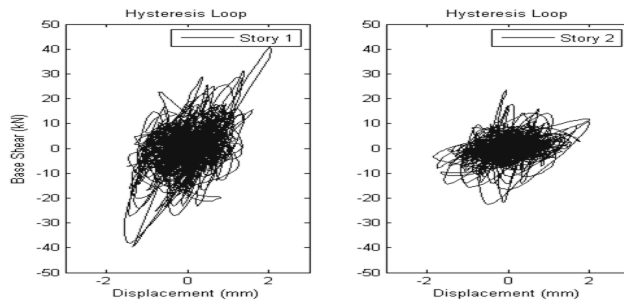
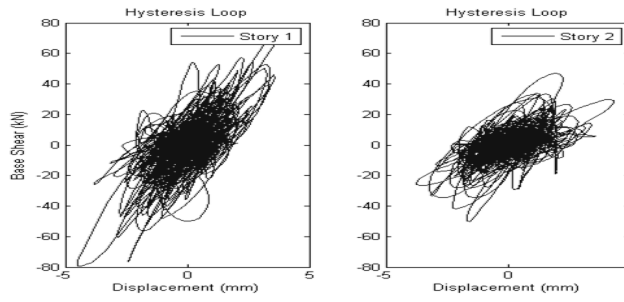


Figure 3.10(b): Restoring diagram of the test structure (P1F) from different input excitation level. (the unit of Y axis is restoring force per unit mass (g))

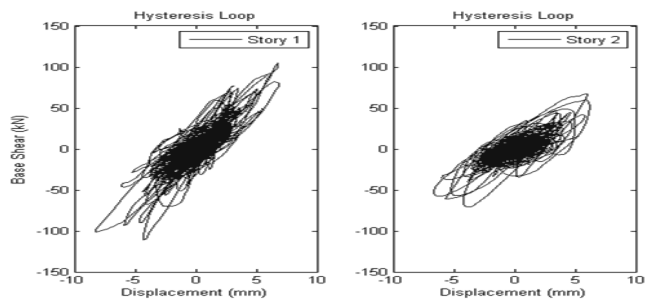
Excitation: 400 gal



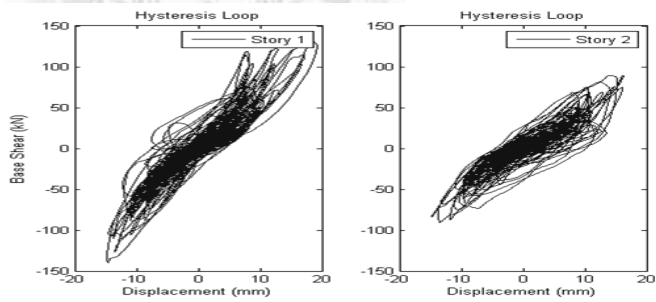
Excitation: 800 gal



Excitation: 1000 gal



Excitation: 1500 gal



Excitation: 2000 gal

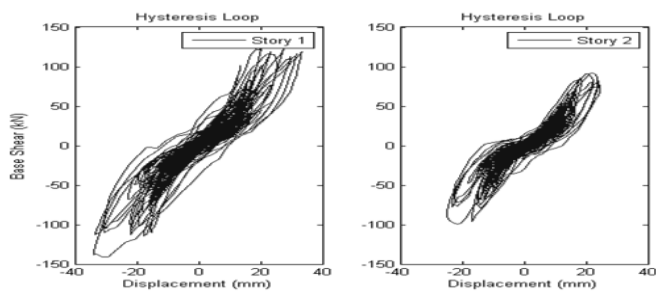


Figure 3.10(c): Restoring diagram of the test structure (P2F) from different input excitation level. (the unit of Y axis is KN)

Results from on-line AR-ARX damage detection: The roof acceleration response from the white noise excitation (normalized to 50 gal peak ground acceleration) of the structure after different damage stage of the structure during earthquake excitation is collected from the wireless sensing and monitoring system for damage detection. Follow the five steps of damage detection procedure which are described ahead, the ratio (F) of AR-ARX two-tier model residual errors can be generated for each damage stage. *Table 3.1* also shows the estimation of the ratio of residual error through wireless damage detection module from the white noise test data of three structures: wall frame structure (A1F), pure frame structure (P1F) and the 2-story RC frame (P2F). Since the data collected from the white noise excitation was analyzed after each earthquake excitation, and the ratio of residual error becomes more and more significant with the increasing of input earthquake excitation level. This ratio of residual error can indicate the degree of damage in the structure. From the observation of *Table 3.1*, it is found that the residual error calculated from the structure after the earthquake excitation with peak acceleration 1000 gal became larger than one which indicates damage was developed in the frame structure after the earthquake excitation with peak acceleration of 1000 gal.

Results from off-line AR-ARX damage detection: In order to verify the accuracy of the damage detection through wireless monitoring and damage detection module,

data collected from wired system (from NCREE data acquisition system) are also used to conduct the offline damage detection using the same two-tier damage detection algorithm. *Figure 3.11* plots the ratio of AR-ARX two-tier model residual error for the three test structures for different test cases using the ambient vibration data (each test data was separated into 6 different segments). It is observed that the estimated residual error also in consistent with the result from on-line almost real-time damage detection. From the observation of the off-line data analysis, the estimated ratio of AR-ARX two-tier model residual error from offline analysis is generally larger than the result from wireless sensing unit. Because of the difference on the sampling rate between these two systems (100Hz for wireless sensing unit and 200Hz for wireless system), the estimated residual error is different from the result of using wireless sensing and monitoring system. But the results all indicate the residual error is exceeding one when the structure was damaged.

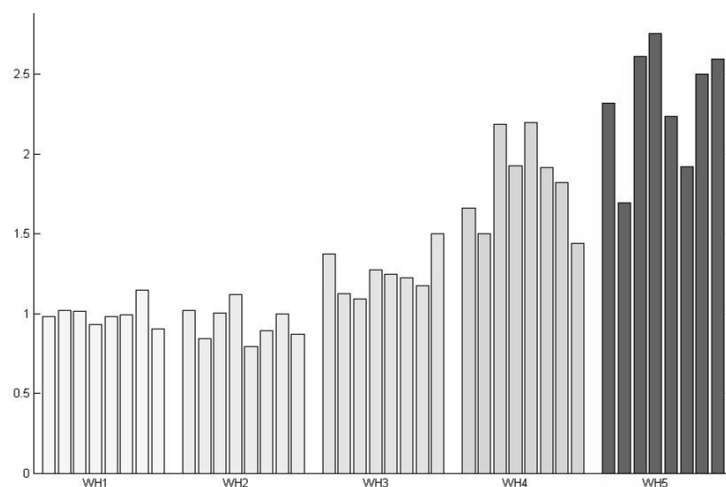


Figure 3.11(a): Ratio of AR-ARX two-tier model residual error from test of RC frame (A1F) using off-line data. (Y axis is damage index)

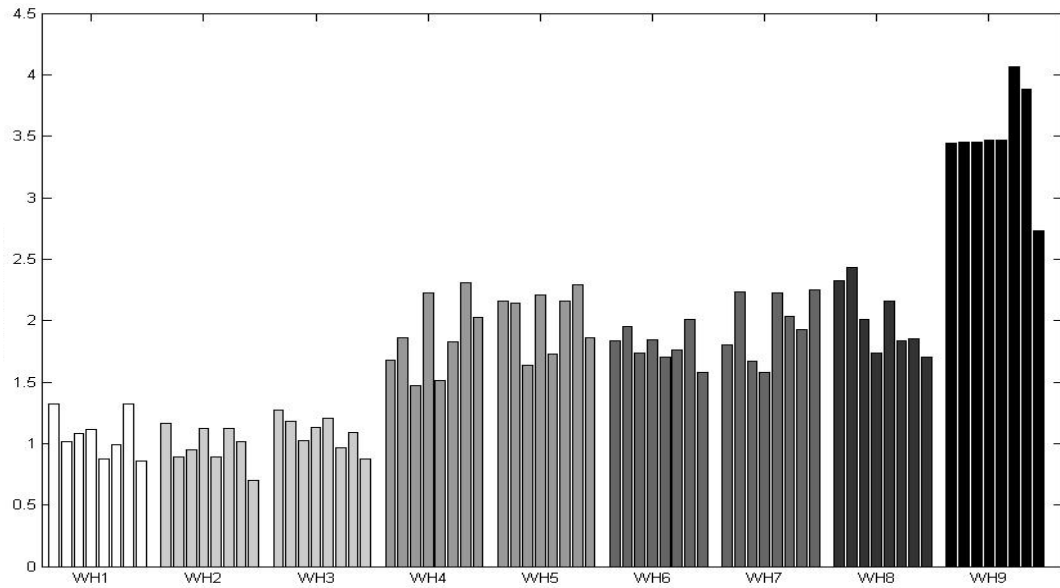


Figure 3.11(b): Ratio of AR-ARX two-tier model residual error from test of RC frame without walls (P1F). (Y axis is damage index)

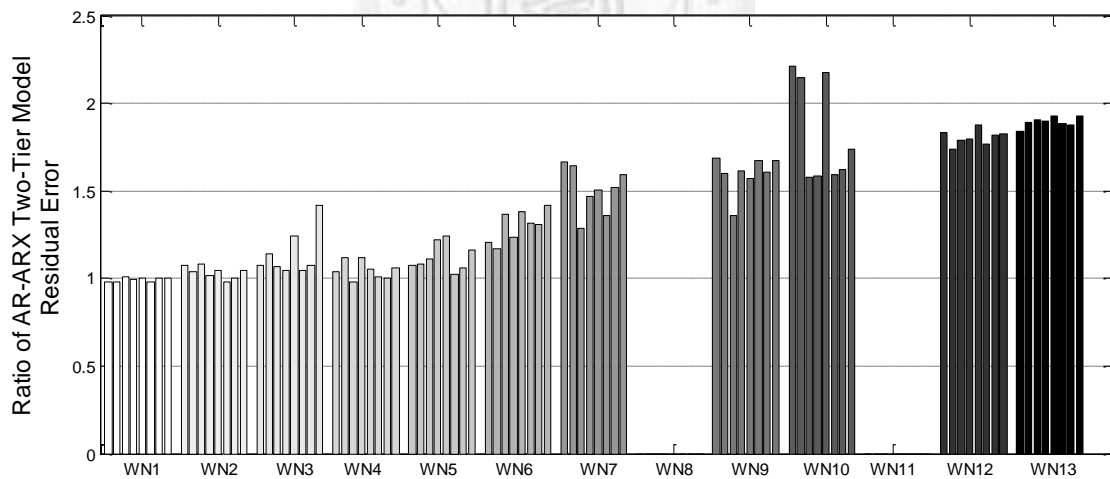


Figure 3.11(c): Ratio of AR-ARX two-tier model residual error from test of 2-story RC frame without walls (P2F).

Graphical User Interface: LabVIEW is a popular Graphically Programming Language. There are three basic communication subroutines in Visualized Interpretation (VI) in LabVIEW: receive wireless package VI, transmit wireless unsigned short, and transmit wireless single float. In this study three major programs are developed under LabVIEW: Real-time display results on AR model estimation and results on damage detection (as shown in *Figure 3.12*. In *Figure 3.12*, there are three pages to display. Page 1 (as shown in *Figure 3.12a*) displays the real time response time history and moving window Fourier amplitude spectrum. Page 2 (as shown in *Figure 3.12b*) displays the results of AR analysis which include the AR coefficients (broadcasted by wireless sensing unit), the roots of transfer function, the poles of transfer function by polar coordinate and the nature frequencies which are extract by solving the poles of transfer function. Page 3 (as shown in *Figure 3.12c*) displays the coefficient of AR-ARX model, and the ratio of the residue error which is received wirelessly from wireless sensing unit. With this setup the almost real-time demonstration of structural response and the residual error calculated by the almost real-time damage detection using two-tier damage detection model can be viewed.

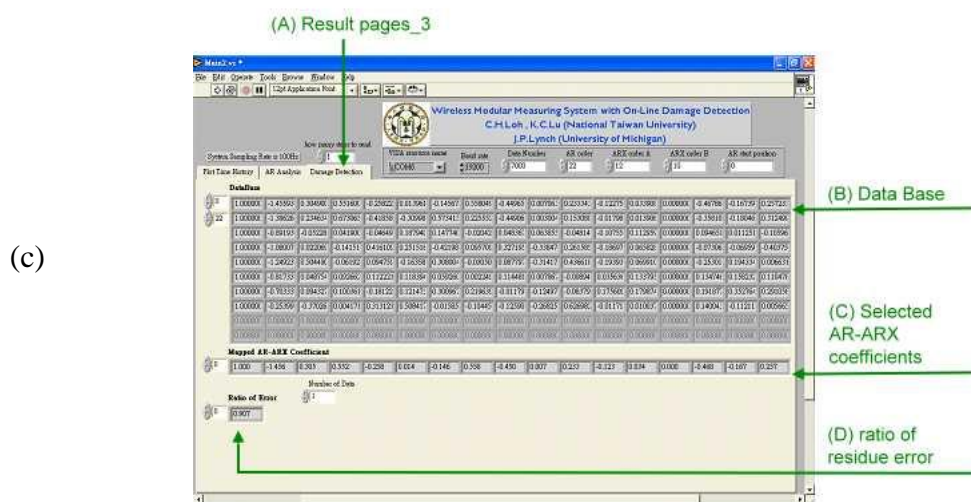
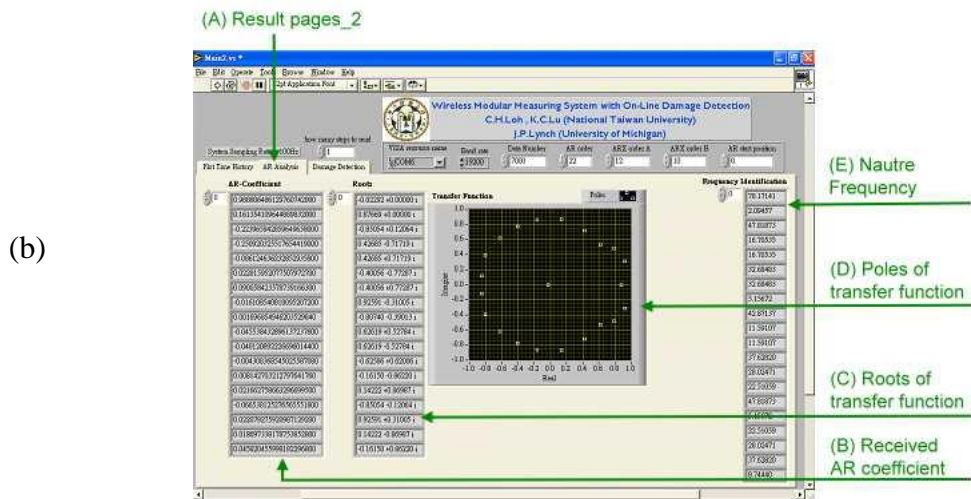
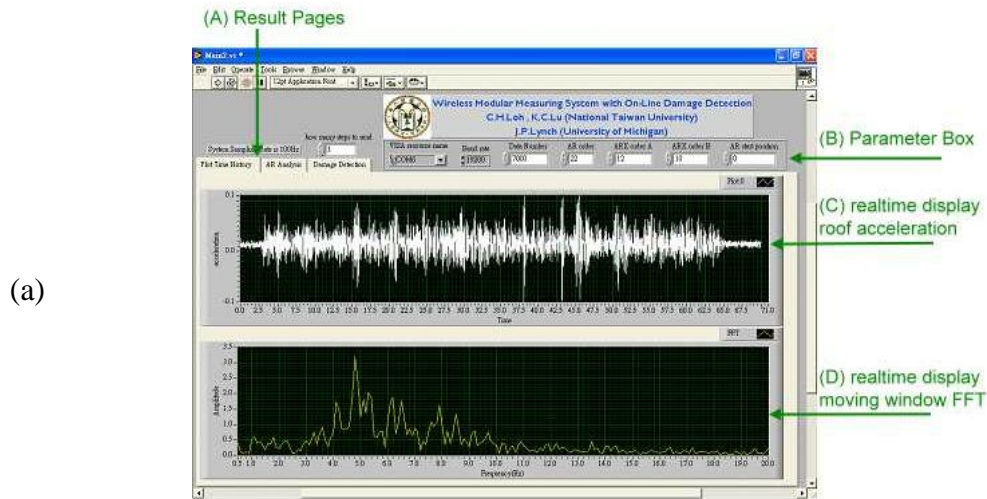


Figure 3.12: Three pages to display from the wireless health monitoring system.

Test Results: This research has explored the use of wireless sensing unit for structural health monitoring. A wireless sensing system is designed for application in structural monitoring and damage detection. Embedded in the wireless monitoring module, a two-tier prediction model, using auto-regressive (AR) and the autoregressive model with exogenous inputs (ARX) is used for obtaining the damage sensitive feature in almost real time monitoring. This approach is basically using the ambient vibration measurement of structure after the excitation of earthquake.

The two-tier damage detection model provides a very convenient and easy to be implemented in the wireless sensing unit for damage detection using ambient vibration response signal. The damage index can be estimated immediately after the ambient vibration survey of the structure.

Two advantages of wireless sensing system are verified in this test, they are:

1. The embedded computing of microcontroller is successfully executed the analysis of AR method which includes a least square method and matrix operations. This means the embedded computing and distributed computation of wireless sensing system is feasible in real applications.
2. The integration of wireless sensing system with graphical user interface is also implemented in this test. Here, the basic functions which are related to the operations of wireless sensing system are deployed on LabVIEW

successfully. In the development environment of LabVIEW, it is easy to implement the required applications (ex. Analysis engine, internet communication and the interface to peripheral hardware.).



3.2.3 Long-term SHM System of NTU CE Research Building

The objective of this experiment is to apply Smart Sensing System to be a continuous monitoring system which can conduct continuous monitoring of a building structure and generate a monitoring report. The building monitoring data will focus on the ambient vibration responses. Two servers are used in this SHM system: 1) wireless measurement server which takes care of measuring and archiving all the structural responses and environmental situation, and 2) analysis server which conducts the signal processing on the received signals. The measurement server is in charge of the collection of signals and broadcast wirelessly from all sensors to the analysis server. Dominant frequencies and mode shapes of the building will be estimated in the analysis server from the continuous monitoring of the ambient vibration data (velocity) of the building by using AR-Model, Frequency Domain Decomposition and Stochastic Subspace Identification methods which are introduced in *Section 3.1*. The proposed continuous monitoring system can effectively identify the building current health condition and generate a report to the owner.

Test Structure (NTU CE research building): The new Civil Engineering research building of NTU was constructed on July 2008. It is an 8-story precast reinforced concrete building with middle-story isolation (isolators were installed in the first story). A typical isolation system layout in the isolation floor is shown in *Figure*

3.13. In this building the Central Weather Bureau (Taiwan) had installed the strong motion instrumentation to monitor the seismic response of the structure during earthquake excitation. All the seismometers installed by CWB are wired system with central data logger which can monitor the seismic response of the building. The objective of this instrumentation is for monitoring the seismic responses of the building. Besides the earthquake monitoring, it is necessary to develop a continuous monitoring system for the building which can monitor the dynamic characteristics of the building continuously using the advance technologies, so as to develop a warning system when the building healthy condition was changed. This monitoring system is designed for continuous monitoring of the building subjected to environmental loading. There are two different types of monitoring systems which are installed in this building: Type-1 monitoring system is for the earthquake monitoring and Type-2 monitoring system is for the continuous monitoring of ambient vibration of the building. Smart Sensing System will adapt to the Type-2 system.

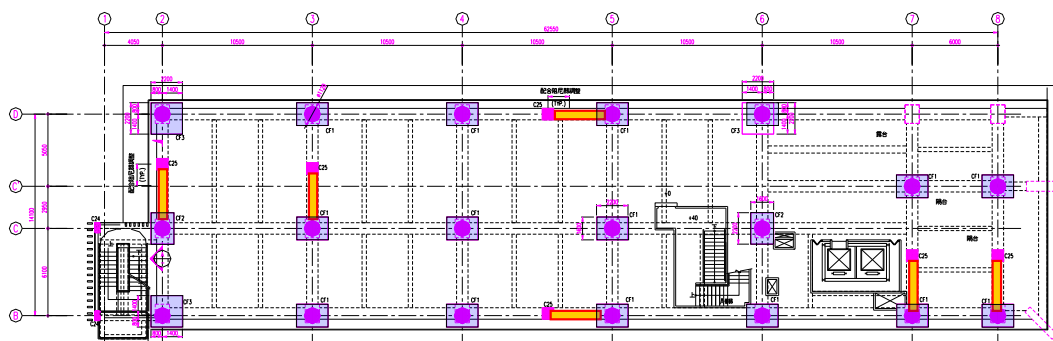


Figure 3.13: Location of dampers and isolators in the isolation floor (between 1st and 2nd floor)

Four different types of sensor are used in this monitoring system which include: accelerometers, anemometers (supported by solar power system), laser displacement gauge and velocity sensors (ambient vibration). The locations of velocity sensors for ambient vibration measurement are shown in *Figure 3.14*.

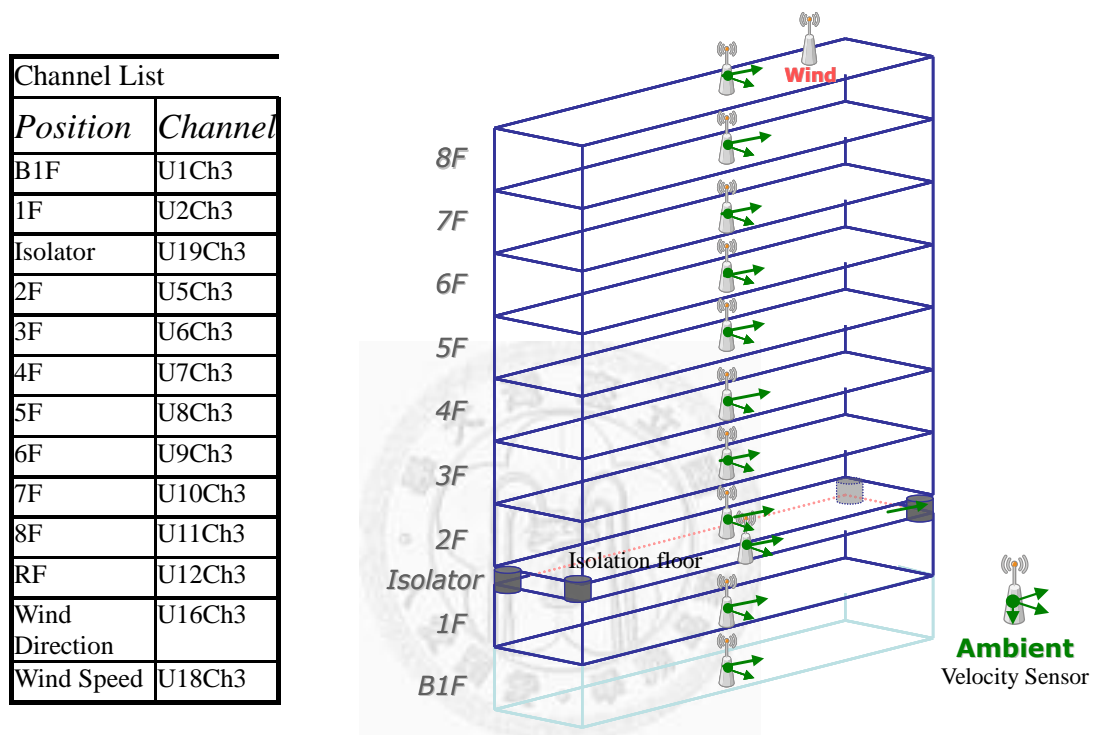


Figure 3.14: Layout of the velocity sensors for ambient vibration monitoring of the building.

The objective of Type-2 monitoring is to develop the reference model of the building. Continuous monitoring of the ambient vibration of the building will be conducted (at least three measurements within a day and each measurement will collect 5 minutes of ambient vibration data). Smart Sensing System will be used in both long term and short term tests. For this test the major works in the project are to develop an

effective and efficient data communication mechanism and data analysis programs so as to extract the dynamic characteristics of the structure right after the collection of the data and perform the damage assessment of the structure if the structure is damaged when it is subjected to environmental excitations. In this building the Central Weather Bureau, Taiwan, also had installed the strong motion instrumentation to monitor the seismic response of the structure during earthquake excitation.

Hardware Organization of Long Term Continuous Monitoring:

For establishing the monitoring system the ambient vibration measurement system will be used. For this monitoring system the instrumentation system consisted of the following components:

- Transducers: Tokyo Sokushin VSE-15D velocity detectors.
- Wireless sensing unit: NTU-WSU-v02a which is introduced in *Section 2.1*.
- Servo Computer: one PC with wireless modem to serve as the trigger and

recording system.

The wireless sensing units were be used in this monitoring system which replaced the traditional data acquisition system that uses cables. The hardware organization is arranged in the following steps (also shown in *Figure 3.15*):

1. The wireless sensing network is based on the Wireless Sensing Unit (NTU-WSU-v02a). The server program is based on LabVIEW which also supports the function of web server, FTP server, remote control and monitoring.
2. The server is a personal computer with LabVIEW can achieve MATLAB solver by ActiveX, and the engineer can easily integrate the developed structural health monitoring program into this system.
3. In the 2nd phase hardware development the server will be replaced by NI Compaq RIO which is a real-time programmable automation controller. In this stage Smart Sensing System will be more robust and simplify. And this phase is already implemented in Smart Sensing System in 2010.

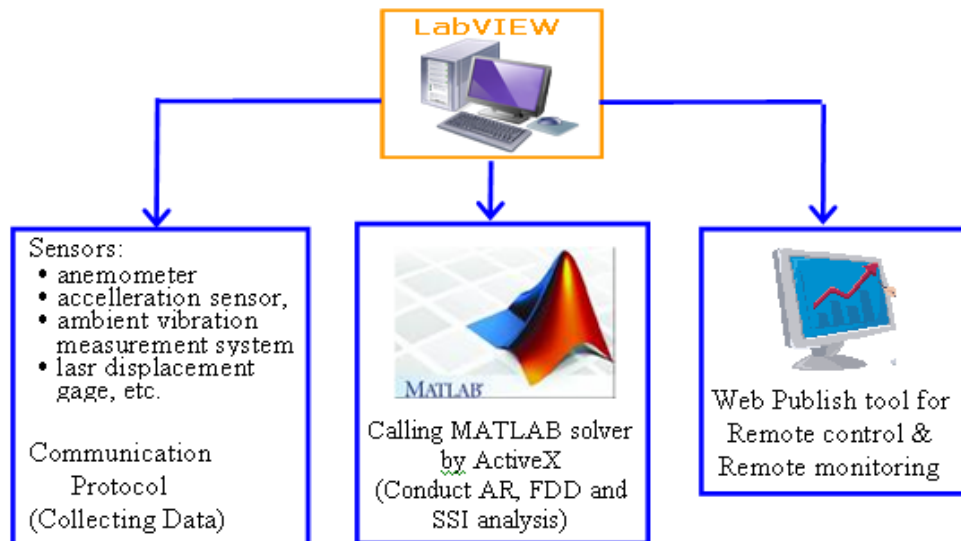


Figure 3.15: Hardware & Software arrangement of structural health monitoring system.

Depend on the objective of the structural monitoring; some computational programs will be embedded into the sensor node. The concept of distributed

computation will be used and in this stage the monitoring system will be highly efficiency and smart.

Software Design for Continuous Monitoring: To start the monitoring system the PC server will send a message to start the program and ask NTU-WSU to collect the data and send the data back to the server for analysis. *Figure 3.16* shows the flow chart of the monitoring system. To ensure there is no mistake during the process of the monitoring, the system was design with several check points and by-pass, so as to make sure no error message in collecting and analyzing the data. The most important one in developing the monitoring system is the communication between the sensing unit and the receiver unit, i.e. to make sure there is no error in the communication between sensing unit and the PC server. To avoid this situation, each action in the sensing unit and in communication must be check without any error message. First, each sensing unit was boot up to collect the vibration signal, then check all units is ready to broadcast the data. Second, make sure all the data was received by the server. Detail of the data communication and check pass is shown in *Figure 3.17*.

Data collected from the wireless sensing system will be processed in the server to extract the dynamic characteristics of the structure. In this test efforts will be put on the development of automatic analysis of ambient vibration data. Three different methods

will be introduced: Least square AR method, frequency domain decomposition method and data-driven output only stochastic subspace identification method.

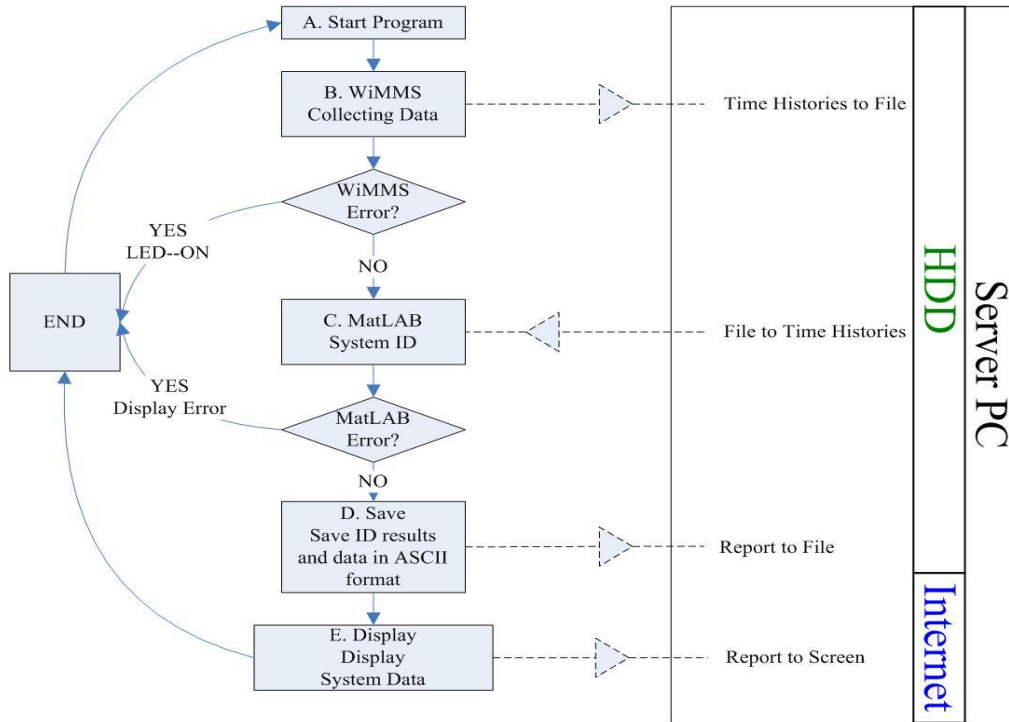


Figure 3.16: Flow chart of the software arrangement for building continuous monitoring.

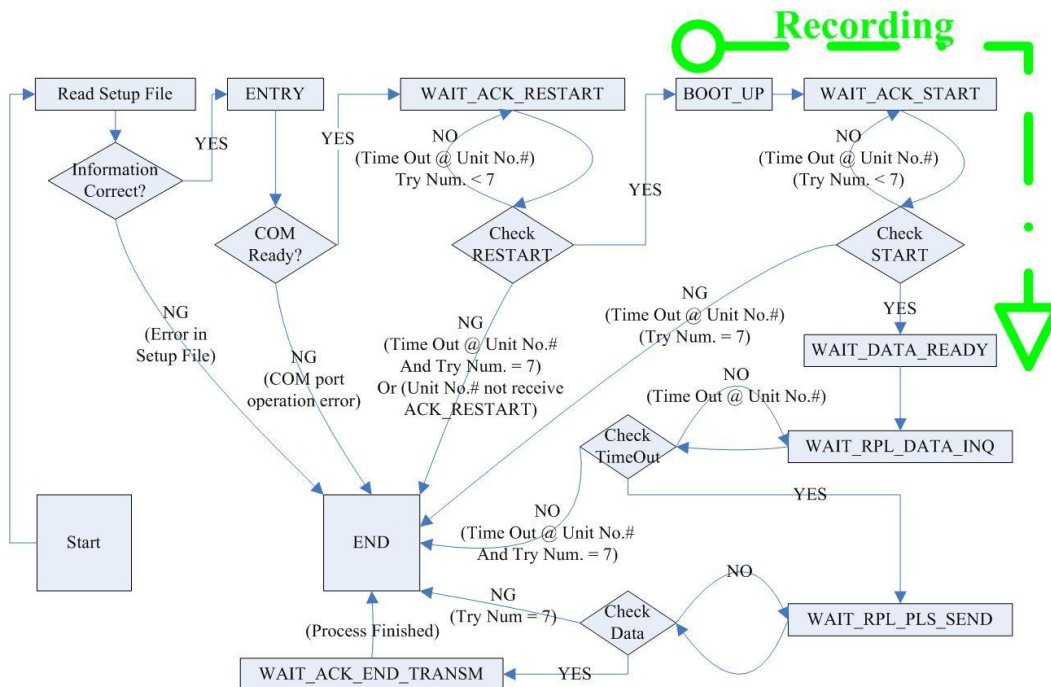


Figure 3.17: Flowchart of the monitoring system in collecting and analyzing the data.

The developed software was implemented in MATLAB and calling MATLAB solver through ActiveX. The theoretical background of these methods is described in *Section 3.1*.

In order to make the process of system identification to be automotive procedure, the automotive program flow is required. The automotive flow chart of AR & FDD method is shown in *Figure 3.18*. In *Figure 3.18*, the setp1~4 are used to extract the system natural frequencies through AR analysis; after the natural frequencies are decided, the step5~11 are used to extract the mode shapes and modal damping ratios. In this procedure, an automotive feature mode selector which is used to pick up the modal frequencies from the results of AR analysis is included, and is shown in *Figure 3.19*. In *Figure 3.19*, there are several criteria included. 1. The roots of AR coefficients must be conjugate pair. 2. The range of natural frequency is limited to 0Hz ~ 20Hz. 3. The system is lightly damped, i.e. the poles must be very close to the unit circle. 4. A statistic of selected frequency range is used to get the natural frequency which is the position of maximum appearance time.

The automotive flow chart of Output only SSI method is shown in *Figure 3.20*. This procedure [19] is base on the description of *Section 3.1* and added an extra step (step 7 in *Figure 3.22*) to distinguish the noise mode. And the detail of step 7 (distinguish the noise mode) is shown in *Figure 3.21*.

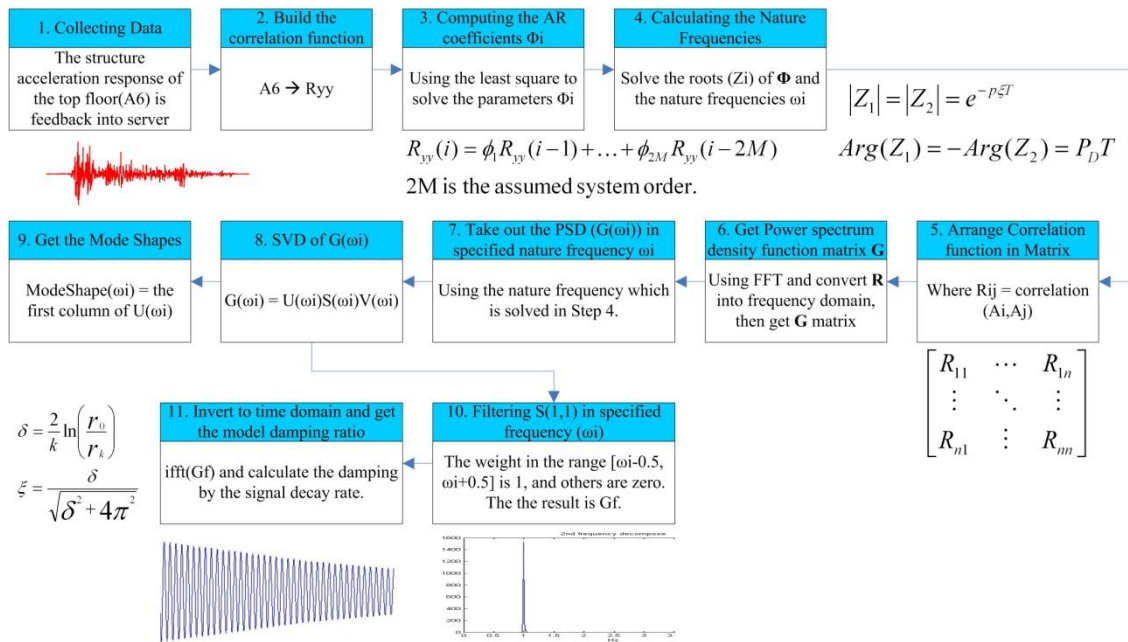


Figure 3.18: The automotive analysis flow chart of AR & FDD method.

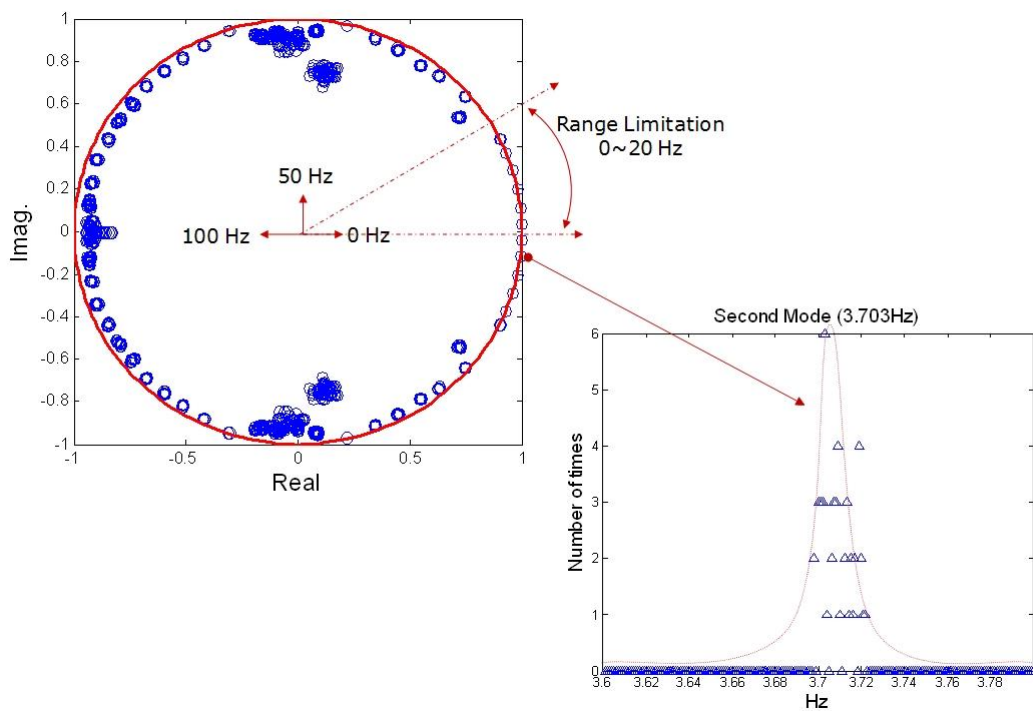


Figure 3.19: The modal frequency selector of AR analysis.

Data-Driven Stochastic Subspace Identification (Data-Driven SSI)

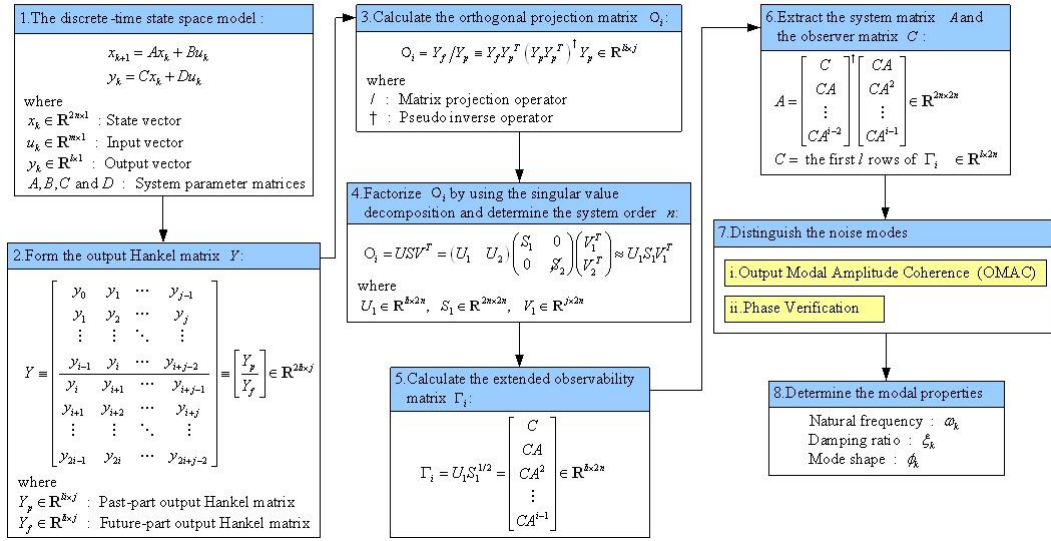
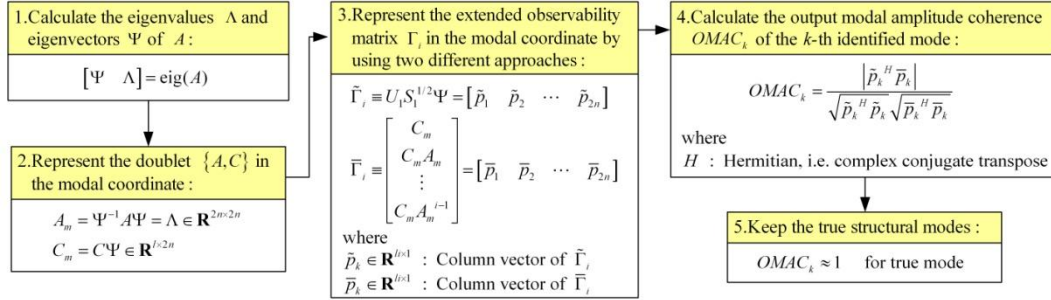


Figure 3.20: The analysis flow chart of data-driven SSI method.

i. Output Modal Amplitude Coherence (OMAC)



ii. Phase Verification

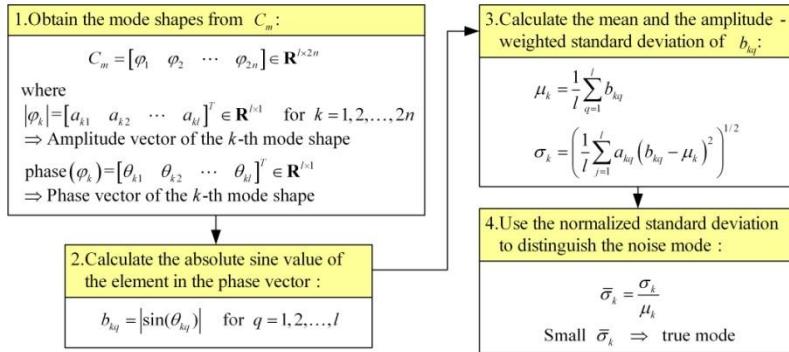


Figure 3.21: The criteria of mode selector of SSI method.

Experimental Results: Through the setup of wireless continuous monitoring system on the new CE research building, the ambient vibration data of the building was collected wirelessly every eight hours. Modal parameters of the building are determined from the velocity signals of ambient vibration. The AR method, FDD method and SSI method are applied to estimate the building natural frequencies and mode shapes. The direct Fourier amplitude spectrum was also calculated directly from the recorded data. For the least-square AR method the order is assigned as 70 and a total of 12,000 samples (with 0.005 sec per sample) were used to extract the modal parameters. For the SSI method the data length is 5000 sample points and the selected Nrow is 30. During the transmission of data the server will display the status of data collection in Wireless Monitoring Module on the screen, as shown in *Figure 3.22*. If error message was shown a check and pass scheme will operate. The operation procedure had been shown in *Figure 3.16*. Based on the established analysis module the following results are generated:

1. Fourier amplitude spectrum of each floor in both longitudinal and transverse directions,
2. Identified system natural frequencies and damping ratios,
3. Generate mode shapes of the building structure in both longitudinal and transverse directions,

Figure 3.23 shows the Fourier amplitude spectrum as well the identified system natural frequencies and damping ratios of the building based on the measurement directions. The fundamental natural frequency in longitudinal direction is 1.75Hz and in transverse direction is 1.46Hz. The identified mode shapes in longitudinal direction is shown in **Figure 3.24**. Comparison on the identified mode shapes among SSI method, FDD method and direct Fourier Transform is also shown in this figure. For the higher mode the discrepancy among the three methods is quite significant. Further study is needed. It has to point out that based on the implemented software the above mentioned analytical results can be generated for each set of measurement.

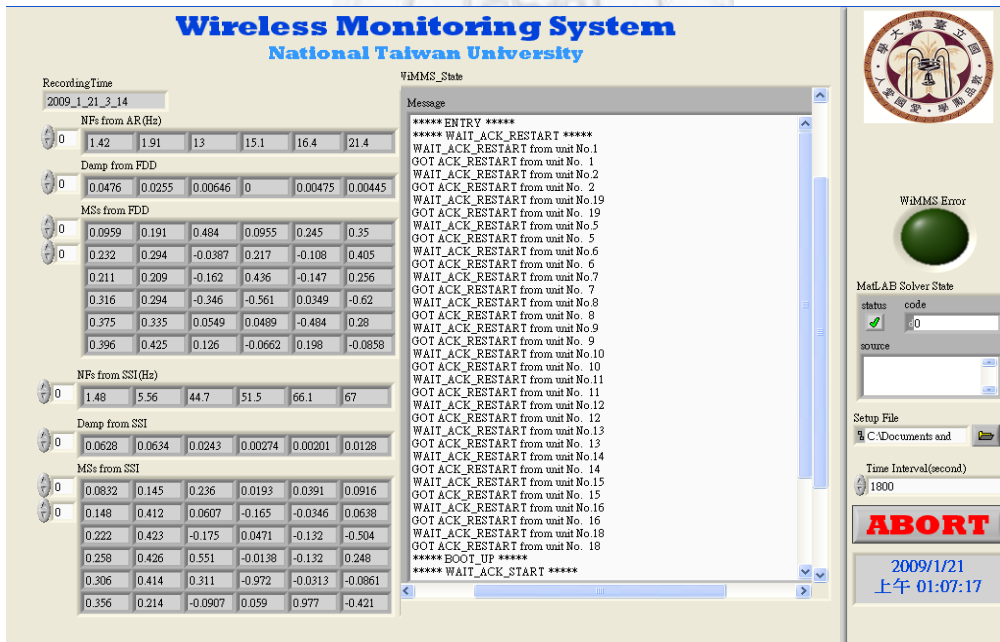


Figure 3.22: Display the status of data collection in Wireless Monitoring Module on the screen

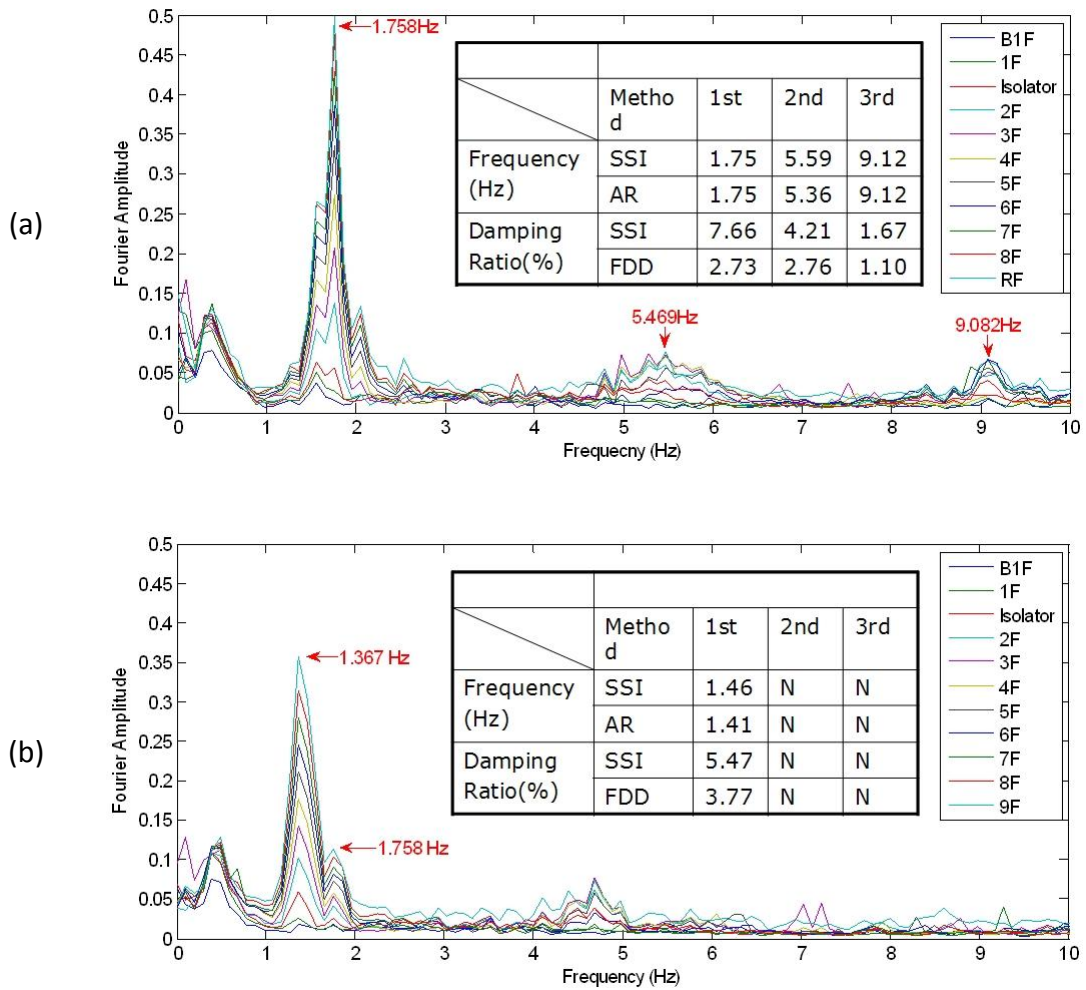


Figure 3.23: Fourier amplitude spectrum from the recorded ambient vibration data of the CE research building in both longitudinal (a) and transverse (b) direction. The identification natural frequencies and damping ratios from SSI method is also shown.

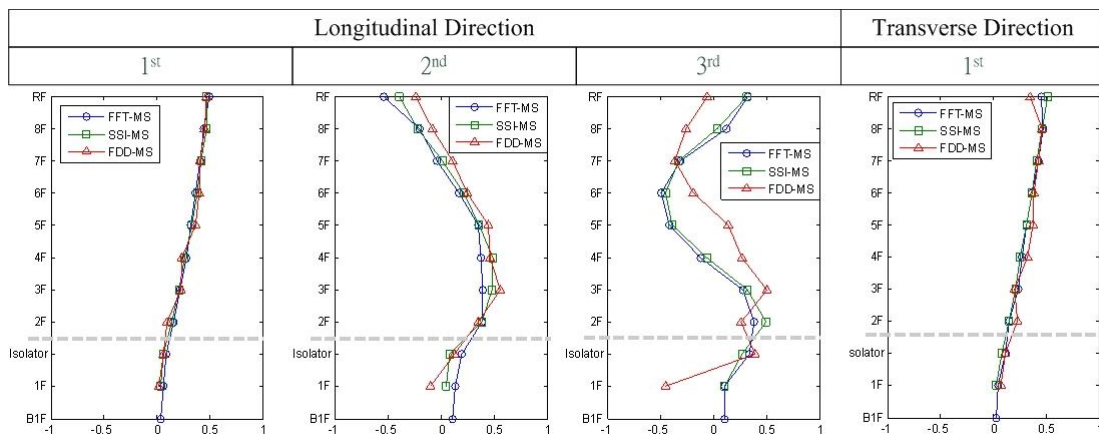


Figure 3.24: Identified mode shapes from three different methods: FFT, FDD and SSI.

3.2.4 Field experiment at Niudou Bridge during typhoon FANAPI

period

Niudou Bridge crosses the Lanyang River and is located in Sanxing Township, Yilan County, Taiwan. Niudou Bridge is a dangerous bridge with serious foundation soil scouring. The bridge is a simple supported bridge with 7 spans and 6 piers; the length of deck in each span is 36.5m and the total length of this bridge is 256m; the width of this bridge is 5m.

FANAPI is a medium-strength typhoon; its center made landfall in the Hualien area and its storm hit Taiwan during 9/19~9/21, 2010. The typhoon's outer bands gave rise to extremely heavy rain at east and southeast of Taiwan, and Lanyan River was swollen with this extremely heavy rain.

The objective of this field experiment is to collect the structural responses of Niudou Bridge under serious flood loading to realize the foundation soil scouring and the flood loading induced structural vibration characteristics. In recent years, the torrential rain induced deluge damages the structural safety of cross-river bridges; the health monitoring and damage detection of bridge are of great urgency. The pioneer step to study this issue is to collect and observe the signals of structural responses under flood loading. Smart Sensing System was adopted in this experiment and provided an easy and effective way to collect structural responses during typhoon period. Both the

software and hardware development of Smart Sensing System is introduced in *Chapter 2*.

Instrumentation of Smart Sensing System on Niudou Bridge: The challenge of this experiment is to get the bridge responses with harsh climate and establish a data base includes the responses under normal condition, flood loading condition and damage condition. Smart Sensing System is applied in this experiment to perform a portable structural monitoring system.

As it is impossible to predict which bridge will meet with the flood loading during the future typhoon. Two dangerous bridges are selected in this experiment; they are Bai-bu-fan Bridge in Taichung County and Niudou Bridge in Yilan County. The plan of this experiment includes two stages. First stage establishes the reference data through the routinely ambient measurements before typhoon season; second stage collects the flood loading structural responses during typhoon period. Fortunately, typhoon FANAPI hit Taiwan during 9/19~9/21, 2010 and swelled the water level of Niudou Bridge (Lanyan River). The following introduction will take Niudou Bridge as example.

The concept and instrumentation of portable structural monitoring system which is performed by Smart Sensing System is shown in *Figure 3.25*. There are totally 5 NTU-WSU units installed on the 2nd to 6th deck of Niudou Bridge and a local site (Host Node) is installed on this bridge. Each NTU-WSU connects with 2 ambient sensors to

measure the vertical and transverse vibrations at the middle point of deck, and totally 10 ambient sensors are installed on this bridge. The site of Niudou Bridge is covered with the signal of 3G Mobile Internet (Chunghwa Telecom) and the signal strength is about 30%. The position of user node is not limited; in this experiment the user node is a laptop and is installed in a hotel. **Figure 3.25** shows that the structural responses are routinely collected by NTU-WSU (WSU1 ~ WSU5), and all of these responses are feedback to local site (Host Node) and stored in the flash memory of Host Node. Host Node connects to internet through 3G mobile router and allows remote user to download these collected structural responses.

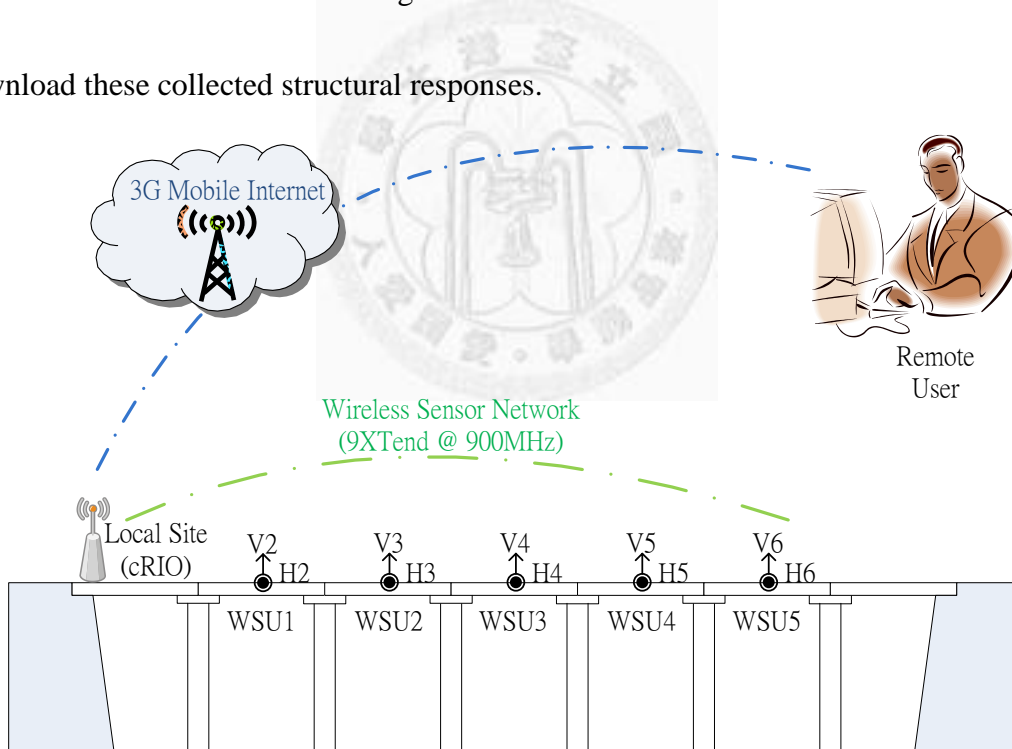


Figure 3.25: the concept and instrument of Smart Sensing System on Niudou Bridge

This system is installed before the land warning of FANAPI is issued, and continuous collects the structural responses of Niudou Bridge during the typhoon period.

The system is set to collect data 15minutes per-time and each time records 15000pts (@ 200Hz) structural responses, these data is saved as a MS EXCEL file which is named with current time and date. Through Internet, remote user can observe the system statuses and the recorded data in office which is safe during this typhoon.



Figure 3.26: The photo of Smart Sensing System on Niudou Bridge

Figure 3.26 shows the photo of Smart Sensing System on Niudou Bridge; **Figure 3.26(a)** shows that Sensing Node installed on the deck of Niudou Bridge, **(b)** shows the Host Node, **(c)** shows the contents of Sensing Node which includes a NTU-WSU, two VSE-15D sensors and a Li battery (supply over 3 days with full loading of Sensing Node); a acrylic housing with alumni plate is used to protect Sensing Node and is mounted on the deck. **Figure 3.26 (d)** shows the serious flood acting on the foundation

of Niudou Bridge. The detail of Sensing Node and Host Node is shown in *Figure 3.27*.

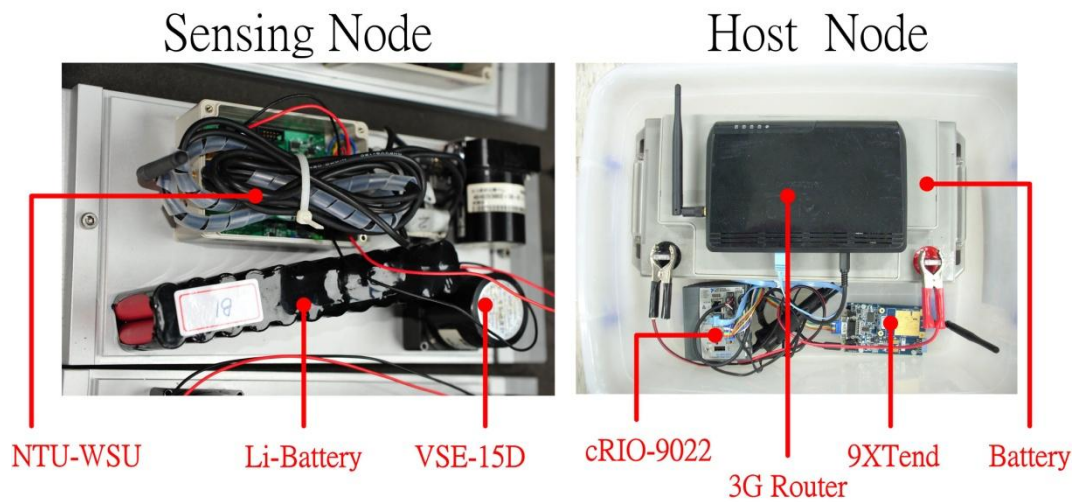


Figure 3.27: The detail on Sensing Node and Host Node

Experiment Results and Discussion: Smart Sensing System is applied on this experiment successfully, and the system performances of Smart Sensing System are also verified. These results are listed as below.

The robustness of NTU-WSU is verified through this operation with harsh climate. During FANAPI typhoon period, the close perfect operation of Smart Sensing System shows the effort on software and hardware design of Smart Sensing System; the system worked correctly without any human maintain on the bridge during typhoon period (ex. system reset or replace battery). The only defect is the poor strength of 3G Mobile Internet at Niudou Bridge. The poor strength of mobile Internet reduces the communication data rate and requires more time to download data (about 10 minutes/per-time). This problem will be improved in the future through the maturity

construction of mobile internet.

The structural responses of Niudou Bridge are collected from 9/19 ~ 9/21 and the reference data base is also established before FANAPI typhoon. Base on these data, **Figure 3.28** shows a roughly results on RSSI analysis which is performed by Dr. J.H. Weng who is also included in this project. In this figure, the response data includes 4/8, 6/9, 7/23 and the typhoon period of FANAPI. The RSSI results show that the frequencies of Niudou Bridge were changed during typhoon period. More advanced results will depend on the future efforts of signal extraction and processing.

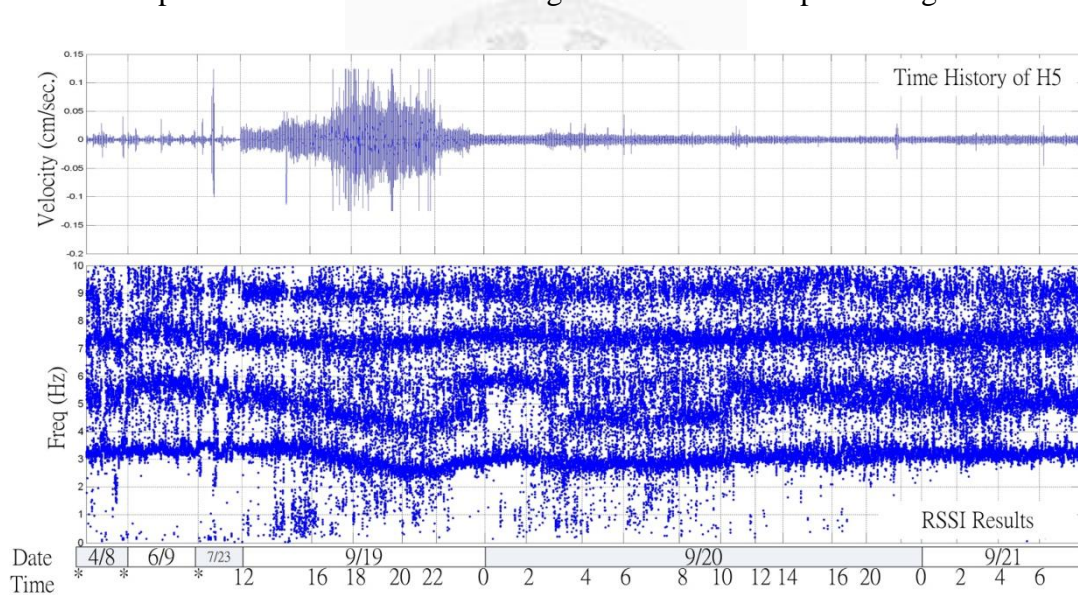


Figure 3.28: The time history of H5 and the analysis results of RSSI

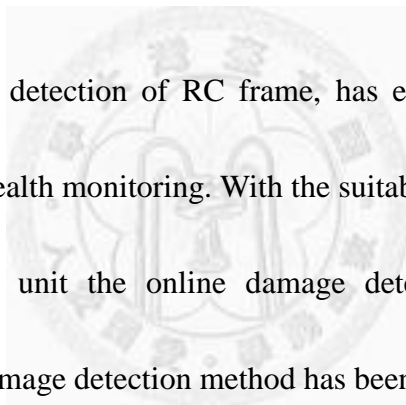
3.3 Summary

The purpose of Gi-Lu Bridge experiment is to conduct an ambient vibration survey of a long-span cable-stayed bridge and to develop a systematic method for the extraction of the dynamic characteristics of the bridge using data collected by the wireless monitoring system. The following conclusions are drawn from the full-scale measurements made on the Gi-Lu Bridge:

1. The wireless sensing units were used in lieu of more costly tethered data acquisition systems. Less effort and man-power were required during the installation of the wireless monitoring system rendering it as ideally suited for rapid short-term field studies. Because the wireless communication range in the open field can reach up to 300 m, it was possible to successfully collect data from at least 10 sensors (in this study) simultaneously with a sampling rate of 100 Hz. During data collection, the wireless monitoring system experienced no data loss as a result of a highly robust communication protocol.
2. The measurement of structural response to ambient levels of wind and traffic has proved to be an effective means of identifying the dynamic properties of a full-scale cable-stayed bridge. The dynamic properties that have been identified from these measured responses are modal frequencies, mode shapes and estimates of modal damping ratios.

3. To autonomously extract the dynamic characteristics of the bridge from structural response time histories, two different approaches were used: the SSI method and the FDD method. Detail description on the time domain dynamic characteristic identification using multiple output identification (SSI method) can extract the mode shape directly. The SSI method can provide a good estimation of the number of modes observed in the structure based on singular values of the Hankel matrix projection. On the other hand, the FDD method can only be applied in the frequency domain if the dominant frequencies are determined a priori.
4. The results of this test have provided conclusive evidence of the complex dynamic behavior of the bridge. The dynamic response of the cable-stayed bridge is characterized by the presence of many closely spaced, coupled modes. For most modes, the analytical and the experimental modal frequencies and mode shapes compare quite well. Based on the analysis of ambient vibration data, it is evident that the vertical vibration of the bridge deck is tightly coupled with the cable vibrations within the frequency range of 0 to 3 Hz.
5. In order to identify the coupling effect between the bridge deck and cables, different instrumentation architectures are adopted (specifically, Test 1, Test 2 and Test 3 in this study). The stochastic subspace identification method provides a very effective way to identify the mode shapes of the structure through the spatially distributed

sensors. It can compress the data while preserving vibration information and also eliminate uncorrelated noise. Through a comparison of the results corresponding to different test setups, separation of dominant frequencies between the bridge deck and cable can be easily identified. As for the damping ratio estimation, the first vibration mode of the deck had a damping ratio of 2.5% on average (depends upon the different sensor locations); the damping values for higher modes are less than 1.0%. More detail study on the estimation of accurate damping ratios is needed in future research.



The research, damage detection of RC frame, has explored the use of wireless sensing unit for structural health monitoring. With the suitable embedded program in the microprocessor of sensing unit the online damage detection of structure can be estimated. The AR-ARX damage detection method has been proved a suitable algorithm within the wireless monitoring system for autonomous execution. To validate the approach, a series of shaking table test of RC frame structure and low level white noise excitation are used, the embedded damage detection algorithm is shown to exhibit sufficient sensitivity to identify damage.

For long-term SHM system, a distributed structural health monitoring system employing wireless sensing system (NTU-WSU_V02) has been developed for the purpose of continuous monitoring and experimentally verified on NTU CE research

building which is a new 8-story mid-floor isolation reinforced concrete building. To realize this monitoring system required various system identification algorithms to be addressed. Middleware services including data acquisition, reliable communication and synchronized sensing. Emphasize in this study is the procedures for error check and pass in this continuous system. The locations of smart sensors can be modified due to the irregularity of the building structure. Integration of different types of sensors can also be used, such as the laser displacement gage for measuring the deformation of isolator, Gill anemometer for measuring the wind speed, etc. Through experimental verification the proposed monitoring system demonstrate the efficacy of the monitoring system developed herein.

The experiment at Niudou Bridge during FANAPI typhoon period demonstrates that Smart Sensing System is fit for field experiment with harsh climate conditions. The efforts on the system design (software and hardware) of Smart Sensing System are proved by this successful experiment. The system layout on Niudou Bridge only takes about 30 minutes, and the strong system robustness makes the system continuous working during FANAPI period which is about three days.

Chapter 4

Smart Structural Control

Smart Structural System includes both sensing and control to mitigate the effects of natural hazards on civil and mechanical infrastructure. Smart Structural Sensing is introduced in *Chapter 2 and 3*. In this chapter, Smart Structural Control is introduced. In general, control system includes three major components, sensor, controller and actuator. The target (controlled structure) is installed with sensors to measure the structural responses; these structural responses are real-time transmitted to the controller to generate the control command; this control command is output to drive actuator to apply force on structure.

Traditionally, structural control system is a centralized control system, the controller is a central computer with control algorithm to acquire structural responses and generate control command. In this operating mechanism, the sensor signals are transmitted to central computer through wired coaxial cables; the central computer runs the control algorithm with these signals to generate the control command. This command is send to actuator through wired coaxial cable. Two important features of this system hamper the real application of civil infrastructure, one is all signals are transmitted through wired coaxial cables which are expensive and difficult to install and maintain; another is the control algorithm requires numerous signals to work out control

command, i.e., an error signal led to the failure on all control commands. The cable wiring is a seriously issue in the real application of civil infrastructure. The number of feedback signals is usually depending on the scale of structure and each feedback signal requires a coaxial cable to connect with controller. When the nodal density is rise up (increasing), the wiring cost is added and the system reliability is dropped. Smart structural control is to find smart ways to avoid these difficulties.

Wireless Control is one of the smart ways. The main idea of wireless control is using the wireless communication technology to replace the traditional wiring of control system. Wireless Control also includes the distributing computation of embedded system with full and partial decentralized control algorithms to improve the computing efficiency and system robustness. This study of wireless control is already performed in 2006 [61].

Base on the passive experiment of wireless control, although the wireless technology makes the control system to be cost down and easy installed by reducing wiring, but the signal reliability and real-time feedback are big challenges on wireless communication technology. This chapter provides another concept of Smart Structural Control which is to develop a standard alone device to perform structural control and this device is called Smart Control Device [62]. Smart Control Device is a control device which integrates sensor, controller and actuator; this device is standard alone

working without any coupling with other system and only requires local feedback to complete the control procedure. The control algorithm of Smart Control Device is decentralized sliding mode control (DSMC) [63] which is one of the decentralized control algorithm and only requires lightly computing.

In software (control algorithm), decentralized sliding mode control is developed to meet the requirements of smart structural control and the theory formulation is presented in *Section 4.1*. Decentralized control algorithm includes two concepts, distributed computation and local measurement. Distributed computation means the control command can be solved individually on local system; local measurement means that only local (near to actuator) response is required to be the input of control algorithm to calculate the local control command.

In hardware (control device), a newly designed platform, Smart Control Device, is used to work with decentralized sliding mode control algorithm to implement the decentralized control on civil infrastructure and it's an embedded system integrates with sensor, controller and actuator. The design of Smart Control Device is presented in *Section 4.2*.

The experiment studies of decentralized sliding mode control algorithm and the system evaluation of Smart Control Device is presented in *Section 4.3*.

4.1 Decentralized Sliding Mode Control

Several decentralized sliding mode control algorithms are developed in this chapter specifically for applications of MR dampers in building structures. Various control algorithms are used for this semi-active control studies, including the proposed decentralized sliding mode control (DSMC), LQR control, and passive-on and passive-off control. Each control algorithm is formulated specifically for the use of MR dampers installed in building structures. Additionally, each algorithm uses measurements of the device velocity and device drift for the determination of the control action to ensure that the algorithm can be implemented in a physical structure. The performance of each algorithm is evaluated based on the results of shaking table tests, and the advantages of each algorithm is compared and discussed. The reduction of story drifts and floor accelerations throughout the structure is examined.

The structural control results of shaking table tests for a steel frame structure is presented to evaluate the performance of a number of proposed semi-active control algorithms using multiple magnetorheological (MR) dampers. The test structure is a six-story steel frame equipped with MR-dampers. Four different cases of damper arrangement in the structure are selected for the control study. In experimental tests, an EL Centro earthquake and Kobe earthquake ground motion data, are used as excitations.

4.1.1 Experimental Setup

Test Structure A 1/4-scale 6-story steel frame was designed by the National Center for Research on Earthquake Engineering (NCREE) for this structural control research.

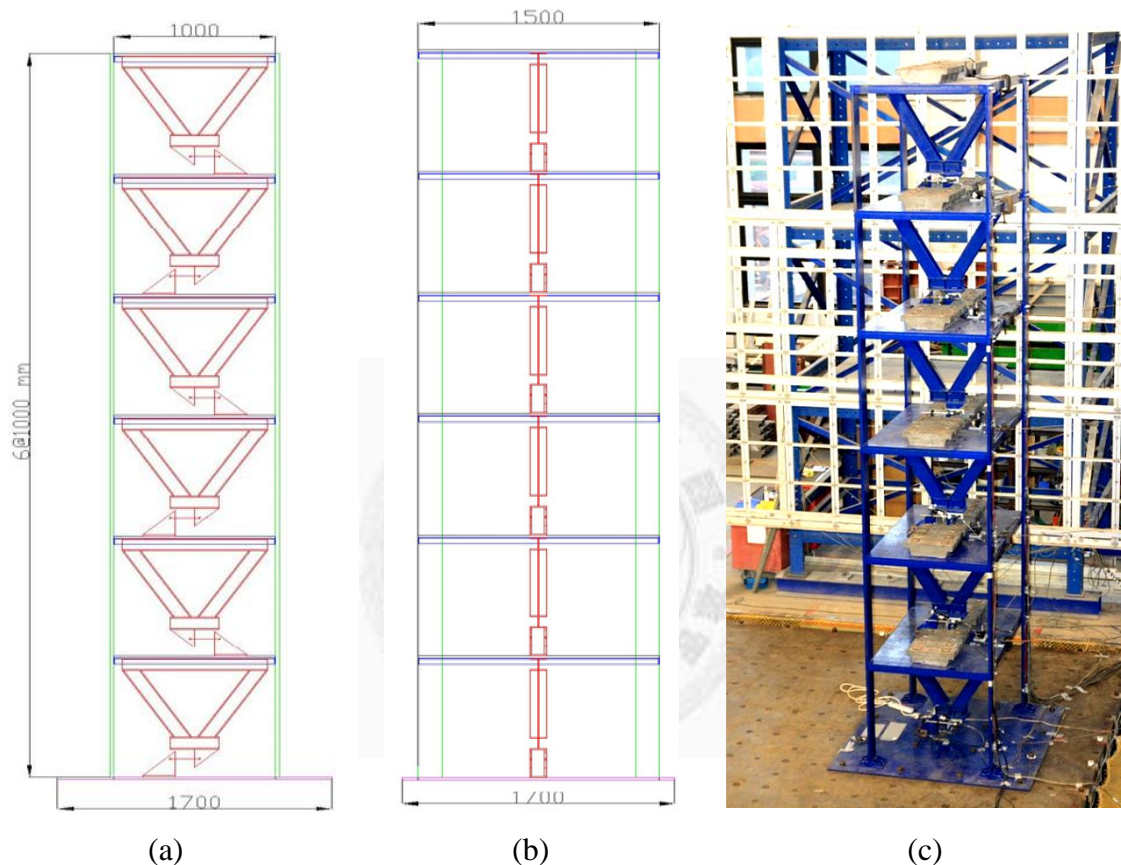


Figure 4.1: (a) & (b) schematic diagrams for side view of 6-story steel frame structure; (c) Photo of the 6-story steel frame structure on NCREE shaking table. The V-shape bracing system is for the installation of damper.

As shown in **Figure 4.1**, the six-story scale-down structure consists of a single bay with a 1.0 m by 1.5 m floor area and 1.0 m story height. The sizes of columns and beams are: Column:150 mm x25 mm (rectangular section), Story height:1000 mm, Floor dimension: 100 mm x 1500 mm, Beam: 50 mm x 50 mm (L-section), Base plate:

1700 mm x 1700 mm. Beam-floor is welded, and both the floor-beam connection and floor-column connection are bolted. Bracing systems for dampers are in bolt connection. Based on the analysis of the low level white noise response data of the structure, the identified first five modal frequencies (using data-driven stochastic subspace identification method [64] are: 1.05 Hz, 3.50 Hz, 6.12Hz, 8.987 Hz and 11.91 Hz and the corresponding modal damping ratios are: 0.2%, 0.99%, 0.09%, 0.79% and 1.86%. The mass, stiffness and damping matrices are shown in **Table 4.1**, which are developed using the finite element model and then are condensed to a 6-story shear-type structure. The detail of bracing is shown in **Figure 4.2**.



Figure 4.2: The detail view on the bracing of 6-story structure

Table 4.1a: Mass matrix of the 6-DOF test structure (Kg)

862.85	0	0	0	0	0
0	862.85	0	0	0	0
0	0	862.85	0	0	0
0	0	0	862.85	0	0
0	0	0	0	862.85	0
0	0	0	0	0	803.98

Table 4.1b: Stiffness matrix of the 6-DOF test structure (N/m)

3.35E+06	-1.87E+06	3.83E+05	-52340	6938.4	-57.82
-1.87E+06	2.98E+06	-1.82E+06	3.76E+05	-51259	6642.4
3.83E+05	-1.82E+06	2.97E+06	-1.82E+06	3.74E+05	-42277
-52340	3.76E+05	-1.82E+06	2.97E+06	-1.80E+06	3.16E+05
6938.4	-51260	3.74E+05	-1.80E+06	2.84E+06	-1.37E+06
-57.82	6642.4	-42277	3.16E+05	-1.37E+06	1.09E+06

Table 4.1c: Damping matrix of the 6-DOF test structure (N/(m/s))

2332.4	-1248.5	256.12	-34.968	4.6355	-0.03863
-1248.5	2085.7	-1214.8	251.51	-34.246	4.4378
256.12	-1214.8	2081	-1213.9	249.66	-28.245
-34.968	251.51	-1213.9	2079.4	-1202.2	211.01
4.6355	-34.247	249.66	-1202.2	1992.3	-914.02
-0.03863	4.4378	-28.245	211.01	-914.02	815.43

MR Damper: In the experiment, the 3kN MR dampers are selected as actuators (semi-active actuators) for this structure. It is a LOAD MR damper (RD 1005-3). The maximum input current (instant value) on the damper is 2.0 Amp. For this particular damper the maximum voltage of 0.8 Volts is corresponding to 1.5 Amps. The V-shape bracing system is added in each story to provide support for the damper installation. The maximum stroke of the damper is ± 20 mm. To install the damper, it is required to

apply a 50 N pre-stress on the damper to re-center it. In the performance test the damper was excited with random stroke (with maximum 15 mm as constraint) under the constant voltage and the results are used to develop the theoretical model of the damper.

The performance test result of the 3kN damper is shown in **Figure 4.3**.

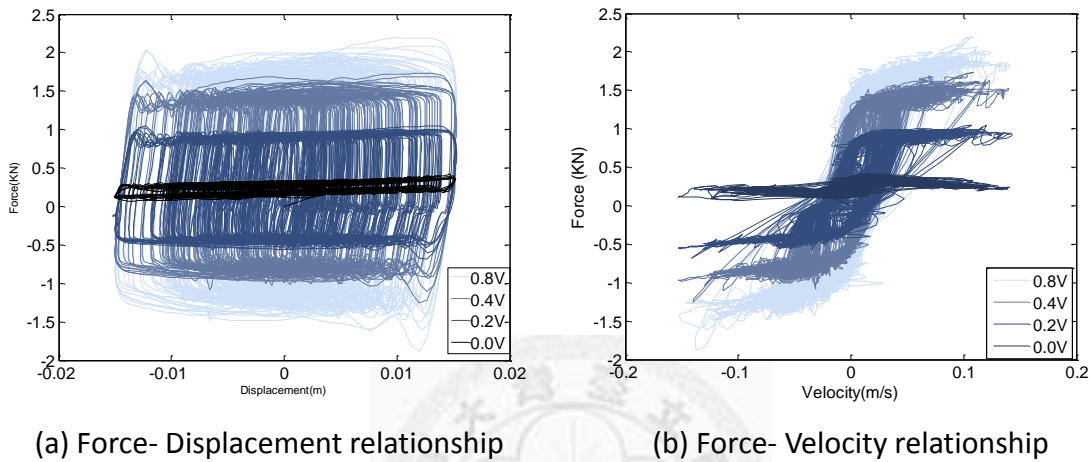


Figure 4.3: Performance test of the 3kN MR damper for four different voltage

Figures 4.3a and **4.3b** shows the force-displacement and force-velocity relationships of the damper for different applied voltages, respectively. The Bouc-Wen model is selected and used to simulate the inelastic behavior of the MR-damper. The damper force is defined as:

$$\text{DamperForce} = Z(k) + \theta_0 \dot{x}_i(k) \quad (4.1)$$

Where

$$\begin{aligned} Z(k) = & Z(k - 1) \\ & + (\theta_1 \dot{x}_i(k) + \theta_2 |\dot{x}_i(k)| Z(k - 1) + \theta_3 \dot{x}_i(k) |Z(k - 1)| \\ & + \theta_4 |\dot{x}_i(k)| |Z(k - 1)| Z(k - 1) + \theta_5 \dot{x}_i(k) |Z(k - 1)|^2) dt \end{aligned} \quad (4.2)$$

And $\theta_1 \sim \theta_5$ are model parameters which are voltage dependent, as shown in **Table 4.2**.

The damper force depends not only on the velocity but also on the voltage.

Table 4.2: Voltage dependent parameters of the model of MR damper

	θ_0	θ_1	θ_2	θ_3	θ_4	θ_5
0.0 Volt	0.5	62.2	-767.6	-333.2	-96.8	-63.8
0.2 Volt	1.6375	734.11	-690.23	-216.99	-429.74	-267.34
0.4 Volt	2.775	1195.3	-468.87	-15.272	-558.87	-365.76
0.6 Volt	3.3875	1289.3	-290.03	128.77	-543.98	-375.22
0.8 Volt	3.5625	1290.6	-231.27	174.48	-528.88	-372.32

If the i^{th} damper is installed in the k_i^{th} story unit, then the control force u_i from the i^{th} damper is a function of the drift x_{ki} and the drift velocity \dot{x}_{ki}

$$u_i = u_i(\rho_i, x_{ki}, \dot{x}_{ki}) \quad (4.3)$$

where ρ_i is the voltage of the MR damper. The capacity of the MR damper is regulated by the voltage that is bounded by

$$0 \leq \rho_{i,\min} \leq \rho_i \leq \rho_{i,\max} \quad (4.4)$$

The damper force from the MR damper can be regulated in real-time operation simply by issuing a command voltage between 0 to 0.8 Volts. For this 3kN MR damper, $\rho_{\min} = 0.0$ Volt and $\rho_{\max} = 0.8$ Volt are defined. The damper in each story can be arranged either active or inactive (disconnected with the bracing system) depending on the selected control method.

In this research, four different damper layouts (configurations) in the building

structure are studied as shown in the following four cases:

Case A: Damper is installed on the 1st floor,

Case B: Damper is installed on 1st and 3rd floors,

Case C: Damper is installed on 1st, 2nd and 3rd floors,

Case D: Damper is installed on 1st, 3rd and 5th floors,

Figure 4 shows the sketch of damper layouts (configurations) in the structure.

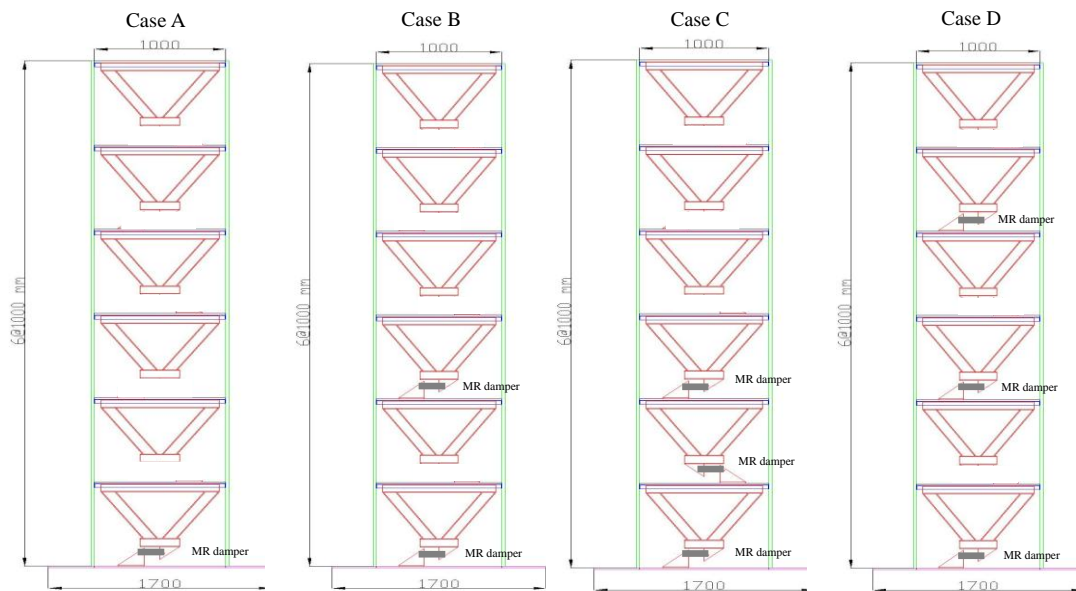


Figure 4.4: Four different cases of MR damper locations (layouts) in the test frame; (i) damper located on 1st floor, (ii) dampers located on the 1st and 3rd floors, (iii) dampers located on the 1st, 2nd and 3rd floors, (iv) dampers located on the 1st, 3rd, and 5th floors.

System Equation of Motion: Consider a general n-degree-freedom building structure subject to a one-dimensional earthquake ground acceleration \ddot{X}_0 . The vector equation of motion is given by

$$\mathbf{M}\ddot{\mathbf{X}}(t) + \mathbf{C}\dot{\mathbf{X}}(t) + \mathbf{K}\mathbf{X}(t) = \mathbf{H}\mathbf{U}(t) + \boldsymbol{\eta}\ddot{\mathbf{x}}_0(t) \quad (4.5)$$

Where $\mathbf{X}(t) = [x_1(t) \ \cdots \ x_n(t)]^T$ is an n -vector with $x_i(t)$ being the i^{th} story drift; $\mathbf{U}(t) = [u_1(t) \ \cdots \ u_r(t)]^T$ is an r -vector consisting of r control forces; \mathbf{H} is a $(n \times r)$ matrix denoting the location of r controllers; and $\boldsymbol{\eta}$ is an n -vector denoting the influence of the earthquake excitation. In Equation (4.5), \mathbf{M} , \mathbf{C} and \mathbf{K} are $(n \times n)$ mass, damping and stiffness matrices, where Rayleigh damping is assumed for the structure.

In the state space representation, Equation (4.5) becomes

$$\dot{\mathbf{Z}}(t) = \mathbf{A}\mathbf{Z}(t) + \mathbf{B}\mathbf{U}(t) + \mathbf{E}(t) \quad (4.6)$$

where $\mathbf{Z}(t)$ is a $2n$ state vector; \mathbf{A} is a $(2n \times 2n)$ system matrix; \mathbf{B} is a $(2n \times r)$ matrix; and $\mathbf{E}(t)$ is a $2n$ excitation vector given, respectively, by

$$\begin{aligned} \mathbf{Z}(t) &= \begin{bmatrix} \mathbf{X}(t) \\ \dot{\mathbf{X}}(t) \end{bmatrix}; \quad \mathbf{E}(t) = \begin{bmatrix} \mathbf{0} \\ \mathbf{M}^{-1}\boldsymbol{\eta} \end{bmatrix} \ddot{\mathbf{x}}_0(t); \\ \mathbf{A} &= \begin{bmatrix} \mathbf{0} & \mathbf{I} \\ -\mathbf{M}^{-1}\mathbf{K} & -\mathbf{M}^{-1}\mathbf{C} \end{bmatrix}; \quad \mathbf{B}(t) = \begin{bmatrix} \mathbf{0} \\ \mathbf{M}^{-1}\mathbf{H} \end{bmatrix} \end{aligned} \quad (4.7)$$

For this particular 6-story building structure for Case D (dampers installed on 1st, 3rd and 5th floors), the mass matrix \mathbf{M} , stiffness matrix \mathbf{K} , location matrix of controllers \mathbf{H} , and influence excitation vector $\boldsymbol{\eta}$ in Equation (4.5) can be expressed as follows:

$$\mathbf{M} = \begin{bmatrix} m_1 & 0 & 0 & 0 & 0 & 0 \\ m_2 & m_2 & 0 & 0 & 0 & 0 \\ m_3 & m_3 & m_3 & 0 & 0 & 0 \\ m_4 & m_4 & m_4 & m_4 & 0 & 0 \\ m_5 & m_5 & m_5 & m_5 & m_5 & 0 \\ m_6 & m_6 & m_6 & m_6 & m_6 & m_6 \end{bmatrix}; \quad \mathbf{H} = \begin{bmatrix} 1 & 0 & 0 \\ 0 & -1 & 0 \\ 0 & 1 & 0 \\ 0 & 0 & -1 \\ 0 & 0 & 1 \\ 0 & 0 & 0 \end{bmatrix}; \quad (4.8)$$

$$\mathbf{K} = \begin{bmatrix} K_1 & -K_2 & 0 & 0 & 0 & 0 \\ 0 & K_2 & -K_3 & 0 & 0 & 0 \\ 0 & 0 & K_3 & -K_4 & 0 & 0 \\ 0 & 0 & 0 & K_4 & -K_5 & 0 \\ 0 & 0 & 0 & 0 & K_5 & -K_6 \\ 0 & 0 & 0 & 0 & 0 & K_6 \end{bmatrix}; \boldsymbol{\eta} = \begin{bmatrix} -m_1 \\ -m_2 \\ -m_3 \\ -m_4 \\ -m_5 \\ -m_6 \end{bmatrix}$$

where m_i ($i=1\sim 6$) is the lumped mass on each floor and K_i ($i=1\sim 6$) is the stiffness of i -th story.

4.1.2 Decentralized Sliding Mode Control Algorithm

Let the i^{th} damper be installed in the k_i^{th} story unit and let r be the total number of dampers (actuators) in the building. The theory of sliding mode control (SMC) is to design controllers to drive the response trajectory into the sliding surface, whereas the motion on the sliding surface is stable. For linear structures, the r -dimensional sliding surface $\mathbf{S} = \mathbf{0}$ for r controllers (dampers) can be a linear combination of the state variables, i.e.

$$\mathbf{S} = \mathbf{PZ} = \mathbf{0} \quad (4.9)$$

where \mathbf{S} is a r -vector consisting of r sliding variable, i.e.,

$$\mathbf{S} = [S_1 \quad S_2 \quad \dots \quad S_r]^T \quad (4.10)$$

and

$$\mathbf{P} = [\mathbf{P}_1^T \quad \mathbf{P}_2^T \quad \dots \quad \mathbf{P}_r^T]^T = (r \times 2n) \text{ matrix} \quad (4.11)$$

$$\begin{aligned} \mathbf{Z} &= [Z_1 \quad Z_2 \quad \dots \quad Z_n \quad Z_{n+1} \quad Z_{n+2} \quad \dots \quad Z_{2n}]^T \\ &= [X_1 \quad X_2 \quad \dots \quad X_n \quad \dot{X}_1 \quad \dot{X}_2 \quad \dots \quad \dot{X}_n]^T \end{aligned} \quad (4.12)$$

In Equations(4.8)~(4.11), X_i is the i^{th} inter-story drift, r is the total number of actuator (damper), n is the total number of DOFs, \mathbf{P} is a $(r \times 2n)$ matrix to be designed such that the motion on the sliding surface, $\mathbf{S}=0$, is stable, and \mathbf{P}_i is the i^{th} row vector of \mathbf{P} with a dimension of $2n$. For the decentralized SMC, the i^{th} sliding variable S_i for the i^{th} damper is chosen as a function of X_{ki} and \dot{X}_{ki} , i.e.,

$$S_i = \alpha_{ki}X_{ki} + \dot{X}_{ki} = 0 \quad (4.13)$$

where $-\alpha_{ki}$ is the pole of the sliding surface. For the motion to be stable on the sliding surface, α_{ki} should be positive, i.e., $\alpha_{ki} > 0$. Consequently, it follows from Equation (4.9) and (4.13) that \mathbf{P}_i , the i^{th} row-vector of \mathbf{P} , is given by

$$\mathbf{P}_i = [0 \quad 0 \quad \dots \quad \alpha_{ki} \quad 0 \quad 0 \quad \dots \quad 1 \quad 0 \quad 0 \quad \dots \quad 0], \text{ for } i = 1, 2, \dots, r \quad (4.14)$$

where the elements “ α_{ki} ” and “1” are at the locations of ki and $ki+n$, respectively.

Based on the sliding mode control, the Lyapunov function is expressed as

$$V = \frac{1}{2} \mathbf{S}^T \mathbf{S} \quad (4.15)$$

The derivative of the Lyapunov function is obtained using Equation (4.9) and (4.6) as

$$\dot{V} = \mathbf{S}^T \dot{\mathbf{S}} = \mathbf{S}^T \mathbf{P} \dot{\mathbf{Z}} = \mathbf{S}^T (\mathbf{PB}) [\mathbf{U} + (\mathbf{PB})^{-1} \mathbf{P} (\mathbf{AZ} + \mathbf{E})] \quad (4.16)$$

Let

$$\boldsymbol{\lambda} = \mathbf{S}^T \mathbf{PB} \text{ and } \mathbf{G} = -(\mathbf{PB})^{-1} \mathbf{P} (\mathbf{AZ} + \mathbf{E}) \quad (4.17)$$

Then, it follows from Equation (4.15) that

$$\dot{V} = \boldsymbol{\lambda} (\mathbf{U} - \mathbf{G}) = \sum_{i=1}^r \lambda_i u_i - \sum_{i=1}^r \lambda_i G_i = \dot{V}_1 + \dot{V}_0 \quad (4.18a)$$

$$\dot{V}_1 = \boldsymbol{\lambda} \mathbf{U} = \sum_{i=1}^r \lambda_i u_i; \quad \dot{V}_0 = -\boldsymbol{\lambda} \mathbf{G} = -\sum_{i=1}^r \lambda_i G_i \quad (4.18b)$$

where u_i = control force from the i^{th} damper. In Equation (4.18), λ_i is the i^{th} element of $\boldsymbol{\lambda}$ vector (r -vector) and G_i is the i^{th} element of the r -column vector \mathbf{G} . Note that \dot{V}_0 is the derivative of the Lyapunov function for the structure without control (i.e., $u_i = 0$). Since the structure without control is stable, we have $\dot{V}_0 \leq 0$. Therefore, to design the control force, it is necessary to guarantee that $\dot{V}_1 \leq 0$. Based on this concept, four different decentralized sliding mode control strategies (DSMC) are proposed in the following.

SMC1 Control Strategy:

To design a sliding mode controller for $\dot{V}_1 \leq 0$, one possible design is obtained by minimizing $\dot{V}_1 = \sum_{i=1}^r \lambda_i u_i$ in Equation (18). Supposed each story is installed with one damper, i.e., $n = r = 6$. The vector $\boldsymbol{\lambda}$ in Equation (4.17) can be expanded as follows:

$$\boldsymbol{\lambda} = \mathbf{S}^T \mathbf{P} \mathbf{B}$$

$$= \begin{bmatrix} \frac{1}{m_1} [(\alpha_1 Z_1 + Z_7) - (\alpha_2 Z_2 + Z_8)] \\ \frac{-1}{m_1} [(\alpha_1 Z_1 + Z_7) - (\alpha_2 Z_2 + Z_8)] + \frac{1}{m_2} [(\alpha_2 Z_2 + Z_8) - (\alpha_3 Z_3 + Z_9)] \\ \frac{-1}{m_2} [(\alpha_2 Z_2 + Z_8) - (\alpha_3 Z_3 + Z_9)] + \frac{1}{m_3} [(\alpha_3 Z_3 + Z_9) - (\alpha_4 Z_4 + Z_{10})] \\ \frac{-1}{m_3} [(\alpha_3 Z_3 + Z_9) - (\alpha_4 Z_4 + Z_{10})] + \frac{1}{m_4} [(\alpha_4 Z_4 + Z_{10}) - (\alpha_5 Z_5 + Z_{11})] \\ \frac{-1}{m_4} [(\alpha_4 Z_4 + Z_{10}) - (\alpha_5 Z_5 + Z_{11})] + \frac{1}{m_5} [(\alpha_5 Z_5 + Z_{11}) - (\alpha_6 Z_6 + Z_{12})] \\ \frac{-1}{m_5} [(\alpha_5 Z_5 + Z_{11}) - (\alpha_6 Z_6 + Z_{12})] + \frac{1}{m_6} (\alpha_6 Z_6 + Z_{12}) \end{bmatrix}^T \quad (4.19)$$

Note that the notations defined previously are $n=6$, $Z_i = X_i$ and $Z_{i+6} = \dot{X}_i$. Further, the

row vector λ is different depending on the damper layout as follows:

Case A structure:

$$\lambda = \frac{1}{m_1} (\alpha_1 Z_1 + Z_7) \quad (4.20)$$

Case B structure:

$$\lambda = \begin{bmatrix} \frac{1}{m_1} (\alpha_1 Z_1 + Z_7) \\ \left(\frac{1}{m_1} + \frac{1}{m_2} \right) (\alpha_3 Z_3 + Z_9) \end{bmatrix}^T \quad (4.21)$$

Case C structure:

$$\lambda = \begin{bmatrix} \frac{1}{m_1} [(\alpha_1 Z_1 + Z_7) - (\alpha_2 Z_2 + Z_8)] \\ \frac{-1}{m_1} [(\alpha_1 Z_1 + Z_7) - (\alpha_2 Z_2 + Z_8)] + \frac{1}{m_2} [(\alpha_2 Z_2 + Z_8) - (\alpha_3 Z_3 + Z_9)] \\ \frac{-1}{m_2} [(\alpha_2 Z_2 + Z_8) - (\alpha_3 Z_3 + Z_9)] + \frac{1}{m_3} (\alpha_3 Z_3 + Z_9) \end{bmatrix}^T \quad (4.22)$$

Case D structure:

$$\lambda = \begin{bmatrix} \frac{1}{m_1} (\alpha_1 Z_1 + Z_7) \\ \left(\frac{1}{m_1} + \frac{1}{m_2} \right) (\alpha_3 Z_3 + Z_9) \\ \left(\frac{1}{m_4} + \frac{1}{m_5} \right) (\alpha_5 Z_5 + Z_{11}) \end{bmatrix}^T \quad (4.23)$$

Hence, the minimization of $\dot{V}_1 = \sum_{i=1}^r \lambda_i u_i$ depends on the signs of λ_i and u_i . If the λ_i value is positive, then a minimum command voltage needs to be selected (equivalent to a minimum control force u_i) to ensure the minimum \dot{V}_1 . On the contrary if the λ_i value is negative, a maximum command voltage (equivalent to a maximum control force u_i) will be selected to ensure the minimum \dot{V}_1 . Based on the above-mentioned

criteria, the following control law is proposed:

- (1) If $\lambda_i > 0$ and $Z_{ki+n} > 0$, then $\rho_i = \rho_{i,\min}$
- (2) If $\lambda_i > 0$ and $Z_{ki+n} < 0$, then $\rho_i = \rho_{i,\max}$
- (3) If $\lambda_i < 0$ and $Z_{ki+n} > 0$, then $\rho_i = \rho_{i,\max}$
- (4) If $\lambda_i < 0$ and $Z_{ki+n} < 0$, then $\rho_i = \rho_{i,\min}$

(4.24)

This SMC1 control algorithm is to assure the minimization of \dot{V}_1 and determine the command voltage for the damper as for the damper lock up [65] will be discussed later. Based on this SMC1 control strategy for Cases A, B and D Structures, using Equation (4.20), (4.21) and (4.23), only relative story velocity and story drift measurements from the story where the damper is located are required. For Case C structure, the measurements for the responses of the lower three stories are needed, but not the full-state. Further discussion will be made for the SMC3 control strategy later. Note that the i^{th} damper is installed in the ki^{th} story where $Z_{ki} = X_{ki}$ and $Z_{ki+n} = \dot{X}_{ki}$.

SMC2 Control Strategy:

The proposed SMC1 control strategy above has been decentralized to the local level, in which the damper force of a damper on a specific floor is determined only by the responses (measurements) of adjacent floors as shown by the vector λ in Equation (4.19). However, there is still the coupling effect between neighboring controllers. It is highly desirable to establish a completely decentralized control strategy, so that the

control force of a damper depends only on the responses (measurements) at that damper location. In this case, sensors can be installed in the damper to measure the required responses for the direct determination of the control force without the requirements of wire communication. A typical example of a completely decentralized control is the so-called resettable semi-active stiffness damper (RSAST) [66, 67].

A careful examination of the λ vector in Equation (4.19) indicates that the coupling effect between adjacent dampers disappears in the SMC1 strategy, if dampers are not installed on the neighboring floors. This is also demonstrated in Equation (4.20), (4.21) and (4.23) for Cases A, B and D structures. Consequently, the proposed SMC1 control strategy is completely decentralized, if dampers are not installed on adjacent floors, such as Cases A, B and D structures. Such a completely decentralized sliding mode control strategy is referred to as SMC2, which is a special case of the SMC1 strategy.

SMC3 Control Strategy:

Based on the classical SMC, the controller is designed to guarantee that $\dot{V} = \lambda(U - G) \leq 0$, see Equation (4.18). Hence, the control force u_i from the i^{th} damper (installed in k_i story) is given by [68, 69]

$$u_i = G_i - \delta_i \lambda_i \quad (4.25)$$

in which $\delta_i > 0$ is referred to as the sliding margin, G_i is the i^{th} element of the

r-vector \mathbf{G} , and λ_i is the i^{th} element of the r-vector λ given by Equation (4.17), substituting Equation (4.25) into Equation (4.18), one can easily show that

$$\dot{V} = \sum \lambda_i (u_i - G_i) = - \sum \lambda_i^2 \delta_i \leq 0 \quad (4.26)$$

The continuous sliding mode controller in Equation (4.25) is a centralized control method [69, 70] indicating that the control force u_i depends on the measurements (or estimates) of the entire state vector \mathbf{Z} of the structure. For decentralized sliding mode control using MR damper, we propose to design each controller (damper) separately, i.e., based on the design of a single damper alone without any interaction with other dampers. In this case, let us consider a single damper installed in the i^{th} story, i.e., $r = 1$, $\mathbf{G} = G_1$, $\lambda = \lambda_1$, and the sliding surface is a scalar, i.e., $\mathbf{S} = S_1$. Further, we consider the static output feedback with co-located sensors, i.e., only $Z_i = X_i$ and $Z_{i+6} = \dot{X}_i$ are measured for feedback. Consequently, the state vector \mathbf{Z} ($2n \times 1$), the \mathbf{P} ($1 \times 2n$) vector in Equation (4.17), and the derivative of the Lyapunov function in Equation (4.17) are as follows

$$\mathbf{Z} = [0 \quad \cdots \quad X_i \quad 0 \quad \cdots \quad \dot{X}_i \quad 0 \quad \cdots \quad 0]^T \quad (4.27)$$

$$\mathbf{P} = [0 \quad \cdots \quad \alpha_i \quad 0 \quad \cdots \quad 1 \quad 0 \quad \cdots \quad 0]$$

$$\dot{V} = \lambda_1 (\mathbf{u}_1 - \mathbf{G}_1) \quad (4.28)$$

in which the elements X_i and α_i are at the i^{th} location and the elements \dot{X}_i and 1 are at the $(i+6)^{\text{th}}$ location. Hence, a stable decentralized sliding mode controller for $\dot{V} \leq 0$

is obtained as

$$u_1 = G_1 - \delta_1 \lambda_1 \quad (4.29)$$

where the sliding margin $\delta_i > 0$ can be adjusted.

The controller u_1 in Equation (4.26) ~ (4.29) is for a single MR damper installed in the i^{th} story. One can repeat the same procedure to design a MR damper in all other stories ($i = 1, 2, \dots, 6$). Consequently, the control force of a damper installed in the i^{th} story, denoted by \bar{u}_i , for $i = 1, 2, \dots, 6$, can be obtained as follows

$$\begin{aligned} \bar{u}_1 &= -m_1[\alpha_1 \dot{X}_1 + (X_1 A_{(7,1)} + \dot{X}_1 A_{(7,7)} - \ddot{X}_0)] - \frac{\delta_1}{m_1} (\alpha_1 X_1 + \dot{X}_1) \\ \bar{u}_2 &= -m_2[\alpha_2 \dot{X}_2 + (X_2 A_{(8,2)} + \dot{X}_2 A_{(8,8)})] - \frac{\delta_2}{m_2} (\alpha_2 X_2 + \dot{X}_2) \\ \bar{u}_3 &= -m_3[\alpha_3 \dot{X}_3 + (X_3 A_{(9,3)} + \dot{X}_3 A_{(9,9)})] - \frac{\delta_3}{m_3} (\alpha_3 X_3 + \dot{X}_3) \\ \bar{u}_4 &= -m_4[\alpha_4 \dot{X}_4 + (X_4 A_{(10,4)} + \dot{X}_4 A_{(10,10)})] - \frac{\delta_4}{m_4} (\alpha_4 X_4 + \dot{X}_4) \\ \bar{u}_5 &= -m_5[\alpha_5 \dot{X}_5 + (X_5 A_{(11,5)} + \dot{X}_5 A_{(11,11)})] - \frac{\delta_5}{m_5} (\alpha_5 X_5 + \dot{X}_5) \\ \bar{u}_6 &= -m_6[\alpha_6 \dot{X}_6 + (X_6 A_{(12,6)} + \dot{X}_6 A_{(12,12)})] - \frac{\delta_6}{m_6} (\alpha_6 X_6 + \dot{X}_6) \end{aligned} \quad (4.30)$$

in which $A_{(i,j)}$ is the i - j^{th} element of the system matrix A in Equation (4.7), $\alpha_i > 0$ and $\delta_i > 0$ ($i = 1, 2, \dots, 6$). Equation (4.30) can be used to calculate the control force of a damper in each story no matter which case of the structure (damper layout) is selected. It is observed from Equation (4.30) that: (i) the sliding mode controllers are completely decentralized, except the MR damper installed in the first story, and (ii) the MR damper installed in the first story requires the measurement of the earthquake

ground acceleration \ddot{X}_0 in addition to the responses of the first story. In practice, the term \ddot{X}_0 may usually be neglected.

The SMC3 controller proposed above is based on the assumption that each damper can be designed independently leading to the decentralized SMC in Equation (4.30). This assumption is justified based on the fact that MR dampers are energy dissipative devices, which will not drive the system to be unstable.

4.2 Smart Control Device

The objective of this section is to develop a prototype of smart control device which integrates the sensing subsystem, computation core (embedded with control algorithm) and the control device (MR-damper), and also can enhance the control reliability and reduce the cabling problem. The smart control device is packaged as a single device which combines the microcontroller (MSP430), the MR-damper and the measurement system. The advantages of implementation of the smart control device are:

- a. Permitting designers to implement their control law on the smart control device,
- b. Easy to setup and maintain the device in the structure,
- c. Highly reliability for long-term operation,
- d. Lower price (Economical condition),

Verification of this smart control device is conducted on the NCREE shaking table by mounting the smart control device in a 6-story 1/4-scale steel frame and verifies the

control effectiveness by using the shaking table test.

4.2.1 Hardware Design of Smart Control Device

The hardware design of Smart Control Device, as shown in *Figure 4.5*, includes three major subsystems: LVDT, MR damper and Driven Box. The LVDT is a displacement meter which is designed to measure the damper stroke (or story drift if the damper is installed between each floor). The measuring range of LVDT is $\pm 50\text{mm}$ and the corresponding signal range is $\pm 10\text{V}$. The power requirement of LVDT is $\pm 15\text{V}$ at maximum of 100mA and minimum of 25mA . The signal measured from LVDT is sent to the driven box where the overall computation of control logic is conducted. Magnetorheological (MR) damper of Smart Control Device is RD1005-3 (Lord Corp.) which is introduced in *Section 4.1*.

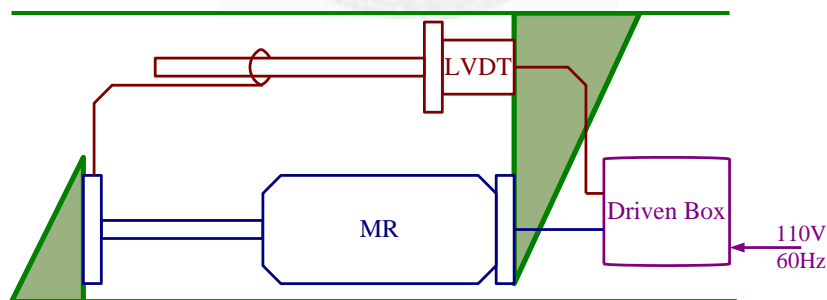


Figure4.5: The detail design of Smart Control Device

Driven Box of Smart Control Device (MSP430):

The key element of the smart control device is the Driven Box. There are six major functions in the driven box, which are:

- a. Power supply unit,
- b. Collect stroke value from LVDT,
- c. Output current command to MR damper,
- d. Run the control logic and decide the control command,
- e. Accept designer to update control law,
- f. Accept user to monitor its operation situation,

In order to offer these functions, the design of driven box includes the following components: power supply, power management, signal condition, VCCS, RS232 communication and microcontroller (MSP430), as shown in **Figure 4.6**. The power supply is a regular power module which outputs the voltage +24V at 3A maximum and +5V at 6A maximum. The +24V power is used to supply the power of MR damper and the +5V power is used in the power management which supplies the power for sensor and the microcontroller.

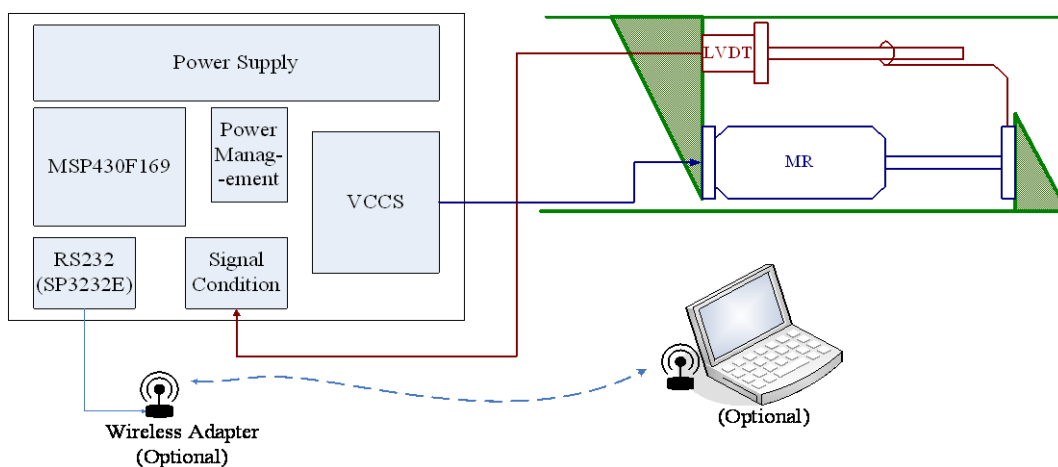


Figure 4.6: The detail components of driven box and its connection with MR damper.

The power management is used to convert the +5V power into +3.3V for microcontroller and +/-15V for LVDT. The MAX743 and L2950 are used in power management. MAX743 (Maxim Integrated Products) is a dual-output, switch-Mode regulator (+5V to +/-15V). LP2950-CZ3.3 (National Semiconductor) is micro-power voltage regulator which converts the +5V to 3.3V for microcontroller. The signal condition is the interface between LVDT and microcontroller (MSP430F169). It converts the LVDT signal (+/-10V) into the internal ADC range of MSP430(0~3.3V). So the mathematical function is: $V_{\text{output}} = (V_{\text{Input}} + 10)/6$. A four channel ultra low noise operational amplifier OP400 (Analog Devices) is selected. And a reference voltage IC REF01 (Analog Devices) is used to offer the +10V reference voltage. The VCCS is a converter to make the output current be linear dependent on the input voltage and regardless the resistance loading. A regular VCCS is selected. (Models 4122Z DC Brush Servo Amplifier from Copley Controls Corp). RS232 is used to communicate with computer to output the monitoring message or debug message. A dual channel RS232 IC SP3232 (Sipex Corp.) is selected. Its function is converting the UART data flow into standard RS232 data flow. The microcontroller is the main core of this driven box. This microcontroller must include ADC which is used to convert the signal from sensor, DAC which is used to output command. A 16-bits ultra low power microcontroller MSP430F169 (Texas Instruments) is selected. It includes 12-bits ADC

channels, Dual 12-bits DAC, 60kB Flash, 2048B RAM and 2 USART. These functions are really matched with the requirement of driven box. In order to monitoring the Smart Control Device a wireless adapter is used to transmit RS232 data wirelessly to PC. An overview of the driven box is shown as **Figure 4.7**. It includes five ports, they are:

PORT 1: Input 110V AC

PORT 2: Connector for LVDT which includes +/-15V power to achieve LVDT and a signal feedback channel.

PORT 3: Connector for MR damper which is used to output the command current to achieve MR damper.

PORT 4: RS232 port which is used to communicate with PC. User can monitor the system situation on the screen. It's an optional connection, the system can work without connect this wire and this wire only supply the function of monitoring.

PORT 5: JTAG port is used to download control law into driven box. This connection is linked only when you want to download the control law. User can edit their control law on laptop and download control law by the linkage between laptop and JATG of smart control device.

A photo of the prototype driven box (without optimal circuit layout) is shown in

Figure 4.8.

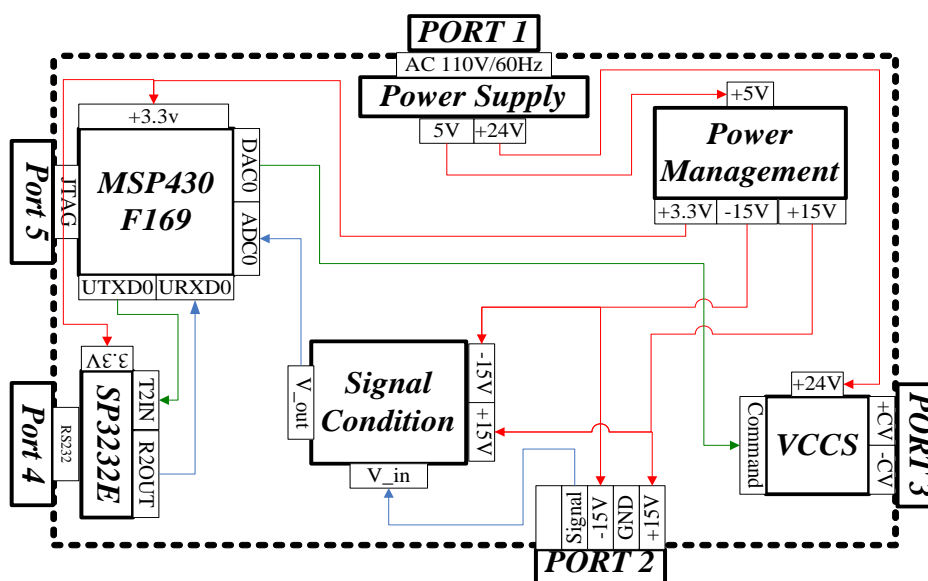


Figure 4.7: Components in the driven box.

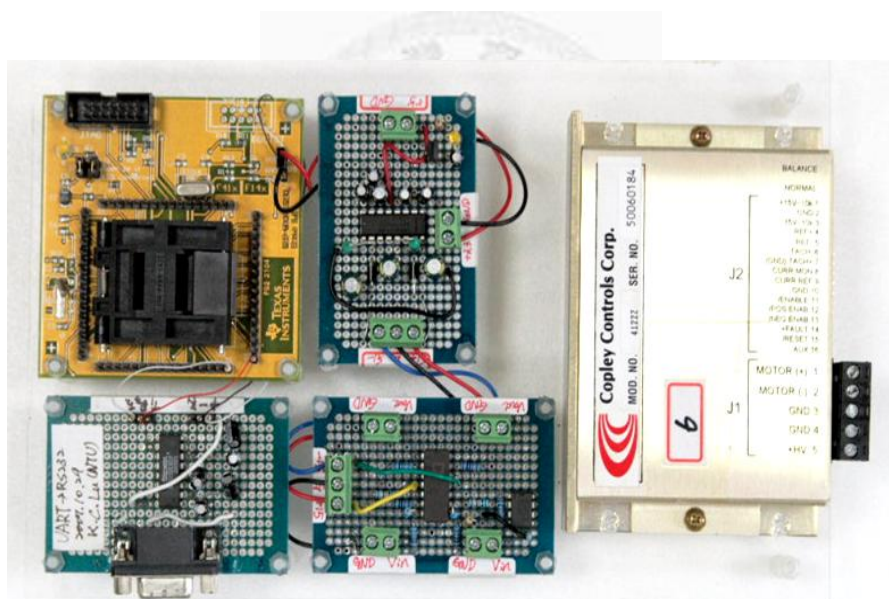


Figure 4.8: Photo of the driven box.

4.2.2 Software Design of Smart Control Device

The software design of MSP430F169 includes three layers, as shown in *Figure 4.9*.

The bottom layer is the microcontroller MSP430F169, the middle layer is the driver and

the top layer is the user design application which includes the software of control logic and signal processing. In the middle layer there are four drivers: ADC driver, DAC driver, UART drive and Timer A driver.

Application	Control Logic			
Driver	ADC	UART	DAC	TimerA
Hardware	MSP430F169			

Figure 4.9: The frame work of software design.

The ADC driver is used to set the ADC parameters and achieve the internal ADC converting the signal and the DAC driver is used to set the internal DAC parameter and convert the digital command to analog voltage. The UART driver includes transmit data package out and receive data package in, which can communicate through UART. The driver of Timer A is used to control the system sampling time (the UART data rate in the driven box the sampling time is 0.005s (200Hz) and UART data rate is 19200bps). After these drivers layout, the application layer can achieve these functions by calling these drivers. And the software of control logic and signal processing is designed and embedded in the application layer. In Smart Control Device, the embedded software in the application layer includes Decentralized Sliding Mode Control (SMC1 Control Strategy in *Section 4.1*) computation and low pass filter. The procedure flow in the application layer is shown in *Figure 4.10*. In each time step, first is the ADC converting

(displacement analog signal from LVDT), second is the differential operation to get the velocity, third is the low pass filtering, then transmit (or input) the digital data of displacement and velocity into the application layer where control logic is embedded. Finally, through the DAC operating the output signal is the control command.

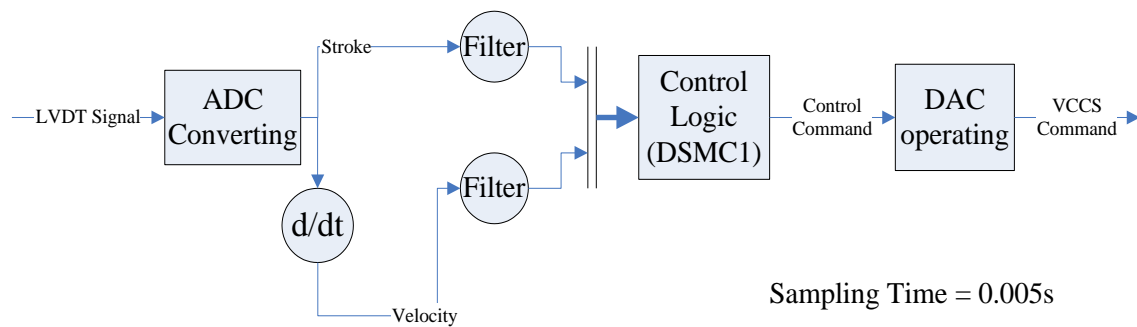


Figure 4.10: Flow chart of calculation in each time step in the microprocessor.

4.3 Discussions on the Experimental Results

Based on the proposed four decentralized sliding mode control algorithms (SMC1~4), the control performance of the test structures with four different cases (CaseA~D) of damper installation (layout) will be examined experimentally. To evaluate the control performance of the proposed control methods, two groups of evaluation criteria proposed by Ohtori et al. [70] are defined, including the peak response values and the root-mean-square (RMS) response values, as shown in **Table4.3**.

Four indices are used: J1= maximum value of inter-story drift normalized to the maximum drift of passive-off case, J2= maximum floor acceleration normalized to the maximum response of passive-off case, J3 & J4 are refer to the root-mean-square value

of the inter-story drift and floor acceleration respectively.

Table 4.3: Evaluation criteria definition of J indices

J1: The maximum normalized story drift		
J1	$\max_{\text{excitation}} \left(\frac{\max_{t,i} \frac{ \text{RelDist}_i(t) }{h_i}}{\text{DriftRatio}_{\max}} \right)$	t: duration of each earthquake record RelDist _i : relative displacement between consecutive floors h _i : the height of i-th floor DriftRatio _{max} : maximum drift ratio in the case of passive-off
J2: The maximum normalized absolute acceleration		
J2	$\max_{\text{excitation}} \left(\frac{\max_{t,i} \text{AbsAcc}_i(t) }{\text{AbsAcc}_{\max}} \right)$	AbsAcc _i : absolute acceleration of i-th floor AbsAcc _{max} : Maximum absolute acceleration in the case of passive-off.
J3: The maximum normalized RMS value of story drift		
J3	$\max_{\text{excitation}} \left(\frac{\max_{t,i} \frac{\ \text{RelDist}_i(t)\ }{h_i}}{\ \text{DriftRatio}\ _{\max}} \right)$	$\ \cdot\ $: root-mean-square value $\ \text{DriftRatio}\ _{\max}$: maximum RMS value of drift ratio in the case of passive-off
J4: The maximum normalized RMS of absolute acceleration		
J4	$\max_{\text{excitation}} \left(\frac{\max_{t,i} \ \text{AbsAcc}_i(t)\ }{\ \text{AbsAcc}\ _{\max}} \right)$	$\ \text{AbsAcc}\ _{\max}$: maximum absolute acceleration of drift ratio in the case of passive-off

The passive-off control (command voltage is set to be 0.0 Volt), passive-on control (command voltage is set to be 0.8 Volts), and LQR control (using full-state feedback control) are also used in this study for comparison. The LQR full-state feedback control method has been quite popular for applications to MR dampers [e.g., 71, 72]. For the LQR controller, Q and R are two (12 × 12) weighting matrices to be adjusted, and a full-state feedback state is measured (or estimated using a Kalman filter). The

passive-off control case will serve as the reference case for all the performance evaluations. Discussion on the control performance will focus on the SMC1 and SMC4 cases because: the SMC2 control method is for the design of the damper locations to achieve a complete decentralized control.

Discussion on control performance using SMC1 method for Case B structure:

The SMC1 control method used in Case B structure is completely decentralized, since only the local relative velocity and displacement of the story, in which the damper is located, are required as feedback signals to calculate the control force. In other words, u_1 requires only the measurements of X_1 and \dot{X}_1 , whereas u_3 is computed only from the measurements X_3 and \dot{X}_3 . These measurements can be obtained by sensors embedded in the respective MR dampers. Further, there are only two parameters, α_1 and α_3 , to be assigned. Four sets of control parameters are selected to study the control performance, referred to as SMC1-1, SMC1-2, SMC1-3, and SMC1-4 as shown in

Table 4.4.

Table 4.4: Four sets of control parameters considered in SMC1 for Case B structure.

	α_1	α_3	Note.
SMC1-1	0.1	0.1	Optimal J1 (Story Drift)
SMC1-2	10	10	Optimal J2 (Acceleration)
SMC1-3	0.001	0.001	Weakly convergence
SMC1-4	1000	1000	Strongly convergence

Figure 4.11 shows the evaluation criteria of the experimental results based on the SMC1 method using different α parameter values, where the El Centro earthquake has been considered as the excitation. Note that $-\alpha$ is the pole of the sliding surface and hence a large α value will result in a faster reduction for the story drifts but frequently at the expense of the floor accelerations. As shown in **Figure 4.11**, the evaluation criteria using SMC1-2 and SMC1-4 methods are larger than other control cases because larger α values are selected. Consequently, for MR dampers using the SMC1 control method, the selection of α value should not be too large.

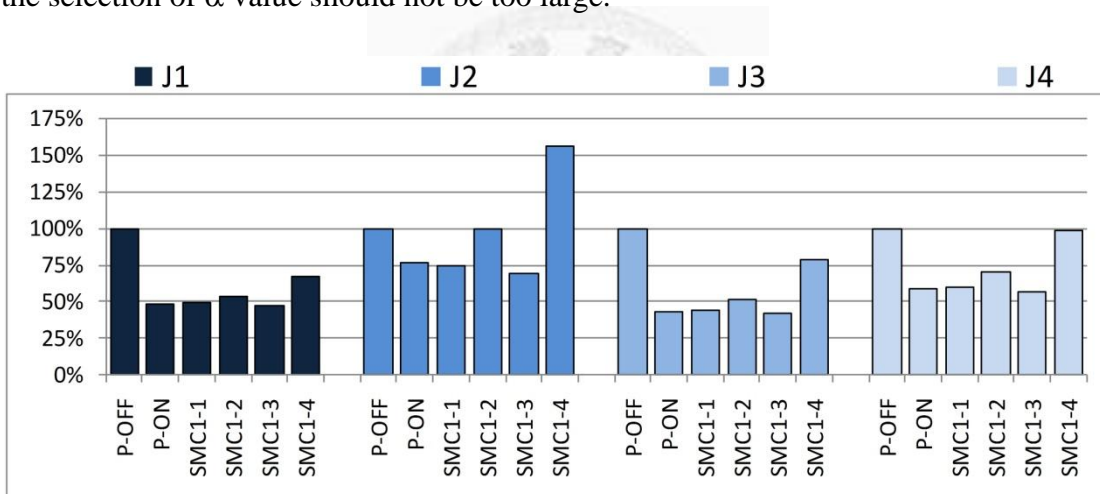


Figure 4.11: Comparison on the performance indices for Case B structure subject to El Centro Earthquake (PGA=100 gal) using the SMC1 method with different sets of control parameters (Passive-off, Passive-on, SMC1-1 ~ 4).

Discussion on control performance using SMC3 method for Case B structure:

For the SMC3 control algorithm, there are four parameters to be assigned for Case B structure (two damper locations), i.e. α_1 , δ_1 , α_3 and δ_3 . For El Centro earthquake excitation, **Table 4.5** shows five different sets of parameters to be used in this study, and

the four performance indices of the experimental results are shown in **Figure 4.12**.

Table 4.5: Five sets of control parameters considered in SMC3 method for Case B structure

	α_1	δ_1	α_3	δ_3	
SMC3-1	1000	10	1000	1.E+05	Optimal J1 (story drift)
SMC3-2	100	1.E+07	1000	1.E+07	Optimal J2 (Acceleration)
SMC3-3	100	10	100	10	α is fixed and with small δ value
SMC3-4	100	1.E+07	100	1.E+07	α is fixed and with medium δ value
SMC3-5	100	1.E+09	100	1.E+09	α is fixed and with large δ value

For the SMC3-1 control case in **Figure 4.12** the control parameters are determined by a minimization of the story drift (J1 index), whereas the control parameters of the SMC3-2 control case are determined by a minimization of the story peak acceleration (J2 index). As shown in **Figure 4.12**, the performance index J2 for all five cases is much larger than the passive-on control case indicating that the selection of control parameters is not good enough.

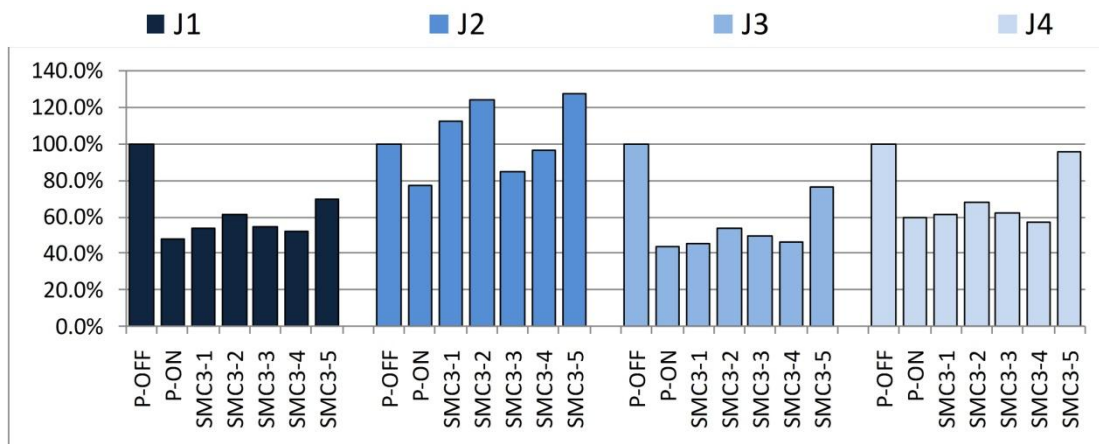


Figure 4.12: Comparison on the performance indices for Case B structure subject to El Centro Earthquake (PGA=100 gal) using the SMC3 method with different sets of control parameters (Passive-off, Passive-on, SMC3-1, SMC3-2, SMC3-3, SMC3-4, and SMC3-5).

Further, we examine the effect of the δ -value (sliding margin) on the behavior of the MR damper. Simulation results indicate that a smaller δ -value produces a negative stiffness for the damper and a larger δ -value induces a positive stiffness for the damper, as shown in the upper part of **Figure 4.13a**, in which $\alpha = \alpha_i = 100$. and $\delta = \delta_i$ for $i = 1$ and 3. This phenomenon is also verified by the experimental results as shown in the lower part of **Figure 4.13a**. Therefore, for a better control performance it is necessary to select a suitable δ -value which can produce a larger area for damper restoring force diagram (hysteretic loop). **Figure 4.13b** shows the comparison of performance indices for the simulation results using four different sets of control parameters. In this figure, the case for $\alpha=0.01$ and $\delta=1.0E+08$ (or $\delta=1.0E+10$) provides a better control performance. It is important to note that the selection of the δ -value plays an important role in this control case, because this parameter determines the shape of the damper hysteretic loop. Therefore, a smaller value of α along with a larger value of δ will have a better performance.

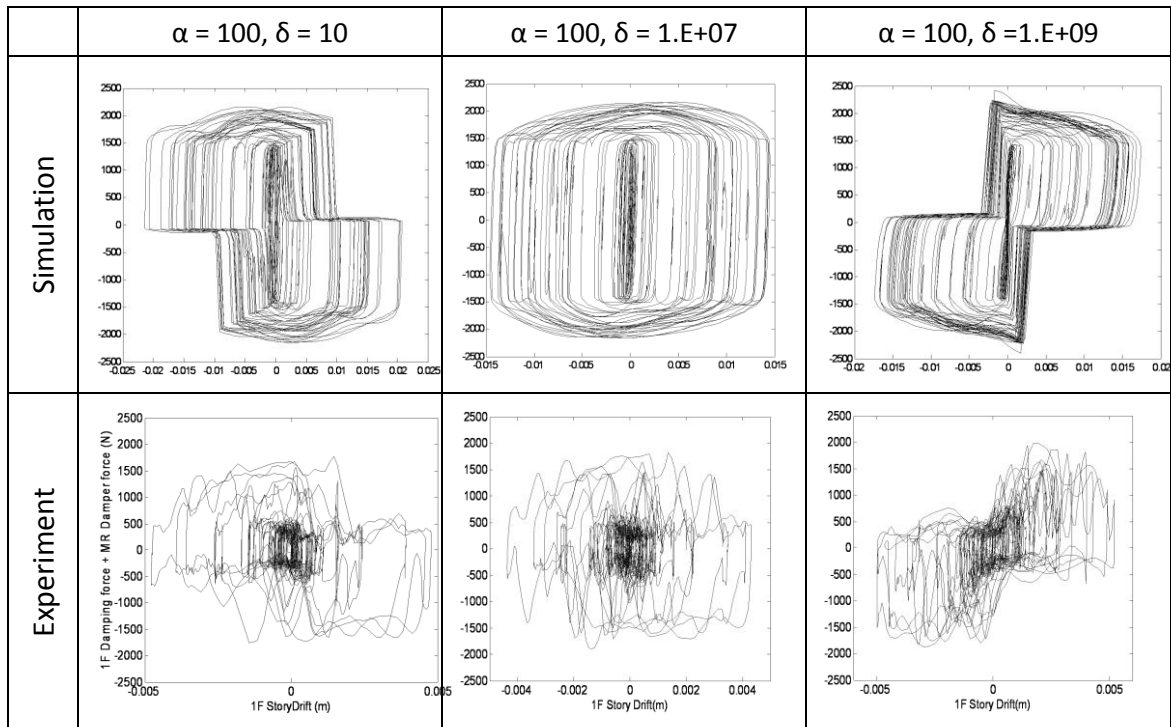


Figure 4.13a: Comparison for the hysteretic loops of damper on the 1st floor between simulation and experiment results using different pairs of α -value and δ -value in the SMC3 control method.

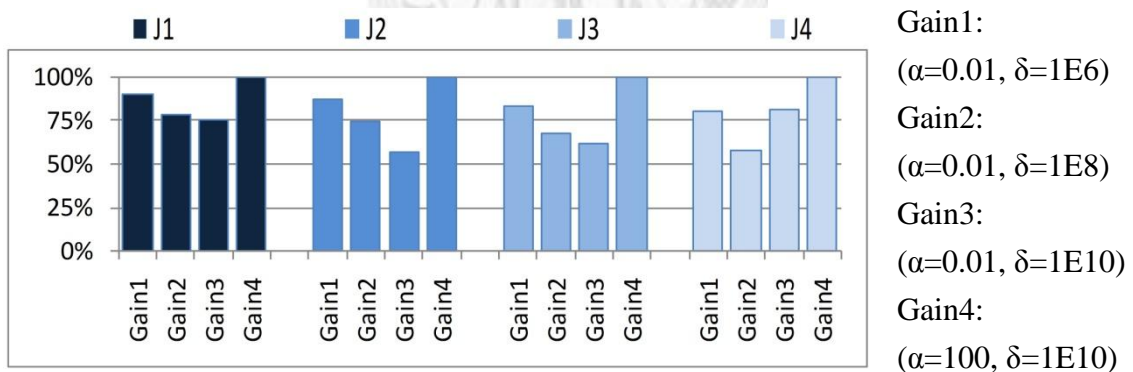


Figure 4.13b: Effects of control parameters, α -value and δ -value, on the performance indices of Case B structure using the SMC3 method.

Discussion for different control methods:

Experimental results for eight control methods, including passive-off (0.0 Volts), passive-on (0.8 Volts), LQR1, LQR2, SMC1-1, SMC1-2, SMC3-1 and SMC3-2, will be

used to examine the control performance of the proposed decentralized sliding mode control methods. For the LQR1 control case, the control parameters are determined by a minimization of the story drift (J1 index), whereas the control parameters for the LQR2 control case are determined by a minimization of the story peak acceleration (J2 index).

Table 4.6: Control parameters and feedback signals for SMC-1, SMC-3 and LQR control methods

	SMC-1		SMC-3		LQR	
	Control parameters	Feedback signals	Control parameters	Feedback signals	Control parameters	Feedback signals
Case A	α_1	X_1, \dot{X}_1	α_1, δ_1	$\ddot{X}_g, X_1, \dot{X}_1$	$[Q]_{12 \times 12}$ R_1	$[Z]_{12 \times 1}$
Case B	α_i $i=1,3$	X_i, \dot{X}_i $i=1,3$	α_i, δ_i $i=1,3$	$\ddot{X}_g, X_1, \dot{X}_1$ $i=1,3$	$[Q]_{12 \times 12}$ R_1, R_3	$[Z]_{12 \times 1}$
Case C	α_i $i=1,2,3$	X_i, \dot{X}_i $i=1,2,3$	α_i, δ_i $i=1,2,3$	$\ddot{X}_g, X_1, \dot{X}_1$ $i=1,2,3$	$[Q]_{12 \times 12}$ R_1, R_2, R_3	$[Z]_{12 \times 1}$
Case D	α_i $i=1,3,5$	X_i, \dot{X}_i $i=1,3,5$	α_i, δ_i $i=1,3,5$	$\ddot{X}_g, X_1, \dot{X}_1$ $i=1,3,5$	$[Q]_{12 \times 12}$ R_1, R_3, R_5	$[Z]_{12 \times 1}$

Control parameters and feedback signals for above-mentioned control methods are shown in **Table 4.6**. Control parameters are selected to study the control performance, referred to as LQR1 and LQR2 as shown in **Table 4.7**. The performance indices of experimental results for four different cases of structural system (damper layout from Case A to Case D) using eight different control methods are shown in **Figure 4.14**, in which the El Centro Earthquake (PGA=100 gal) has been used as the excitation. In general, the decentralized sliding mode control strategies perform better than the LQR control as observed from performance indices in **Figure 4.14**.

Table 4.7 shows the number of control parameters and feedback signals needed for

different control methods. Note that the SMC1 or SMC3 control methods are decentralized so that each damper depends only on the relative velocity and drift of the story, in which the damper is installed, to calculate the control force, eliminating the requirement of wire communications. Therefore, the reliability of the control system using the proposed DSMC strategies is better. Comparison for the experimental control performance using passive-on, LQR1 and SMC1-1 for four different cases of damper placement (layout) in the structure is also shown in *Figure 4.15*. As observed from *Figure 4.15*, the Case C control layout provides good control performance.

Table 4.7: Control parameters for the control methods LQR1 and LQR2 in four test structures

Case A	LQR1	Q1	Q2	Q3	Q4	Q5	Q6	Q7	Q8	Q9	Q10	Q11	Q12	R		
		1	1	1	1	1	1	1000	10	10	10	10	10	10	1.E-06	
	LQR2	Q1	Q2	Q3	Q4	Q5	Q6	Q7	Q8	Q9	Q10	Q11	Q12	R		
		1	1	1	1	1	1	1000	100	10	10	10	10	10	1.E-05	
Case B	LQR1	Q1	Q2	Q3	Q4	Q5	Q6	Q7	Q8	Q9	Q10	Q11	Q12	R1	R3	
		1	1	1	1	1	1	1000	1000	10	10	10	1000	1.E-05	1.E-05	
	LQR2	Q1	Q2	Q3	Q4	Q5	Q6	Q7	Q8	Q9	Q10	Q11	Q12	R1	R3	
		1	1	1	1	1	1	1000	1000	100	10	10	1000	1.E-05	1.E-06	
Case C	LQR1	Q1	Q2	Q3	Q4	Q5	Q6	Q7	Q8	Q9	Q10	Q11	Q12	R1	R2	R3
		1	1	1	1	1	1	1000	1000	1000	10	10	1000	1.E-05	1.E-05	1.E-05
	LQR2	Q1	Q2	Q3	Q4	Q5	Q6	Q7	Q8	Q9	Q10	Q11	Q12	R1	R2	R3
		1	1	1	1	1	1	10	10	10	10	10	10	1.E-06	1.E-06	1.E-06
Case D	LQR1	Q1	Q2	Q3	Q4	Q5	Q6	Q7	Q8	Q9	Q10	Q11	Q12	R1	R3	R5
		1	1	1	1	1	1	1000	10	1000	10	1000	1000	1.E-05	1.E-05	1.E-05
	LQR2	Q1	Q2	Q3	Q4	Q5	Q6	Q7	Q8	Q9	Q10	Q11	Q12	R1	R3	R3
		1	1	1	1	1	1	10	10	10	10	10	10	1.E-06	1.E-06	1.E-06

Table 4.8: Comparison on the number of control parameters and feedback signals for different control method

	Number of parameters				Number of feedback Signals			
	Case A	Case B	Case C	Case D	Case A	Case B	Case C	Case D
LQR	13	14	15	15	12	12	12	12
SMC1	1	2	3	3	2	4	6	6
SMC2	1	2	3	3	2	4	N	6
SMC3	2	4	6	6	3	5	7	7

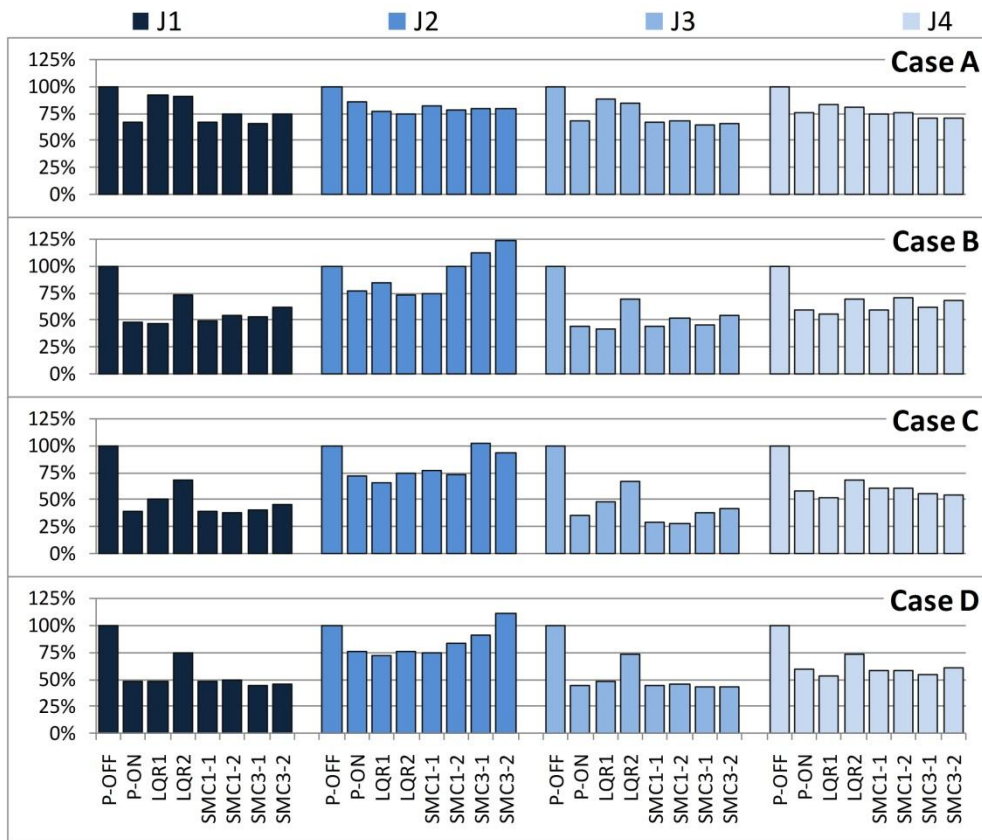


Figure 4.14: Comparison on the control performance for four different structural systems (from Case A to Case D) using eight different control methods (Passive-off, Passive-on, LQR1, LQR2, SMC1-1, SMC1-2, SMC3-1 and SMC3-1) with El Centro Earthquake (PGA=100 gal) as excitation.

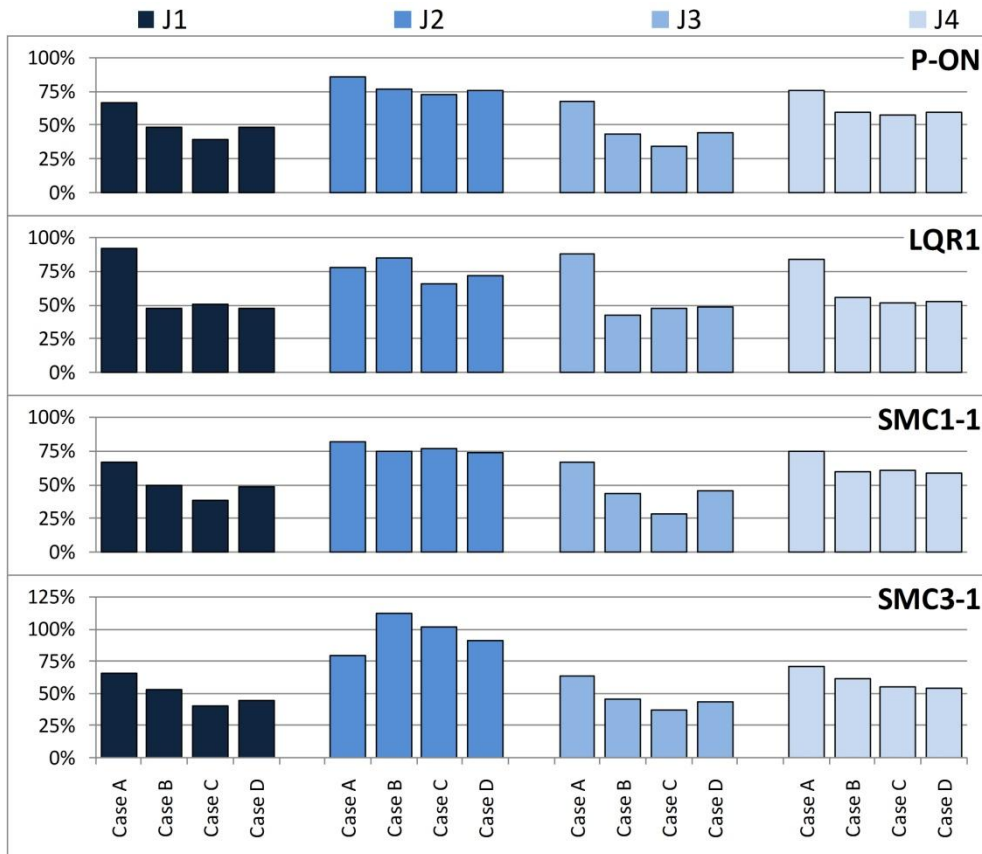


Figure 4.15: Comparison on the performance indices using three different control methods, Passive-on, LQR1, SMC1-1 and SMC3-1, on four different cases of structural systems.

Discussion for the control performance among different earthquake excitation:

Four earthquake records (EL Centro-100 gal, EL Centro-200 gal, Kobe-100 gal, Kobe-150 gal; where 1000 gal=981 cm/sec²) are selected as input excitations to examine the effect of different seismic excitations on the performance of various control algorithms. **Figure 4.16** shows the performance indices of the experimental results for the Case A structure using the passive-on, LQR1, SMC1-1 and SMC3-1 control algorithms.

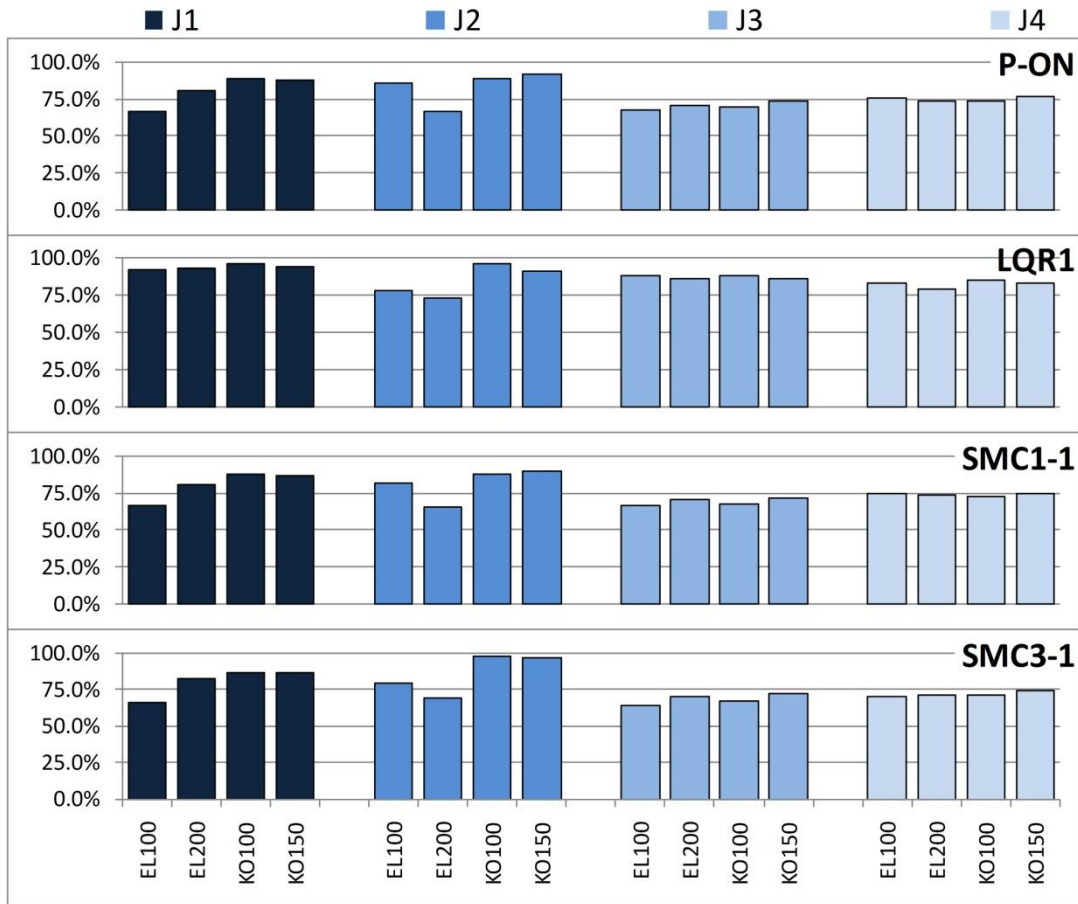


Figure 4.16: Comparison on performance indices of Case A structure subjected to four different earthquake excitations (EL Centro-100gal, EL Centro-200gal, Kobe-100gal, Kobe-150gal);

As observed from **Figure 4.16**, the variances of the performance indices for different ground motions are not significant, and the control performance based on passive-on (identical to SMC2), LQR1, SMC1-1 and SMC3-1 control algorithms are plausible. Comparison on the roof acceleration response between passive-off case (0 Volt) and four different control cases (Passive-on (0.8Volt0, LQR1, SMC1 and SMC3)) is also shown in **Figure 4.17** for comparison.

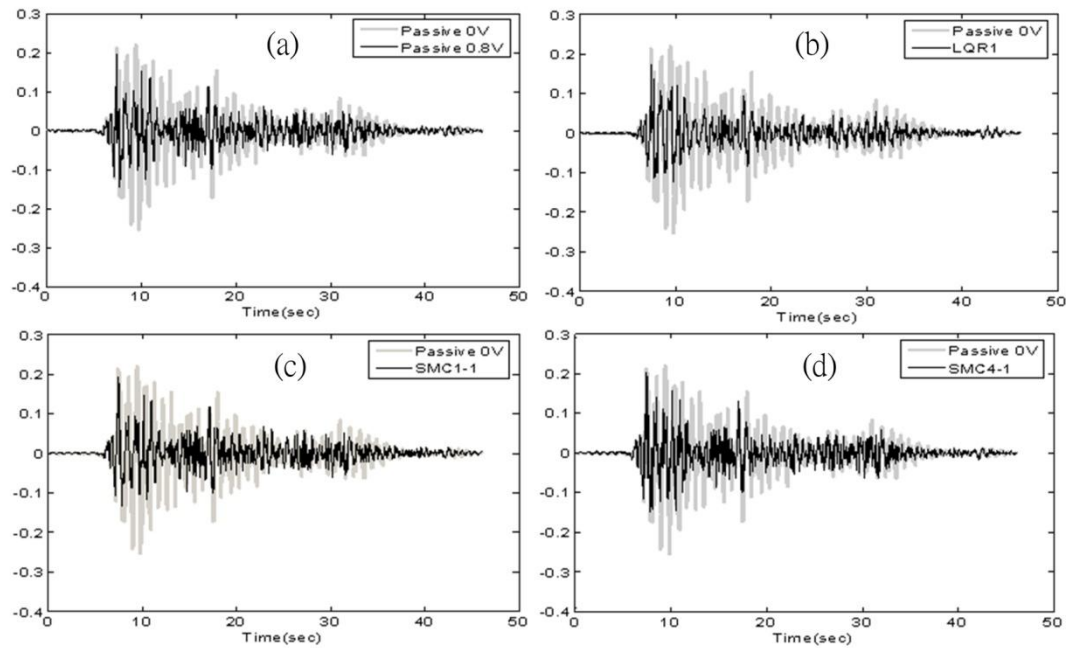


Figure 4.17: Comparison on the 6th floor acceleration response for case B structure between; (a) Passive-off (0 Volt) and passive-on (0.8Volt) control cases, (b) Passive-off (0 Volt) and LQR1 control cases, (c) Passive-off (0 Volt) and SMC1-1 control cases, (d) Passive-off (0 Volt) and SMC3-1 control cases.

Evaluate the system performance of Smart Control Device:

The experimental setup of *Section 4.1* is also used to verify this prototype of Smart Control Device (SCD). Considering the limited number of Smart Control Device, only the first story of test structure is installed with Smart Control Device and others are not, so only Case A is considered. El Centro earthquake with $PGA=100gal$ are used as the input ground motion of shaking table. There are four control methods in Case A, Passive-Off, Passive-On, SCD-SMC1, dSPACE-SMC1. SCD-SMC1 is the method that using Smart Control Device with SMC1 Control Strategy; dSPACE-SMC1 is the method that using dSPACE with SMC1 Control Strategy. The SMC1 control strategy is

introduced in *Section 4.1* and the control law is shown in Equation (4.24). Base on the experimental results of *Section 4.1*, two control gains (G1 and G2) are used in this test, G1 ($\alpha = 0.01$) is weak convergence , G2 ($\alpha = 100$) is strong convergence. dSPACE is a popular control system for structural control and vehicle control and is used to verify with Smart Control Device in this test.

Figure 4.18 shows the photo of the installation of the smart control device in the first floor. The Smart Control Device is integrated with the MR damper which is installed under the V-shape bracing. The design of V-shape bracing needs to be rigid enough. The LVDT is also installed under the bracing to measure the story drift. The relative velocity is the differential results of LVDT signal. And the Smart Control Device required an AC 110V/60Hz power.

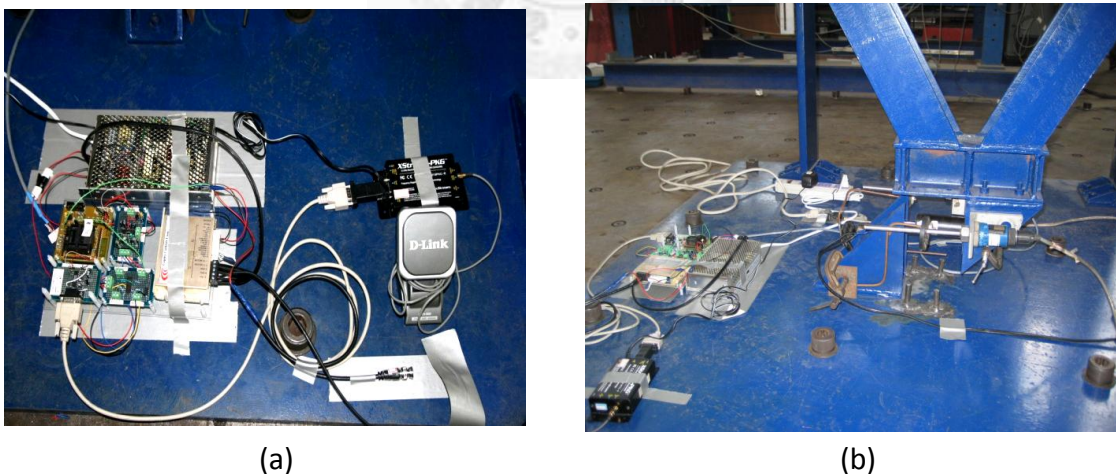


Figure 4.18: Photos of the Smart Control Device in the first story to control the MR damper.

The control results are shown in *Figure 4.19*, the performance indices (J1, J2, J3

and J4) are defined in **Table 4.3**, SCD-SMC1-G1 means SCD-SMC1 with control gain G1 ($\alpha = 0.01$) and so on. By comparing the performance indices of SCD-SMC1 and dSPACE-SMC1, the indices are closed when they apply the same control gain, this means that the performance of Smart Control Device is almost the same as dSPACE. The control performance of G1 is better than G2, it means the control gain for strong convergence is not good in this control scenario and concurs with the results of **Section 4.1**.

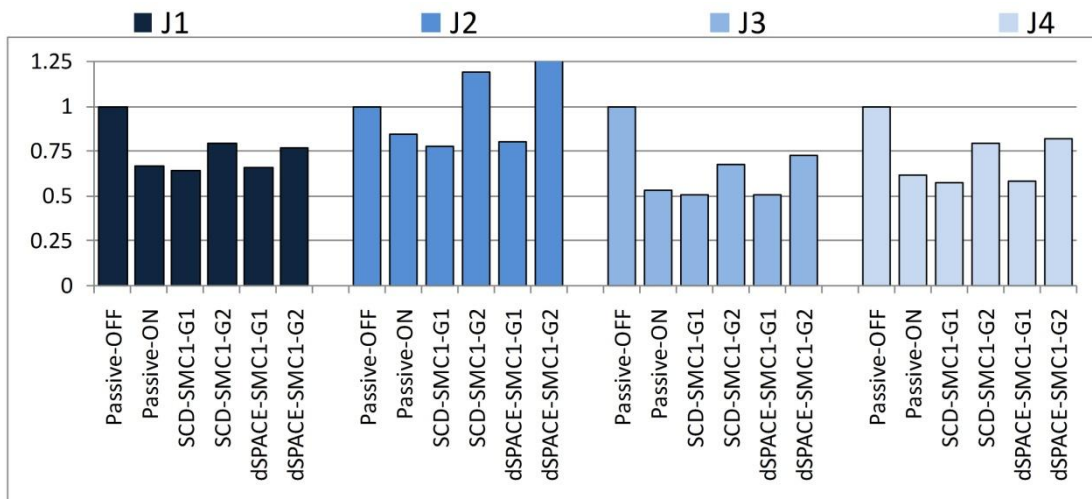


Figure 4.19: The performance indices of Case A. (Input is El Centro 100gal)

To verify the accuracy of signal processing in the Smart Control Device (in MSP430 microprocessor) the output displacement (story drift of the 1st floor) signal from the SCD is broadcast through wireless communication module and compared with the data recorded by NCREE wired data acquisition system, as shown in **Figure 4.20**.

The recorded stroke signal of Smart Control Device and NCREE system are quite

matched. But the signal issued by the Smart Control Device has lower resolution as compared with the NCREE system. This because the resolution of MS430 is 12bits and the NCREE system is 16-bits. So the signal of Smart Control Device is not as good as NCREE system. But the decided command voltage of smart control device is the same as the real command which is recorded by NCREE system.

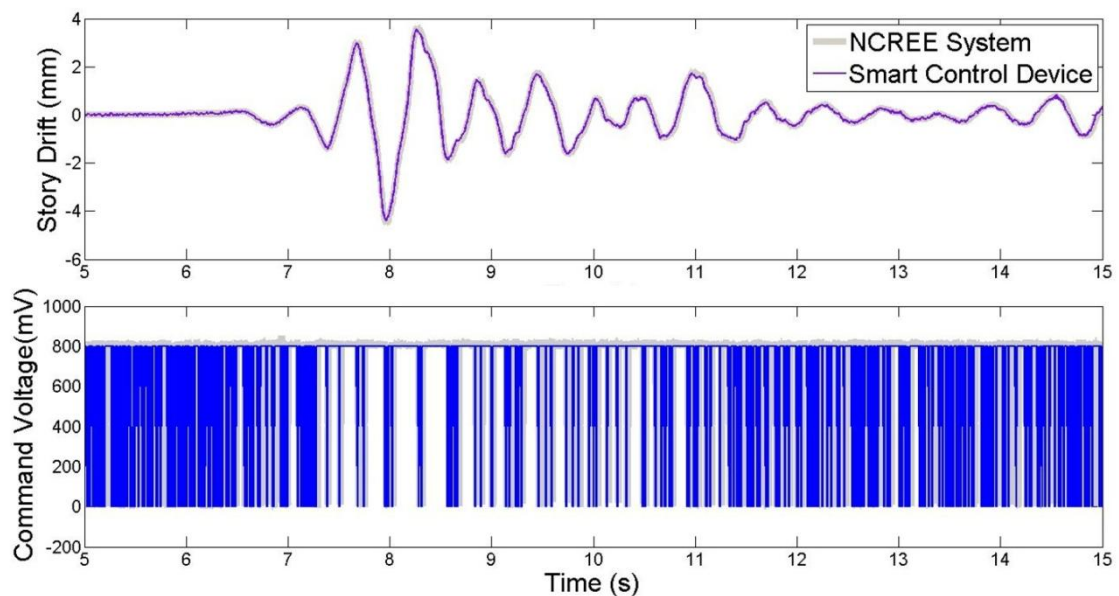


Figure 4.20: Comparison on the stroke signal and the command voltage issued by NCREE system and the MSP 430 microprocessor of Smart Control Device.

4.4 Summary

The structural control results of shaking table tests for a steel frame structure in order to evaluate the performance of a number of proposed decentralized sliding mode control algorithms for multiple magnetorheological (MR) dampers. Various control

algorithms have been used for this semi-active control study, including several proposed decentralized sliding mode control (DSMC) methods, LQR control method, and passive-on and passive-off control. Through both experimental and numerical simulation studies for the test structure, it is concluded that the proposed decentralized sliding mode control methods perform very well as observed from the experimental performance indices, in addition to the advantages of decentralizations. For example, the SMC1 and SMC3 control strategies require only local signals to calculate the control force without wire communication as compare to the traditional LQR full-state feedback control. Therefore, the reliability of the control system using the DSMC strategies is better. The experimental results demonstrate that: (1) the proposed DSMC methods have the capability to reduce the response of seismic-excited building structures using limited feedback signals, and (2) the control performance using the proposed DSMC methods is quite comparable with or even better than the popular full-state LQR control for MR dampers.

From the number of control parameters and feedback signals needed for different control methods it is realized that the reliability of the control system using the proposed DSMC strategies is better because each damper depends only on the feedback signals of relative velocity and drift of the story where damper located to calculate the control force. Although the traditional LQR control also can be used this system for

requirement of less sensors and using the Kalman estimator to estimate the full states with less sensors, but still need to define the large number of control parameters. The SMC system is used in lieu of more costly tethered data acquisition systems. Less effort is required during the installation of the communication and increase the reliability of the control system.

The objective of *Section 4.2* is to develop a smart control device which integrates with sensing subsystem and computation core (embedded with control algorithm). The smart control device is packaged as a single device which combines the microcontroller (MSP430) embedded with control algorithm, the MR-damper signal converter (Voltage Covert to Current), and the measurement system. The advantage of using the smart control device must integrate the decentralized control algorithm, so as to reduce the cabling issue in structural control and increase the system reliability. From the shaking table test of a 6 DOF system verification of the smart control device was performed. It was proved that with the embedded decentralized sliding mode control algorithm in the microcontroller the smart control device performs very well as compare to the wired control system (dSPACE).

Chapter 5

Conclusions and Future work

5.1 Conclusions

The objective of this thesis is to implement the concept of Smart Structural System in civil infrastructure. Both structural sensing and control are studied in this research and two systems are developed, Smart Sensing System and Smart Control Device. In *Chapter 2*, the concept of Smart Sensing System is introduced first then the detail constructions of hardware and software are presented. In the development of Smart Sensing System, there are several important results that make the concept of smart sensing to be implemented and they are outlined as below.

1. A new wireless sensing unit (NTU-WSU) is successful designed to perform the sensing process of Smart Sensing System. The high resolution and excellent noise rejection designs of the hardware of NTU-WSU makes the sampling quality of structural ambient responses as good as the official system (SPC51). In the software design of NTU-WSU, the program architecture which includes idle mode and implicit state machine enhances the robustness of NTU-WSU and improves the feasibility of the wireless sensing unit to implement on field test.
2. Through the integration of industrial real-time controller (NI cRIO), Smart Sensing System can be easy to communicate with other industrial equipments. This feature

makes Smart Sensing System possible to extend to support other application in the future. The software development environment of NI-cRIO is LabVIEW which supports several methods to embed other software (ex. C language, ActiveX and Dynamic Link Library). In civil engineering, the analysis software is usually coded in Matlab or C language, LabVIEW provides an easy interface to integrate the analysis software into Smart Sensing System.

3. The internet techniques, 3G mobile router and Dynamic Domain Name Service (DDNS), establish the communication bridge between local site (Smart Sensing System) and remote users. The 3G mobile router (DLink DIR-455) offers the Smart Sensing System an Ethernet port to link internet in field which is a environment without internet; Dynamic Domain Name Service breaks the bottleneck of accessing to a floating IP address which is provided by 3G internet and user can link to Smart Sensing System through a static hostname (ex. <http://polarbearlu.homelinux.org>).

After the system design of Smart Sensing System, this research surveys four well-developed techniques of Structural Health Monitoring (AR, FDD, SSI and Two Stage AR-ARX damage detection) and designs their automated analysis processes. The system performance of Smart Sensing System and the designed automated analysis processes of SHM techniques are verified through the experimental studies of *Section 3.2*, and the results are concluded as below.

1. In the test of Gi-Lu Bridge, the SHM techniques (AR, FDD and SSI) successfully extract the structural dynamic features which include modal frequencies, modal damping and mode shapes. The wireless sensing units (NTU-WSU-V02a) are successfully applied on Gi-Lu Bridge test in the field and propagate the wireless data to the host node which is 2km away from Gi-Lu Bridge.
2. In the damage detection of RC frame, the capabilities of analysis computing and bi-directional wireless communication of wireless sensing unit are verified in this test; the two stage AR-ARX damage detection method is also implemented and verified with wireless sensing system.
3. In the experiment of long-term SHM, the full system verification of Smart Sensing System with an on-line SHM analysis processes is established. This experiment demonstrates the concept of smart sensing which includes the self-data processing (distributed computing), on-line SHM analysis and the wireless sensing for large-scale office building.
4. The field experiment at Niudou Bridge during FANAPI typhoon period demonstrates that Smart Sensing System is reliable and is able to put in field structures under harsh climate. The two-layer communication architecture which includes wireless sensor network and 3G Mobile Internet is also verified in this test. By observing the analysis results of RSSI method, the frequency contents of structure are changed during

FANAPI typhoon period.

In *Chapter 4*, a new idea of structural control, Smart Control Device, is preliminary constructed on control theory and control hardware, and the results are concluded as below.

1. The algorithm of decentralized sliding mode control meets the concept of Smart Control Device which includes local feedback and solving control command on local machine.
2. A prototype of Smart Control Device is designed and verified with a shaking table test. The signal sampling, control processing and command issuing are all handled by microcontroller (MSP430F1611), i.e. a single chip supports all functions of Smart Control Device. This design improves the system reliability significantly and makes the control system possible to implement on real building.

5.2 Future works

The future development of smart structural sensing on civil engineering may emphasize on several issues pointed out as below.

The architecture of embedded system of wireless sensing unit may be improved the reliability and robustness by simplifying the overall bill-of-material (BOM). Recently, several semiconductor manufactures focus on the system-on-chip (SoC) solution for wireless sensing. Such as CC2530 (Texas Instruments) is a system-on-chip solution for

2.4GHz IEEE 802.15.4. The CC2530 integrates the RF transceiver with an 8051 MCU and also supports 12-bits ADC channels. This single chip solution is quite suitable for the application of structural responses measurement under strong ground motion excitation. For accurate vibration measurement, such as structural ambient responses, the embedded system of wireless sensing unit should emphasize on the excellent performance of signal sampling, a series of analog-intensive MCU which is launched by Silicon Laboratories Inc. integrates high performance analog sampling circuit with MCU. C8051F350 is one of this series MCU which includes 24-bits resolution ADC, 8-input multiplexer and programmable gain amplifier (1X to 128X).

For the wireless communication techniques, extending the wireless communication range and overcoming the building shielding induced wireless signal hindrance are important targets in the future. The multi-hopping and router functions are used to improve these difficulties. Zigbee is one of the multi-hopping communication protocols and is suitable for the application scenario which is low data rate, low power and short distance. The 9XTend wireless module which is adopted in NTU-WSU is also support the advanced hopping network which includes the router function to extend wireless signal range. These suggestions may be implemented for the future development of wireless sensing unit. WiMAX (Worldwide Interoperability for Microwave Access) is a new telecommunications protocol of mobile internet and provides higher data rate and

wider signal covering range than 3.5G mobile internet. This technique should be considered to upgrade Smart Sensing System to improve the communication performances.

For the sensor development, the ambient sensor (VSE-15D) is too expensive (about 5000 USD). The future work of this issue should try to find or build alternative sensors which are low price and small size to replace VSE-15D.

The future development of SHM techniques should emphasize on the features of automation and on-line analysis or even real-time, these features make the structural health information to be continuously generated and monitored.

A concept of Smart Control Device is demoed in this thesis. In the future, this concept may extend to integrate with other actuators to improve the adjustability on the features of hysteresis loop. On the other hand, decentralized control algorithms should be developed with the consideration on the limitations of real application in the future.

Finally, the techniques change with each passing day. The future development of smart structure system should focus on interdisciplinary collaboration. The communication interface plays an important role between these different fields of research. The research of civil engineering should put more efforts on system integration and interdisciplinary collaboration.

Reference

- [1] Straser, E.G. and Kiremidjian, A.S., 1998, "A modular, wireless damage monitoring system for structures", The John A. Blume Earthquake Engineering Center Technical Report, 128.
- [2] Lynch, J.P., Law, K.H., Kiremidjian, A.S., Carryer, E., Kenny, T.W. et al., 2002, "Validation of a wireless modular monitoring system for structures", Proceeding of SPIE Smart Structures and Materials: Smart systems for Bridges, Structures, and Highways, San Diego, CA 4696(2), 17-21.
- [3] Lynch, J.P., Wang, Y., Law, K.H., Yi, J.H., Lee, C.G. and Yun, C.B., 2005, "Validation of a large-scale wireless structural monitoring system on the Geumdang bridge" Proceeding of the International Conference on Safety and Structural Reliability, Rome, Italy.
- [4] Tanner, N.A., Wait, J.R., Farrar, C.R., and Sohn, H., 2003, "Structural health monitoring using modular wireless sensors", J. of Intelligent Material Systems and Structures, 14(1), 43-56.
- [5] Nagayama, T., Ruiz-Sandoval, M., Spencer B.F., Mechitov, K.A., Agha, G., 2004, "Wireless strain sensor development for civil infrastructure", Proceeding of 1st Int. Workshop on Networked Sensing Systems, Tokyo, Japan, 97-100.
- [6] Nitta, Y., Nagayama, T., Spencer B.F., Nishitani, A., 2005, "Rapid damage assessment for the structure utilizing smart sensor MICA2 MOTE", Proceeding of 5th International Workshop on Structural Health Monitoring, Stanford, CA., 283-290.
- [7] Jian-Huang Weng, Chin-Hsiung Loh, Lynch, J.P., Kung-Chun Lu, P.Y. Lin, Wang, Y., 2008, "Output-Only Modal Identification of a Cable-Stayed Bridge Using Wireless Monitoring Systems", J. of Engineering Structure, 30 (2), 1802-1830.
- [8] Lynch J.P., Sundararajan A, Law, K.H., Kiremidjian A.S., Carryer E., 2004, "Embedding damage detection algorithms in a wireless sensing unit for operational power efficiency", Smart Materials and Structures, 13(4): 800-810.
- [9] Lynch J.P., Sundararajan A, Law, K.H., Kiremidjian A.S., Kenny TW, Carryer E., 2003, "Embedment of structural monitoring algorithms in a wireless sensing unit", Structural Engineering and Mechanics, 15(3): 285-297.
- [10] Lynch J.P., 2007, "An overview of wireless structural health monitoring for civil structures", Philosophical Transactions of the Royal Society of London. Series A, Mathematical and Physical Sciences, 365(1851): 345-372.
- [11] Lynch J.P., Wang Y., Loh K, Yi JH, Yun CB., 2006, "Performance Monitoring of the Geumdang Bridge using a Dense Network of High-Resolution Wireless Sensors", Smart Materials and Structures, 15(6): 1561-1575.
- [12] Vahid Sotoudeh, 1986, "Measurement and Analysis of Structural Vibrations", Ph.D. Dissertation, Stanford. Stanford University
- [13] Erdal Safak, M.ASCE, 1991, "Identification of Linear Structures Using Discrete-Time Filters", Journal of Structural Engineering, Vol. 117, No. 10, October 1991, pp. 3064-3085

- [14] Rune Brincker, Lingmi Zhang, Palle Andersen, 2000, “*Modal Identification from Ambient Responses using Frequency Domain Decomposition*”, Proceeding of the 18th International Modal Analysis Conference (IMAC), San Antonio, Texas.
- [15] Rune Brincker, Lingmi Zhang, Palle Andersen, 2000, “*Output-only Modal Analysis by Frequency Domain Decomposition*”, Proceeding of ISMA 25, Volume 2
- [16] Rune Brincker, Lingmi Zhang and Palle Andersen, 2001, “*Modal Identification of Output-only Systems Using Frequency Domain Decomposition*”, Smart Materials and Structures, 10, 441-445
- [17] Rune Brincker, Carlos E. Ventura, Palle Andersen, 2001, “*Damping Estimation by Frequency Domain Decomposition*”, Proceeding of the 19th International Modal Analysis Conference (IMAC), Kissimee, Florida
- [18] Jian-Huang Weng, 2010, “*Application of Subspace Identification in System Identification and Structural Damage Detection*”, Ph.D. Dissertation, National Taiwan University
- [19] Jian-Huang Weng, Chin-Hsiung Loh and Yang J N, 2009, “*Experimental Study of Damage Detection by Data-Driven Stochastic Subspace Identification and Finite Element Model Updating*,” J. of Structural Engineering, 135(12) 1533-1544, 2009.
- [20] Chin-Hsiung Loh, C.H. Mao, S.H. Chao and Jian-Huang Weng, 2010, “*Feature Extraction and System Identification of Reinforced Concrete Structures Considering Degrading Hysteresis*,” Accepted for publication in J. of Structural Control & Health Monitoring, Article first published online: 5 JUL 2010
- [21] Chin-Hsiung Loh and Jian-Huang Weng, 2009, “*Damage Detection Using Stochastic Subspace Identification with Partial Measurements*,” The 7th international workshop on structural health monitoring – 2009, 9-11 September 2009.
- [22] Jian-Huang Weng and Chin-Hsiung Loh, 2009, “*Structural Health Monitoring of Arch Dam from Dynamic Measurements*,” 12th international conference on engineering, science, construction and operations in challenging environments (Earth & Space 2010), 14-17 March 2010.
- [23] Doebling, S. W., Farr, C. R., Prime, M. B., and Shevitz, D. W., 1996, “*Damage identification and health monitoring of structural and mechanical systems from changes in their vibration characteristics: A literature review*”, Los Alamos National Laboratory, Tech. Rep., May.
- [24] Kondo, I. and Hamamoto, T., 1996, “*Seismic damage detection of multi-story building using vibration monitoring*”, Eleventh World Conference on Earthquake Engineering, Paper No. 988.
- [25] Safak, E., 1989, “*Adaptive modeling, identification, and control of dynamic structural systems: I - Theory*”, J. Eng. Mech., ASCE, 115(11), 2386-2405.
- [26] Safak, E., 1989, “*Adaptive modeling, identification, and control of dynamic structural systems: II - Application*”, Journal of Engineering Mechanics, Vol. 115, No. 11, pp. 2406-2426
- [27] Andersson, P., 1985, “*Adaptive forgetting in recursive identification through multiple models*”, Int. J. Control, 42(5), 1175-1193.
- [28] Chin-Hsiung Loh and Lin, H. M., 1996, “*Application of off line and on line identification techniques to building seismic response data*”, Earthq. Eng. Struct. Dyn., 25(3), 269-290.

- [29] Sohn, H., Farrar, C. R., Hunter, N. And Worden, K., 2001, “*Applying the LANL statistical pattern recognition paradigm for structural health monitoring to data from a surface-effect fast patrol boat*”, Los Alamos National Laboratory Report No. LA-13761-MS, University of California, Los Alamos, NM.
- [30] Sohn, H. and Farrar, C. R., 2001, “*Damage diagnosis using time series analysis of vibration signals*”, Smart Mater. Struct., 10, 446-451.
- [31] Dyke S J and Spencer B.F., 1995. “The role of control-structure interaction in predictive system design”, J. Eng. Mech. ASCE 121, 322-338.
- [32] Dyke S J, Spencer B.F., Quest P, Sain M K, Kapari D C and Soong T T, 1996. “*Acceleration feedback control of MDOF structures*”, J. Eng. Mech. ASCE, 122, 907-918.
- [33] Suhardjo J, Spencer B.F. and Kareem A, 1992. “*Frequency domain optimal control of wind excited building*”, J. Eng. Mech. ASCE, 118, 2463-2481.
- [34] Schmitendorf W E, Jabbari F and Yang J N, 1994. “*Robust control techniques for buildings under earthquake excitation*”, Earthquake Eng. Struct. Dyn. 23(5), 539-552.
- [35] Jabbari F, Schmitendorf W E and Yang J N, 1995, “*H ∞ control for seismic-excited building with acceleration feedback*”, J. Eng. Mech. ASCE, 121(9), 994-1002.
- [36] Kose I E, Schmitendorf W E, Jabbari F and Yang J N, 1996, “*H ∞ active seismic response control using static output feedback*”, J. Eng. Mech. ASCE, 122(7), 651-659.
- [37] Chin-Hsiung Loh, Chia-Ming Chang, 2006, “*Vibration control assessment of ASCE benchmark model of cable-stayed bridge*”, Journal of International Association Structural Control and Monitoring, Vol. 13, Issue 4, 825-848, July 2006
- [38] Chin-Hsiung Loh, Chia-Ming Chang, 2007, “*MATLAB-based seismic response control of a cable-stayed bridge: cable vibration*”, urnal of International Association Structural Control and Monitoring, Vol. 14, Issue 1, 109-143, Feb. 2007
- [39] Chin-Hisung Loh, Chia-Ming Chang, 2008, “*Application of Centralized and Decentralized Control to Building Structure: Analytical Study*”, J. Engrg. Mech., Vel. 134, Issue 11, 970-982, Nov. 2008
- [40] Yang J N, Wu J C, and Agrawal A K, 1995, “*Sliding mode control of seismic-excited linear structures*”, J. of Engineering Mechanics, ASCE, Vol.121, No.12, 1386-1390.
- [41] Yang J N, Wu J C and Agrawal J, 1995, “*Sliding mode control for nonlinear and hysteretic structures*”, J. Eng. Mech. ASCE 121(12), 1330-1339.
- [42] Yang J N, Wu J C, Kawashima K and Unjoh S, 1995, “*Hybrid control of seismic-excited bridge structures*”, Earthquake Engineering and Structural Dynamics, 24 (11), 1437-1995.
- [43] Yang J N, Wu J C, Reinhorn A M and Riley M, 1996, “*Control of sliding isolated buildings using sliding mode control*”, J. of Struct. Eng. ASCE, 122(2), 83-91.
- [44] Yang J N, Wu J C, Agrawal A K and Hsu S Y, 1997, “*Sliding mode control with compensator for wind and seismic response control*”, Earthquake Engineering and Structural Dynamics,26(11), 1137-1156.
- [45] Hiemenz G J and Wereley N M, 2000, “*Seismic response of civil structures utilizing semi- active ER and MR bracing systems*”, J. of Intelligent Materials and Structures,10(8): 646- 651.

- [46] Hiemenz G J, Choi Y T and Wereley N M, 2003, “*Seismic control of civil structures utilizing semi-active MR braces*”, J. of Computer-Aided Civil and Infrastructure Engineering, 18, 31-44.
- [47] Spencer B F, Dyke S J, Sain M K and Carlson J D, 1997, “*Phenomenological model for magnetorheological dampers*”, Journal of Engineering Mechanics ASCE, 123:230-238.
- [48] Kung-Chun Lu and Chin-Hsiung Loh, 2010, “*Development of Wireless Sensing System for Structural Health Monitoring*”, The proceeding of 12th International Conference on Engineering, Science, Construction, and Operations in Challenging Environments, Honolulu, Hawaii, March 14-17, 2010.
- [49] Kung-Chun Lu, Chin-Hsiung Loh, and Jian-Huang Weng, 2010, “*Development of smart sensing system for structural health monitoring*”, the proceeding of SPIE on Smart Structures and Materials + Nondestructive Evaluation and Health Monitoring, vol. 7647, 7-11 March.
- [50] Wang, Y., Lynch, J.P. and Law, K.H., 2007, “*A wireless structural health monitoring system with multithreaded sensing devices: design and validation*”, Structure and Infrastructure Engineering, 3(2), 103-120.
- [51] Atmel Corporation, 2004, “*Atmel AVR Atmega128 Datasheet: 8-bit AVR Microcontroller with 128Kbytes In-System Programmable Flash*”, San Jose, CA.
- [52] *Datasheet of ADS8341EB*, <http://focus.ti.com/docs/prod/folders/print/ads8341.html>
- [53] *Datasheet of VSE-15D*, <http://www.to-soku.co.jp>
- [54] Bendat J S and Piersol A G, 1986, “*Random Data, Analysis and Measurement Procedures*” (New York: Wiley)
- [55] Brincker, R., Ventura, C.E., Andersen, P., 2001, “*Damping estimation by frequency domain decomposition*”, Proceedings of the 19th Int’l Modal Analysis Conference (IMAC), 698-703.
- [56] Analog Devices, Inc., 2003, “*OP400 Datasheet – Quad Low Offset, Low Power Operational Amplifier*”, MA, USA
- [57] Kung-Chun Lu, Wang Y., Lynch J.P., Chin-Hsiung Loh, Y. J. Chen, P. Y. Lin, and Z. K. Lee, 2006, “*Ambient Vibration Study of the Gi-Lu Cable-Stay Bridge: Application of Wireless Sensing Units*”, SPIE 13th Annual International Symposium on Smart Structures and Materials, San Diego, CA, February 26 - March 2, 2006.
- [58] Kung-Chun Lu, Yuan-Sen Yang, Chin-Hsiung Loh, Lynch J.P. and Law, K.H., 2006, “*Structural Health Monitoring and Damage Diagnosis: Based on Embedded Algorithm and Visualized User Interface*”, Proceedings of the US-Taiwan Workshop on Smart Structural Technology for Seismic Hazard Mitigation, Taipei, Taiwan, October 12-14, 2006.
- [59] Kung-Chun Lu, Chin-Hsiung Loh, Yuan-Sen Yang, Lynch J.P., Law, K.H., 2008, “*Real-time structural damage detection using wireless sensing and monitoring system*”, Journal of Smart Structures and Systems, Volume 4, Number 6, pp.759-778, November.
- [60] Kung-Chun Lu, Jian-Huang Weng, Chin-Hsiung Loh, 2009, “*Turning the building into a smart structure: Integrating health monitoring*”, SPIE 16th Annual International Symposium on Smart Structures and Materials & Nondestructive Evaluation and Health Monitoring, San Diego, CA, March 9-12, 2009.

- [61] Chin-Hsiung Loh, Lynch J.P., Kung-Chun Lu, Wang Y., Chia-Ming Chang, P.Y. Lin and Ting-Hei Yeh, 2007, “*Experimental verification of a wireless sensing and control system for structural control using MR damper*”, *Earthquake Engineering and Structural Dynamics*, 2007, Vol.36, 1303-1328
- [62] Kung-Chun Lu, Chin-Hsiung Loh, 2008, “*Structural control using Smart Control Devices*”, *Proceedings of Cansmart 2008 International Workshop*, Montreal, Quebec, Canada, October 2008.
- [63] Kung-Chun Lu, Chin-Hsiung Loh, Yang J N and P. Y. Lin, 2008, “*Decentralized sliding mode control of a building using MR dampers*”, *Smart Materials and Structures*, Vol.17, 055006
- [64] Verhaegen M and Dewilde P, 1992, “*Subspace model identification, Part I: The output-error state space model identification class of algorithms*”, *Int. J. Control*, Vol 56 1187-1210.
- [65] Hiemenz G J, Choi Y T and Wereley N M, 2003, “*Seismic control of civil structures utilizing semi-active MR braces*”, *J. of Computer-Aided Civil and Infrastructure Engineering*, 18, 31-44.
- [66] Yang J N, Kim, J H and Agrawal, A K, 2000, “*A Resetting Semi-Active Stiffness Damper for Seismic Response Control*”, *J. of Structural Engineering*, ASCE, 126(12); 1427-1433.
- [67] Yang J N, Bobrow J, Jabbari F, Leavitt J, Cheng C P and P.Y. Lin, 2007, “*Full-Scale Experimental Verification of Resettable Semi-Active Stiffness Dampers*”, *Journal of Earthquake Engineering and Structural Dynamics*, Vol. 36, 1255-1273.
- [68] Yang J N, Wu J C, and Agrawal A K, 1995, “*Sliding mode control of seismic-excited linear structures*”, *J. of Engineering Mechanics*, ASCE, Vol.121, No.12, 1386-1390.
- [69] Yang J N, Wu J C and Agrawal J, 1995, “*Sliding mode control for nonlinear and hysteretic structures*”, *J. Engng. Mech. ASCE* 121(12), 1330-1339.
- [70] Ohtori Y, Christenson R E, Spencer B F and Dyke S J, 2004, “*Benchmark control problem for seismically excited nonlinear buildings*”, *J. of Engineering Mechanics*, ASCE; 130: 366- 385.
- [71] Jung H J, Choi K M, Spencer B F and Lee I W, 2006, “*Application of some semi-active control algorithms to a smart base-isolated building employing MR dampers*”, *J. Structural Control and Health Monitoring*; 13:693-704.
- [72] Jansen L M and Dyke S J, 2000, “*Semi-active control strategies for MR dampers: comparative study*”, *Journal of Engineering Mechanics ASCE*, 126; 8:795-803.

簡歷



姓名：盧恭君 (Kung-Chun Lu)

出生地：台灣 (Taiwan)

出生時：中華民國七十一年七月十九日 (1982.07.19)

E-mail: d95521003@ntu.edu.tw

學經歷：國立新竹高級中學

淡江大學 土木工程系 學士

國立台灣大學 土木工程所結構工程組 碩士

國立台灣大學 土木工程所結構工程組 博士